

**PREDICTION OF SPACE VEHICLE
THERMAL CHARACTERISTICS**

*J. T. BEVANS
T. ISHIMOTO
B. R. LOYA
E. E. LUEDKE*

TRW SYSTEMS GROUP

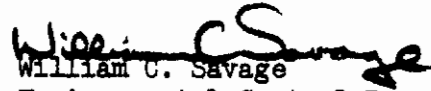
FOREWORD

The following report was prepared by TRW Systems Group, under USAF Contract No. AF 33(615)-1725 as part of Project 6146, Task 614617. The program was administered by the Air Force Flight Dynamics Laboratory, Research and Technology Division, Wright-Patterson Air Force Base. The Technical Monitor was Mr. C. J. Feldmanis.

The program was performed by J. T. Bevans, T. Ishimoto, B. R. Loya, and E. E. Luedke. Dr. D. K. Edwards of the University of California, at Los Angeles, was consultant throughout the study.

The manuscript was released by the authors 31 August 1965, for publication as an RTD Technical Report.

This technical report has been reviewed and is approved.


William C. Savage
Environmental Control Branch
Vehicle Equipment Division
AF Flight Dynamics Laboratory

ABSTRACT

The work reported herein is the first phase of a program to improve the prediction of spacecraft thermal performance. The study has consisted of measuring actual joint thermal conductances, correlation of the measured joint conductances, programming an improved method of thermal radiation analysis, and performing an experimental comparison of predicted radiation exchange for a simple geometrical system.

Three types of structural and three sizes of component mounting joints were tested and the conductances measured. A successful method of correlation was developed for the unfilled component mounting joints. All joints were selected for their applicability to the next phase of the program, a thermal test of a spacecraft model.

A method of radiation analysis has been programmed which uses directional thermal radiation properties and accounts for the specularity and/or diffuseness of these properties. The results of this program can be readily incorporated into most existing thermal analysis programs. The user has the choice of the specular, the diffuse, or the specular-diffuse assumption. The prediction of radiation exchange using these assumptions for simple geometrical arrangements has been compared to experiment. Although the results were within the overall experimental tolerances, further improvement in the predicted values is believed possible.

The study has developed several important technical areas which are worthy of further evaluation. The first is the extension of the correlation techniques to include filled component joints and filled or unfilled structural joints. Continuation of the general measurement of joints to develop a large knowledge of practical joint conductances is also indicated. The comparison of experimental and predicted radiation exchange has shown that a more extensive study is needed of thermal radiation properties to determine the division of these properties into specular and diffuse components. The non-gray error of radiation analysis has also been shown to be an important area for further study.

Contrails

TABLE OF CONTENTS

	PAGE
1. Introduction and Summary	1
2. Spacecraft Model Selection	2
3. Thermal Conductance of Joints	4
4. Development of Analytical Methods for Thermal Performance Analysis	21
5. Computer Program for Directional Specular- Diffuse Method	32
6. Experimental Comparison of Specular, Diffuse and Directional Specular-Diffuse Analyses	46
7. Correlation of Component Joint Experimental Results	60
8. Conclusions and Recommendations	75
Appendix I Experimental Data--Component Joints	79
Appendix II Structural Joint Tests	104
Appendix III Script F Computer Program Print Out	124
Appendix IV Experimental Data--Radiation Exchange Experiment.	165
Appendix V Bibliography for Joint Thermal Conductance	171
Appendix VI Component Joint Test Data used for Correlation Task	173

ILLUSTRATIONS

FIGURE	PAGE
1. Spacecraft Model - Size and Shape	3
2. Component Joints	5
3. Structural Joints	6
4. Typical Component Joint	8
5. Component Joint Ready for Testing	9
6. Power Circuit for Joint Testing	10
7. Typical Structural Joint	16
8. Computer Program Flow Chart	33-35
9. Program Input Format	37
10. Load Sheet for Two Parallel Infinite Diffuse Strips of Unit Width and Separation	39
11. Load Sheet for Sample Problem; Diffuse Assumption	41
12. Load Sheet for Sample Problem; Specular Assumption	43
13. Load Sheet for Sample Problem; Directional Specular- Diffuse Assumption	45
14. Configurations Used for Test of Radiation Analysis	47
15. Test Configuration in Test Fixture	48
16. Test Configuration Ready for Testing	49
17. Experimental Matrix for Test of Radiation Analysis	51
18. Directional Reflectance of 3M Flat Black Paint to a 540°R Black Body as a Function of Angle	53
19. Directional Reflectance of Vacuum Deposited Aluminum to a 540°R Black Body as a Function of Angle	54
20. Directional Reflectance of Sulfuric Soft Anodized Aluminum (Type 1100), 0.0005 Inches Thick to a 540°R Black Body as a Function of Angle	55

ILLUSTRATIONS

FIGURE	PAGE
21. Directional Reflectance of Rinshed-Mason Leafing Aluminum Paint to a 540°R Black Body as a Function of Angle	56
22. STL Goniometric Reflectometer	58
23. Analytical Models for Bolted Component Joint Correlation	62
24. The Quantity $[\eta_0^2 - (\eta_0^4/4) - \ln \eta_0 - 3/4]^{-1}$ as a Function of η_0	65
25. The Thermal Conductance of a Single Contact Junction as a Function of Contact Radius (R_0) for an Aluminum Plate 1/16th Inch Thick	66
26. The Thermal Conductance of a Peripheral Contact Junction for an Aluminum Plate 1/16th Inch Thick	67
27. Stress Distribution in a Bolted Plate for Uniform Bolt Pressure	69
28. The Pressure Distribution Under the Nut of a Bolted Plate According to Equation 7-12	69
29. Method of Subdividing the Test Configurations to Predict Overall Thermal Conductance	72
30. Thermal Circuit for Calculating Overall Thermal Conductance	70
31. 6" x 6" Component Joint Thermocouple Location	82
32. 6" x 12" Component Joint Thermocouple Location	83
33. 12" x 12" Component Joint Thermocouple Location	84
34. 6 Inch Structural Joint, Configurations 1 and 2, Thermocouple Locations	107
35. 9 Inch Structural Joint, Configurations 1 and 2, Thermocouple Locations	108
36. 6 Inch Structural Joint, Configuration 3, Thermocouple Locations	109
37. 9 Inch Structural Joint, Configuration 3, Thermocouple Locations	110
38. Measured Heat Loss from Test Surfaces of Radiation Experiment	168
39. Bolt Locations for Correlation Task Experiments	175

Contracts

TABLES

TABLE	PAGE
1. Component Joint Thermal Conductance Experimental Results 6 inch by 6 inch joint	12
2. Component Joint Thermal Conductance Experimental Results 6 inch by 12 inch joint	13
3. Component Joint Thermal Conductance Experimental Results 12 inch by 12 inch joint	13
4. Structural Joint Conductance, BTU/hr ft ² °F Configuration 1	17
5. Structural Joint Conductance, BTU/hr ft ² °F Configuration 2	18
6. Structural Joint Conductance, BTU/hr ft ² °F Configuration 3	19
7. Summary of Radiation Exchange Analyses and Experiment	57
8. Comparison of Predicted and Measured Component Joint Conductances	73
9. Experimental Data--6 by 6 Inch Component Joints	85-97
10. Experimental Data--6 by 12 Inch Component Joints	98-100
11. Experimental Data--12 by 12 Inch Component Joint	101-103
12. Experimental Data--Structural Joint Configuration 1	111-114
13. Experimental Data--Structural Joint Configuration 2	115-119
14. Experimental Data--Structural Joint Configuration 3	120-123
15. Summary of the Data Obtained in the Experimental Testing of the Analytical Prediction	169-170
16. Additional Component Joint Correlation Data	176

Contrails

SYMBOLS

Section 3

A	Area - ft^2
h	Thermal conductance - $\text{Btu/hr ft}^2 \text{ } ^\circ\text{F}$; h_{eff} = effective h
q	Heat flow - Btu/hr
t	Temperature - $^\circ\text{F}$

Section 4

A	Area of a surface - ft^2
B	Quantity introduced by Gebhart - $\text{Btu/hr ft}^2 \text{ } ^\circ\text{R}^4$ (Section 4.1)
C	Heat capacity - Btu/hr
D	Diffuse irradiation - $\text{Btu/hr ft}^2 \text{ ster.}$ (Section 4.2)
F	Geometrical shape factor
\mathcal{F}	"Script F"
J	Radiosity - Btu/hr ft^2
M	Number of surfaces within the enclosure
N	Number of time intervals
R	Thermal conduction resistance - $\text{hr } ^\circ\text{F/Btu}$ (Equation 4-3)
R	Hottel's radiant power leaving a surface - $\text{Btu/hr ft}^2 \text{ } ^\circ\text{R}^4$ (Section 4.1)
T	Absolute temperature - $^\circ\text{R}$
a	Coefficient (Section 4.2)
b	Coefficient (Section 4.2)
c	Coefficient (Section 4.2)
d	Coefficient (Section 4.2)
i, j, k	Indices representing surfaces within the enclosure
q	Heat flow Btu/hr
x, y, z	Indices
α	Absorptance
ϵ	Emittance
η	Convergence factor (Equation 4-8)
π	3.1415927
ρ	Reflectance
σ	Stefan-Boltzmann constant - $\text{Btu/hr ft}^2 \text{ } ^\circ\text{R}^4$
θ	Time

SYMBOLS (Cont.)

[]	Square matrix
[] ⁻¹	Inverse square matrix
{ }	Column matrix

Section 5

Symbols defined in the text.

Section 6

Q_s	Source heat flow - Btu/hr
$\rho(\theta)$	Directional reflectance at angle θ
θ	Angle between the normal to the surface and the incident or reflected radiation - degrees

Section 7

A	Area, ft ²
Q	Heat flux, Btu/hr ft ²
R	Radius - in.
T	Temperature, °F
a	Bolt diameter, in.
b	Twice the plate thickness, in.
c	Effective contact radius, in.
d	Bolt major thread dia.
h	Thermal conductance - Btu/hr ft ² °F
k	Thermal conductivity - Btu/hr ft °F
r	Radial position, in.
t	Plate thickness - ft.
η	Nondimensional radius ratio - r/R
η_o	Nondimensional radius constant R_o/R

Appendix IV

T_R	= "Receiver" temperature °R
T_M	= "Mirror" temperature °R
T_o	= "Sink" (cold wall) temperature °R
T_s	= "Source" temperature °R

Contrails

Contrails

1. INTRODUCTION AND SUMMARY

The program, "Prediction of Space Vehicle Thermal Performance," was initiated on 1 July 1964, under Contract AF 33(615)-1725. The purpose of the study can be stated as: Given the necessary analytical methods and experimental data, how well can the thermal performance of a space vehicle be predicted? The subject program was the first step towards securing an answer to this question.

The problem provides two natural divisions. The first is the examination of the analytical procedures needed and the experimental information required for analysis. The second is the verification of the predictions of analysis by a thermal test of a model space vehicle. The present program was intended to satisfy the first need and to provide a transition to the second. Since a model is required to verify analysis, its design will dictate the nature and scope of the experimental studies performed to support analysis. In particular, the subsequent construction of a test model will require the selection of structural and component joints in anticipation of the design. Depending upon the type of joint selected and the degree of experimental measurements made, the thermal resistance of the joints can be critical to the experimental verification of any predictions made. Consequently, it was necessary at the start of the present program to select, in reasonable detail, the model configuration. The experimental measurements of joint thermal resistance were restricted to those joints to be used in the model. Only in this manner could the end purpose of the study, the test of prediction, be achieved within the allocated resources and time.

The specific tasks undertaken in the study were:

- (a) Selection of a model for determination of the experimental joint thermal conductance measurements
- (b) Experimental measurement of component and structural joint thermal conductance
- (c) Examination of the results of the joint thermal conductance results to ascertain if a correlation were possible
- (d) Comparison of the analytical techniques of Hottel (1), Gebhart (2), and Oppenheim (3).
- (e) Development of a computer program for a specular-diffuse analysis (4)
- (f) Experimental measurement of radiation exchange with real surfaces

The following report will consider the above tasks in the order shown. It should be re-emphasized that the purpose of the program and hence, the goal of each task, is to provide the necessary data for a comparison of thermal analysis and thermal test of a spacecraft model.

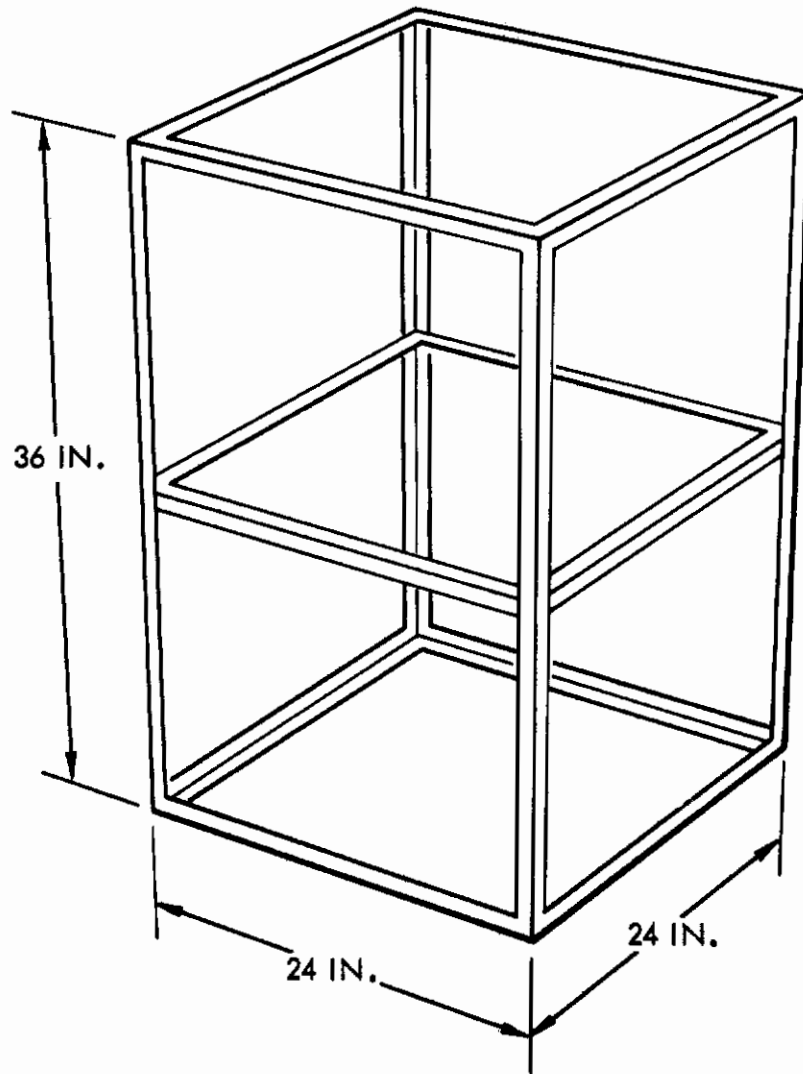
2. SPACECRAFT MODEL SELECTION

An important initial task was the conceptual design of the model of the space vehicle to be tested in the subsequent phase of the program. The size, method of construction and shape of the model greatly affects the type of fasteners, the physical dimensions and the shape of the joints.

The model which has been selected is shown in Figure 1. Alternative shapes, cylindrical and spherical, were considered but the rectangular parallelepiped was chosen for economy and ease of fabrication. Furthermore, the geometrical shape can not be a critical factor in a test of the prediction of thermal performance. The indicated dimensions, 24" x 24" x 36", are sufficiently large to demonstrate the effects of construction variations, thermal gradients, and internal dissipation. The model will conveniently fit into most environmental test chambers and available solar simulation facilities. Also, the size is representative of many present day space vehicles.

A welded framework is indicated. This method of construction was selected to reduce the number of structural joints that had to be tested. There are three structural joints with the frame: the side panels, the end panels, and the component mounting platform. The side and end panels are 1/16-inch aluminum; i.e., thin enough to sustain a thermal gradient. The mounting platform is 1/8-inch aluminum. In actual space vehicle construction, this mounting plate would probably be a honeycomb structure to reduce weight. Such materials are anisotropic and the thermal conductance in the x, y, and z directions are variable from sample to sample of the same material. The conductance also varies widely for different types of honeycomb. Thus, use of a honeycomb structure would introduce a major undetermined factor in the thermal analysis. This could easily obscure the validity of the comparison of prediction and experiment. The aluminum mounting plate avoids this without affecting the value of the test to be conducted. Thus, if the analysis can properly predict for the aluminum plate, it will be satisfactory for application to a honeycomb material (assuming the properties of the honeycomb are known).

The external panels can be changed to provide different external thermal radiation properties. This may not be important in the initial testing to be performed with the model but will be useful should further testing be desired or required. These panels can be coated to simulate solar cell thermal radiation properties, low α/ϵ properties or even be insulated without affecting the basic model physically. A louver system could be used in place of any panel to determine the effects of variable emission. Hence, the model will be of much more value than just for the program contemplated in Phase II.



ALUMINUM FRAME-HELI ARC CONSTRUCTION

Figure 1. Spacecraft Model - Size and Shape

3. THERMAL CONDUCTANCE OF JOINTS

Completely riveted joints were excluded from the study. In spacecraft practice, riveted systems are used in order to save weight. However, the thermal conductance of such joints is not considered reproducible and variations of 100 percent have been found in supposedly identical joints (5). Since the goal of the program is to test the ability to predict thermal performance with reliable input information, the introduction of such an uncontrolled thermal resistance is not desired. This would not test the prediction of thermal performance but only the uncertainty of knowledge. The effect of the variable thermal resistance can be demonstrated analytically, once the analysis has been verified.

Two general types of joints were studied: component and structural joints. The component joints are shown in Figure 2. The dimensions were chosen as representative of typical component base sizes. Simulation of the actual component box was not deemed necessary since this would only involve changes in the radiation shape factors used. The assumption was made that the base plates would have a uniform areal power dissipation. The experimental variables examined were bolt-torque, power dissipation level, filler material and reproducibility of the joints. A detailed description of the test method and the results will be given in Section 3.1.

The structural joints tested are presented in Figure 3 and all are bolted joints. The structural joints were selected to satisfy the requirements of the proposed space vehicle model (see Section 2). The first configuration corresponds to the joint between the side panels and the frame. The end panels are bolted to the frame by means of nut plates which are riveted in place (second joint). This joint can be considered to be a combination of a rivet and bolt fastener. The third joint shown represents the joint between the component mounting platform and the frame. As with the component joints, the variables of power dissipation level, filler material and reproducibility were examined. The experimental test method and results are given in Section 3.2.

These joints are "practical" ones; i.e., representing actual fabricated joints. As a result, variations in the thermal conductance must be expected from "identical" joints. An attempt was made to apply idealized theories to these joints to obtain a correlation of the test data. The results of this effort are given in Section 7.

3.1 COMPONENT JOINT EXPERIMENTAL TESTS

The component joints were simulated by bolting a plate 1/16 inch thick of the necessary dimensions to a base plate 1/8 inch thick. The component base plate dimensions used were 6 inches square, 6 inches by 12 inches, and 12 inches square. The plates upon which the base plates were mounted were 2 inches greater in each dimension than the component plate; e.g., 8 inches square for the 6-inch square component plate. The bolt size and placement for each joint are shown in Figure 2. A heater made of 40 gage constantan wire sandwiched between 1 mil Mylar was bonded to the upper surface of each component base plate. The mounting plate had 1/4 inch

Contrails

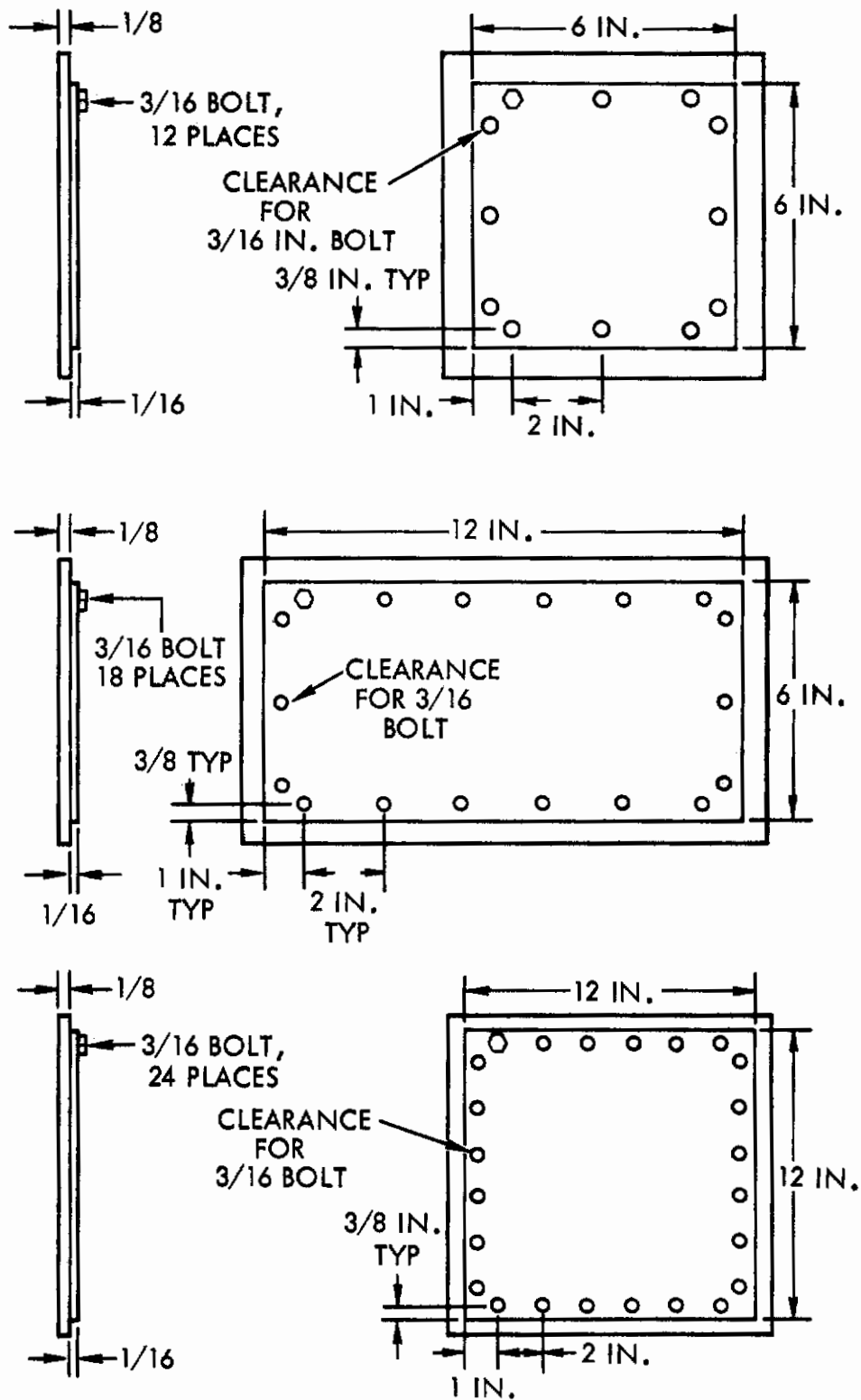


Figure 2. Component Joints

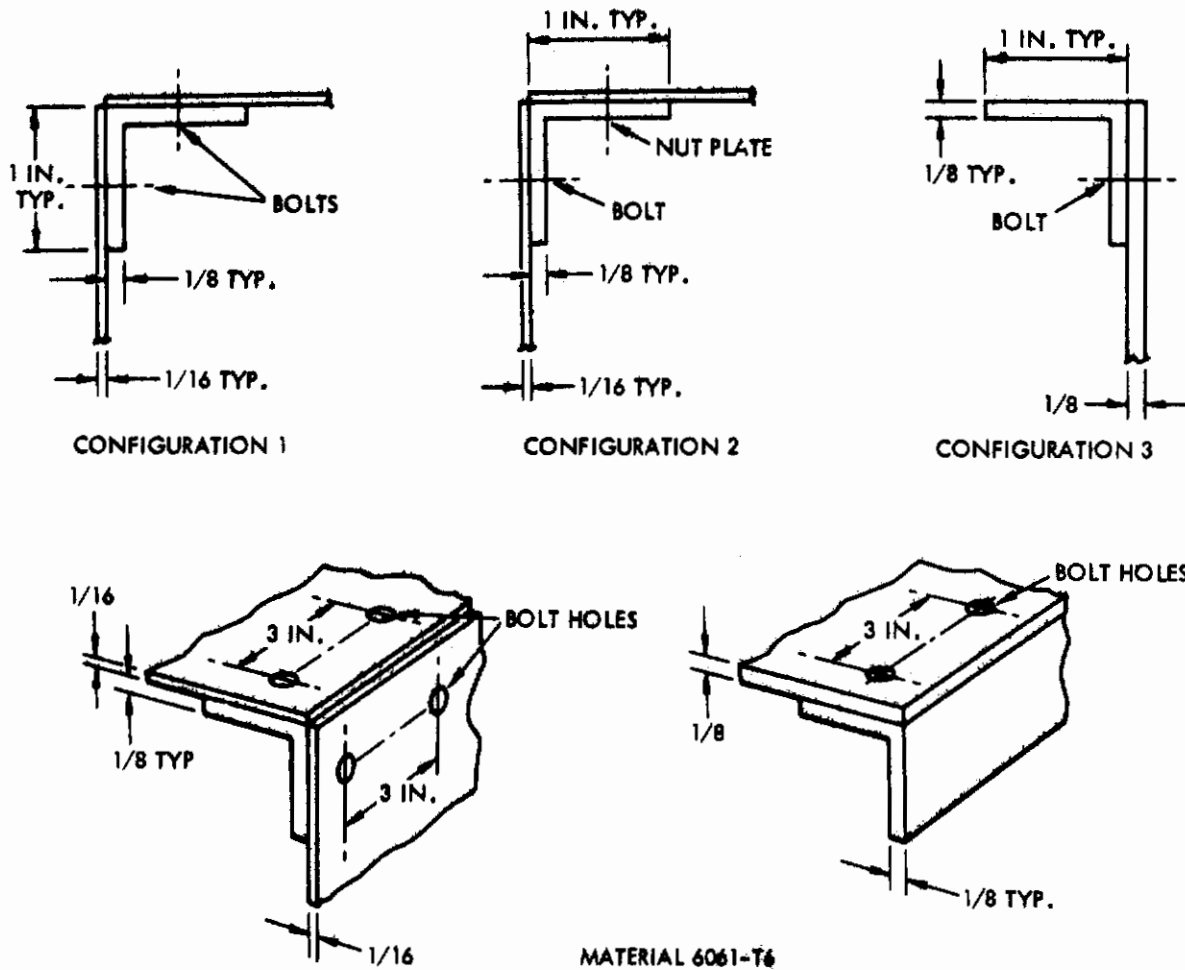


Figure 3. Structural Joints

Contrails

copper cooling coils attached to its underside. The whole assembly was wrapped in 20 layers of super insulation and suspended within a bell jar. This bell jar was evacuated to a pressure less than 10^{-5} torr. Figure 4 shows a component joint after testing; the final assembly and the vacuum system are illustrated in Figure 5. The thermocouples have been removed from this sample so that surface roughness measurements can be made.

The test procedure consisted of placing the insulated and instrumented joint within the bell jar, securing a vacuum on the system, and setting the initial heating rate. Equilibrium was determined by plotting the various temperatures as a function of time. Once these temperatures had stabilized to less than plus or minus 1°F per hour, a set of data was taken. The observed temperature drift was caused by drift in the cooling water temperature.

The electrical circuit used to measure the power dissipated by the heater is shown in Figure 6. The power was determined by measuring the voltage across the heater terminals at the component joint and measuring the current flowing in the heater with a standard resistor. This procedure is commonly referred to as the four terminal resistor technique. The potentiometer used for these two measurements was a Leeds and Northrup Type K-3 Potentiometer. This instrument has three ranges: 1.6 volts, 0.16 volts, and 16 millivolts. The least count on these three ranges is 50, 5, and 0.5 microvolts, respectively.

Initially, temperatures were to be measured with nickel resistance temperature sensors. These sensors were obtained from the RdF Corp., Hudson, New Hampshire, and were calibrated by the vendor to within plus or minus 0.5°F. The first tests did not yield consistent results. This was traced to the resistance sensors. Deviations as large as 2°F were found between initial and final calibrations for a run. Since the temperature differences across a joint were generally smaller than 2°F, this initial data had to be discarded and the sensors replaced with differential copper-constantan thermocouples. The subsequent data was reproducible and consistent for a given test configuration.

Resistance thermometry has the inherent advantage of measuring an area rather than a point; i.e., a local average. When properly calibrated, it is also a more accurate sensor since the impurities in the metals used are less important in resistance than in thermoelectric effects. However, this accuracy can only be achieved at a significant increase in cost relative to thermocouples. The instrumentation method required for differential resistance thermometry is quite different than that used for resistance thermometry. The ratio of the resistances of two elements must be measured, the absolute value of one of these elements is needed, and two sets of lead resistance corrections are necessary. This involves two different bridge circuits (and/or instruments) and a means for electrical switching. The alternative use of thermocouples can provide a differential accuracy of approximately plus or minus 0.1°F if the thermocouples are cut from the same roll of wire and careful experimental procedures used. The cost is much less, both in construction and use. This is offset by the "point" measurement characteristics of a thermocouple. For this series of tests, the thermal conductivity of the aluminum joint material was sufficient to minimize this problem.

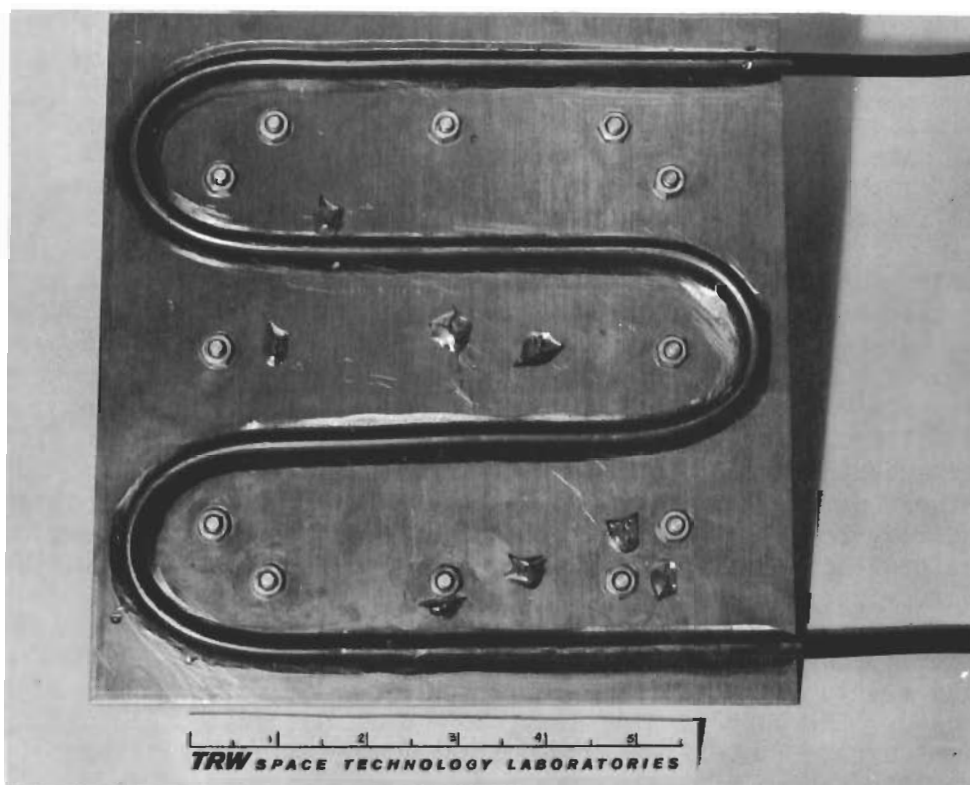
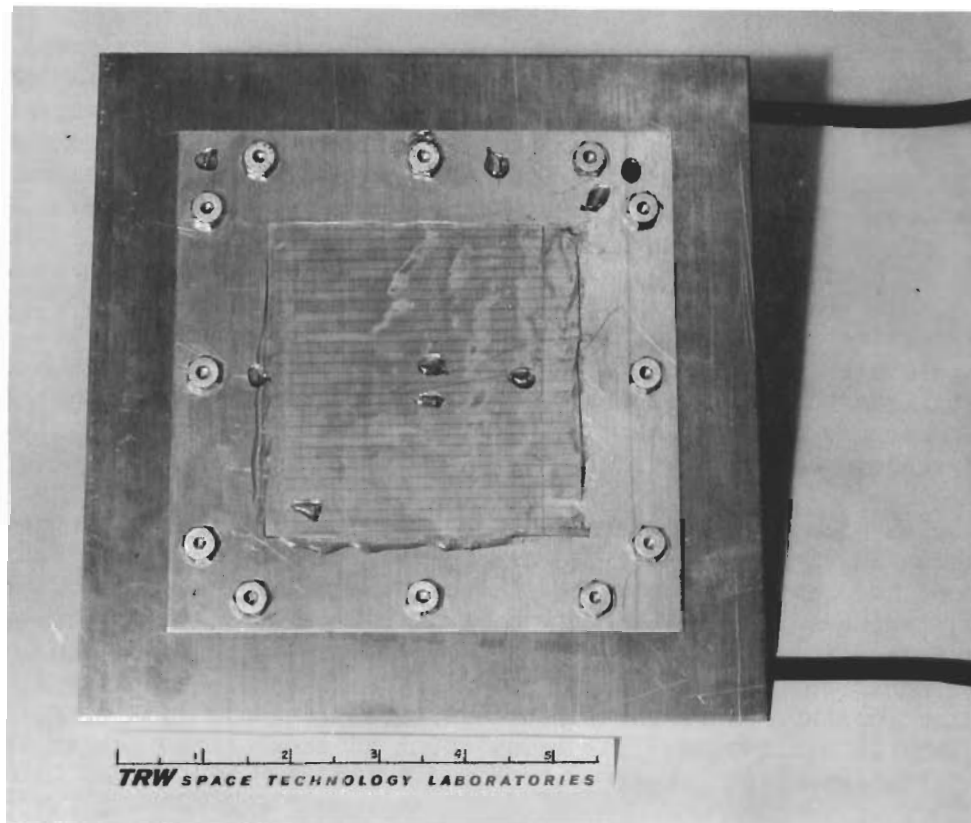


Figure 4. Typical Component Joint



Figure 5. Component Joint Ready for Testing

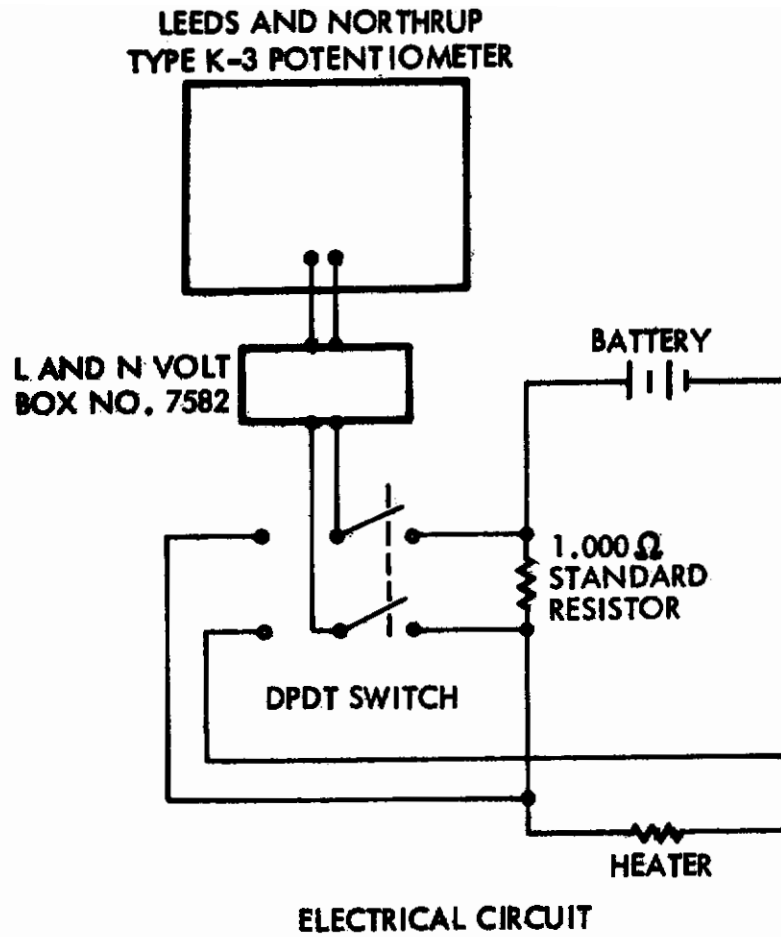


Figure 6. Power Circuit for Joint Testing

Contrails

The emf of the test thermocouples was measured with a Leeds and Northrup Type K-3 Potentiometer. On the millivolt range, this instrument has a least count of 0.5 microvolts. Deutch No. 14657-37T vacuum feed throughs were used for the thermocouples to avoid a discontinuity in the thermocouple circuitry. When a filler material was used, it was applied by placing two 0.050 inch wires on the surface of the mounting plate, putting an ample quantity of the filler material between the wires and scraping the excess off with a straight edge resting on the wires. Before the material set, in the case of RTV-11 filler material, the component plate was placed on the mounting plate and bolted down. The bolt torques for all joints were set with a calibrated torque wrench. No special instructions were given to the person assembling the joint relative to the order of tightening the bolts. This was intentional since the randomness of a fabricated joint was desired.

The results are summarized in Tables 1, 2, and 3; the actual data and the techniques used in its reduction are given in Appendix I. Included in the Appendix are schematic diagrams showing the placement of the temperature sensors. Three specimens of each joint were run with the exception of the G 683 silicone grease filler.* This material was found to be less suitable for use as filler than the silicone rubber. The primary difficulty with the grease was the contamination of the other areas around the joint; i.e., it was messy. Furthermore, it did not yield joint conductances as large as the RTV-11 material.

The results for the 6-inch square joint (Table 1) shows that the effect of heat flux level was small. This was a temperature gradient effect and for the small range involved in this test (from 2.5°F to 10°F for a typical case), it was not important. Similarly, the change in bolt torque from 12 to 30 inch-pounds was not significant. The effect of the RTV-11 was, however, quite significant. It increased the thermal conductance of the 6-inch square joints by a factor of 4 and the larger joints by a factor between 5 and 6.

The most obvious result of the tests was the inconsistency of the results for "identical" joints. Joint No. 2 of the 6-inch square joints is a good example. An examination of the second joint showed the component base plate to be bowed by 0.007 inches (concave upwards); Joint No. 1 was bowed 0.003 inches (concave downwards); and Joint No. 3 was bowed 0.003 inches (concave upwards). Thus a trend of increased conductance with upward concavity is indicated by these limited tests. In actual fabrication, a flatness tolerance can be imposed, e.g., plus or minus .003 inches, which would minimize this effect. Such a constraint is not unreasonable. The surface roughness of the test plates was measured using a diamond stylus profilometer. The results were consistent for all the plates and yielded 11 μ in. rms across the roll marks and 4 μ in. rms with the roll marks. The surfaces were randomly mated, that is the roll marks placed either parallel or perpendicular, but recorded. The results show no correlation between striation alignment and conductance values.

* Manufactured by General Electric Company, Silicone Products Department

TABLE 1
COMPONENT JOINT THERMAL CONDUCTANCE EXPERIMENTAL RESULTS
THERMAL CONDUCTANCE - BTU/HR FT² °F

6 inch by 6 inch plate, 1/16 inch thick, bolted to
8 inch by 8 inch plate, 1/8 inch thick, using 12 bolts

<u>Sample No.</u>	<u>Bolt Torque</u>			<u>30 in-lb</u>	<u>Filler</u>	
	<u>12 in-lb</u>	<u>24 in-lb</u>	<u>30 in-lb</u>			
	10 Watts	4.9 Watts	8.6 Watts	13.4 Watts	18.4 Watts	
1		22.8	23.2	22.9	23.1	None
2	28.5	29.1	30.1	30.1	30.0	None
3	24.8	22.1	25.9	26.2	26.6	None
* 1		76.9	81.5	82.5	83.2	RTV-11
2	123.0	128.1	127.0	129.0	130.0	RTV-11
3	84.1	91.0	93.5	94.8	95.4	RTV-11
* 1		63.0	65.0	66.1	67.1	G-683
2	55.5	47.3	48.2	48.8	49.5	G-683
3	47.0					G-683

12

* Same samples as above, with filler added.

Contrails

TABLE 2
COMPONENT JOINT THERMAL CONDUCTANCE EXPERIMENTAL RESULTS
THERMAL CONDUCTANCE - BTU/HR FT² °F

6 inch by 12 inch plate, 1/16 inch thick, mounted to 8
inch by 14 inch plate, 1/8 inch thick using 18 bolts;
bolt torque 24 in-lb

Sample No.	Power Dissipation			Filler Material
	10 Watts	20 Watts	40 Watts	
1	18.5	18.9	18.5	None
1	103	101.5	98	RTV-11
2	103	101	97	RTV-11
3	90	92	92	RTV-11

TABLE 3
COMPONENT JOINT THERMAL CONDUCTANCE EXPERIMENTAL RESULTS
THERMAL CONDUCTANCE - BTU/HR FT² °F

12 inch by 12 inch plate, 1/16 inch thick, mounted to
14 inch by 14 inch plate, 1/8 inch thick using 24 bolts;
bolt torque 24 in-lb

Sample No.	Power Dissipation			Filler Material
	20 Watts	40 Watts	80 Watts	
1	8.4	8.3	8.3	None
1	56.6	55.8	56.1	RTV-11
2	51.7	52.8	51	RTV-11
3	51.4	51.9	52.4	RTV-11

Contrails

The value of the filler for component mounting boxes is apparent. For the proposed test of a spacecraft model, the component boxes will be simulated by resistances dissipating pre-determined values of power. This is very similar to an actual spacecraft system. The higher values of conductance will permit the same heat flow with 1/3 to 1/4 of the temperature difference or conversely, 3 to 4 times the heat flow for the same temperature difference. This should make this type of thermal resistance less critical in the thermal analysis and prediction.

The effect of using filled joints must be investigated for each specific application under consideration. While much higher conductance values were obtained, the scatter in the data was larger for filled than unfilled joints. Therefore, the selection of filled or unfilled joints depends upon whether joints of high conductance, not precisely defined or joints of low conductance, more accurately described, are desired.

The differences in conductance for different sized component mounting plates was also of interest. The filled conductance decreased by a factor of 2 when the dimensions of the square component base was increased from 6 to 12 inches. This decrease is expected since the number of bolts doubled while the total area increased four times. This effectively causes an increase in the conduction pathlength of the mounting plate. These factors will be considered in more detail in Section 7, "Correlation of Experimental Results."

The overall accuracy of the tests is difficult to assess properly. However, the experimental accuracy of the various tests quantities can be given:

Inaccuracy in temperature difference measurement: $\pm 0.1^{\circ}\text{F}$

Inaccuracy in temperature measurement: $\pm 0.5^{\circ}\text{F}$

Inaccuracy in power dissipation (including insulation loss): $\pm .5\%$

Inaccuracy in area measurement: $\pm .050 \text{ in}^2$

Inaccuracy in bolt torque: $\pm 0.5 \text{ inch-pounds}$

These values may be combined in a linear error analysis to approximate the total measurement inaccuracy. That is, the error in measured conductance (h) of a typical unfilled joint is:

$$\frac{\Delta h}{h} = \frac{\Delta(\Delta t)}{\Delta t} + \frac{\Delta q}{q} + \frac{\Delta A}{A} = \frac{.1}{1} + \frac{.025}{5} + \frac{.05}{36}$$

or

$$\frac{\Delta h}{h} = 10.5\%$$

The significance of this inaccuracy must be appraised in terms of the application of the data. The error in the measurement of a single joint is less than the lack of reproducibility between joints. Hence, the more

important factor is the variation of the conductance of "identical" joints. As shown in Tables 1, 2, and 3, this is approximately plus or minus 25 percent. However the influence of such a variation upon a thermal analysis can be either large or small, depending upon the system examined. For example, if a spacecraft thermal control system is conduction controlled, this variation might be critical; conversely, if it were radiation dominated, the differences might be negligible. To determine the importance of these variations requires an error analysis of the specific configuration.

3.2 STRUCTURAL JOINT EXPERIMENTAL TESTS

The test procedures used for the structural joint measurements were identical to those used with the component joints. The structural joints tested are shown schematically in Figure 3; an actual test joint is shown in Figure 7. A 40 gage constantan and Mylar heater was bonded to one edge of the joint. On the opposite edge, a 1/4 inch copper cooling tube was bonded to provide the necessary heat sink. This whole assembly was wrapped in 20 layers of super insulation and suspended in a bell jar (similar to Figure 5). The remainder of the test procedure was identical to that used for the component joints, e.g., the electrical measurement circuit was that given in Figure 6. Based upon the experience with the component joints, only thermocouples were used as the temperature sensors. The Leeds and Northrup Type K-3 Potentiometer was again used for measuring the thermocouple voltages.

The test results are given in Tables 4, 5, and 6; the actual data from which these results were reduced are given in Appendix II. The first joint tested, Configuration 1 of Figure 3, is representative of the trends indicated for all three joints. Within the range of power dissipations used, no dependency upon power level is indicated for the unfilled joint; i.e., for small temperature differences, the conductance is a constant. A much higher value of joint conductance was obtained with the use of a filler material along with an apparent heat flow dependency. Configuration 2 used nut plates on one side instead of bolts. This had little effect upon conductance for the unfilled case. However, opposite results were obtained for two different RTV-11 filled joints with this configuration; i.e., in one case the nut plate side had a higher conductance and in the other, it had a lower one. No difference between a bolted joint and a nut plate joint could be concluded from the results for Configuration 1 and 2 because of this conflicting data. A strong dependency with heat flow is also noted for the filled joint.

The results of the filled structural joint tests show wide variations in calculated conductance. The most probable reason for these variations is the temperature measurement error. The temperature difference across the interface was of the same order of magnitude as the expected temperature error. In ideal joint conductance tests appearing in the literature (see Section 3.3), the temperature profile of the mating parts is accurately plotted and the data projected to the interface to obtain the temperature difference. The heat flows are normally much higher than in the present study and much higher temperature differences result. In the

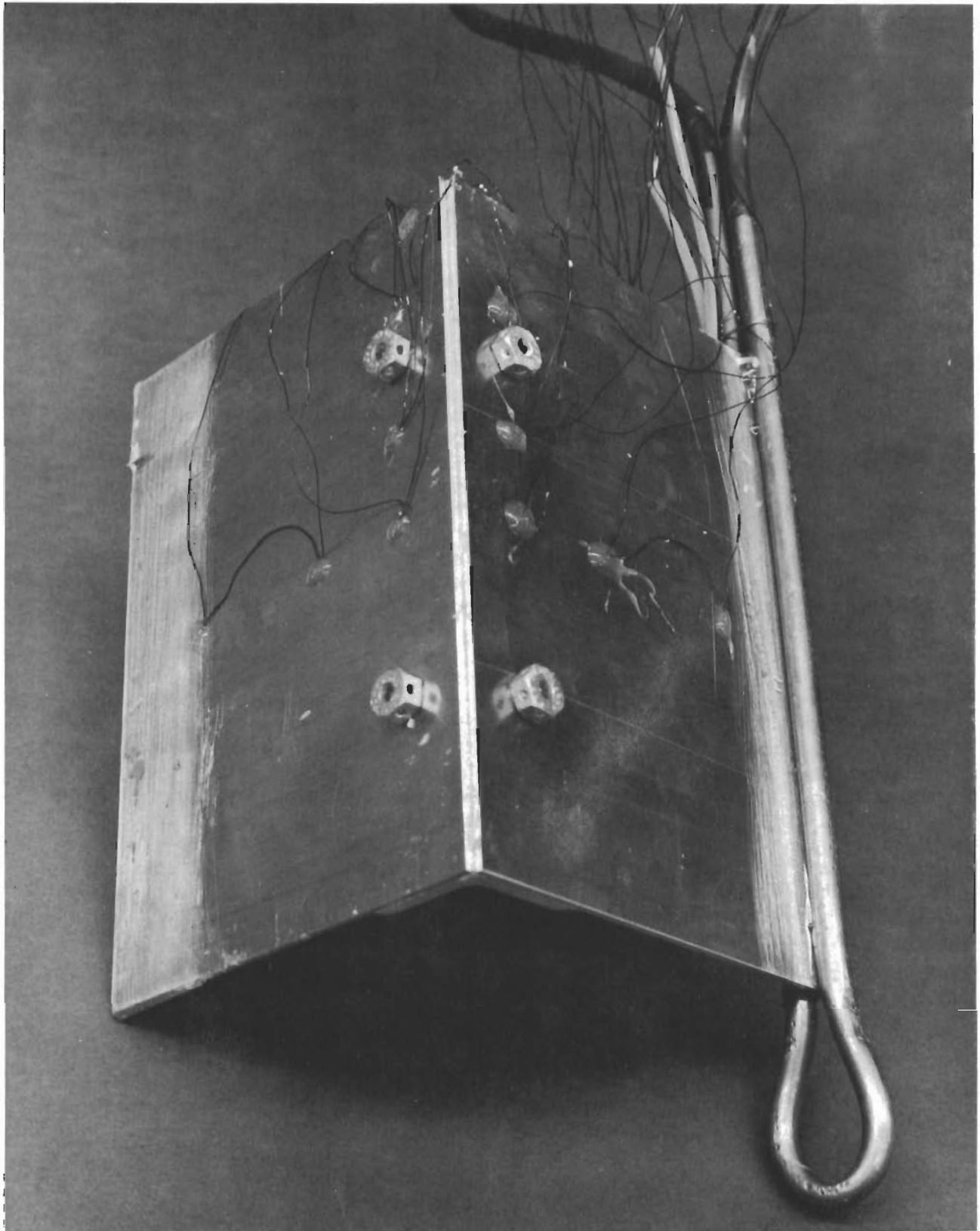


Figure 7. Typical Structural Joint

Contrails

TABLE 4
STRUCTURAL JOINT CONDUCTANCE - BTU/HR FT² °F

6 inch joint, 2 bolts, 24 inch-pounds torque, Configuration 1

Joint No.*	Q - Heat Supplied			Filler
	5 Watts	15 Watts	25 Watts	
1a	70.3	74.2	75.7	None
1b	80.5	80.6	85.3	None
2a	103.5	100.1	100.9	None
2b	88.5	90	96.5	None
3a	78.5	79.4	77.0	None
3b	77.5	79.8	81.8	None
1a	1042	906	715	RTV-11
1b	1042	995	895	RTV-11
1a	602	595	542	G-683
1b	681	652	645	G-683

9 inch joint, 3 bolts, 24 inch-pounds torque, Configuration 1

Joint No.*	Q - Heat Supplied			Filler
	7.5 Watts	22.5 Watts	37.5 Watts	
1a	116.0	98.5	100.8	None
1b	74.0	75.3	77.9	None

*The notation a and b are used to distinguish the side of the joint next to the heater and the cooling coil, respectively.

TABLE 5
STRUCTURAL JOINT CONDUCTANCE, BTU HR FT² °F

6 inch joint, 2 bolts, 24 inch-pounds torque, Configuration 2

Joint No.	Watts			Filler
	5 Watts	15 Watts	25 Watts	
1a (Bolt)	84.2	81.5	85.0	None
1b (Nut Plate)	99.0	100.8	110.3	None
2a (Bolt)	105.5	102	100.8	None
2b (Nut Plate)	82.4	81.4	83.2	None
3a (Bolt)	89.5	88.5	92.6	None
3b (Nut Plate)	93.5	99.3	105.2	None
1a (Bolt)	1427	1227	1050	RTV-11
1b (Nut Plate)	520	514	490	RTV-11
1a (Bolt)	438	425	420	G-683
1b (Nut Plate)	341	345	375	G-683
2a (Bolt)	889	795	669	RTV-11
2b (Nut Plate)	1892	1466	800	RTV-11

9 inch joint, 3 bolts, 24 inch-pounds torque, Configuration 2

Joint No.	Watts			Filler
	7.5 Watts	22.5 Watts	37.5 Watts	
1a (Bolt)	93.5	95.2	94.1	None
1b (Nut Plate)	84.1	87.8	97.6	None

Contrails

TABLE 6
STRUCTURAL JOINT CONDUCTANCE, BTU HR FT² °F

6 inch joint, 2 bolts, 24 inch-pounds torque, Configuration 3

Joint No.				Filler
	5 Watts	15 Watts	25 Watts	
1	147.0	144.2	142.0	None
2	194.0	180.0	174.0	None
3	112.2	108.5	106.5	None
1	1110	1273	1242	RTV-11
1	1328	1262	1231	G-683

9 inch joint, 3 bolts, 24 inch-pounds torque, Configuration 3

Joint No.				Filler
	7.5 Watts	22.5 Watts	27.5 Watts	
1	142.2	139.0	135.5	None

Contrails

present investigation, the real joints had two dimensional heat flows. It was not possible to project gradient measurements to the interface. Furthermore, the heat fluxes used were selected as representative of those to be encountered in an actual spacecraft, and the temperature gradients were correspondingly small.

Two values of joint conductance are given in Table 4 and 5 (Configurations 1 and 2) for each test joint. The experimental system was instrumented to obtain the conductance from either plate to the angle. The effective conductance from plate to plate is determined (by analogy to an electrical circuit) as:

$$h_{\text{eff}} = \frac{1}{\frac{1}{h_1} + \frac{1}{h_2}}$$

If this effective conductance is computed for "identical" joints and conditions, the variations between the measurements are reduced significantly for the unfilled joints. In the case of Configuration 1, the variations in total conductance are less than plus or minus 15 percent; for Configuration 2, it is less than plus or minus 7.5 percent. The filled joints have a much wider variation as is indicated by the measurements.

Two lengths of joint were tested for all three configurations. No significant differences in the measured conductances were observed. Hence, the end losses from the test joint are considered to have been negligible.

The third configuration tested was the one to be used for connecting the internal mounting plate to the frame. The measured results were similar to those obtained for the other two configurations.

The test results obtained indicate a filled structural joint to be more variable than an unfilled one. The conductance is significantly higher, of course. This variability may be nullified by the higher value obtained. As discussed in Section 3.1, this can only be assessed by performing an analysis of an actual spacecraft system using these opposing conditions. The choice will depend upon the relative importance of the two modes of heat transfer, radiation and conduction, for the joint analyzed and the particular system used. However, if filled joints are used, a formerly conduction dominated system may become radiation controlled. For example, the total effective conductance of an unfilled joint is of the order of 40 to 50 Btu/hr ft² °F where as an RTV-11 filled joint has a conductance of over 500 Btu/hr ft² °F.

4. DEVELOPMENT OF ANALYTICAL METHODS FOR THERMAL PERFORMANCE ANALYSIS

The transient energy equation which must be solved for each surface in space vehicle thermal analysis is:

$$C_i \frac{dT_i}{d\theta} = (q_x)_i + (q_r)_i + (q_c)_i \quad 4-1$$

where q_x = net heat transfer from an external source or by internal dissipation

q_r = net heat transfer by radiation

q_c = net heat transfer by conduction

The quantity q_x is generally a function of time. This is a result of orbital conditions and/or of mission imposed duty cycles. Solutions of Equation 4-1 are required for each surface of the spacecraft (internal and external) as a function of time in orbit.

For computer solution, the technique of finite differences is used. Equation 4-1 is written

$$T_i(\theta + \Delta\theta) = T_i(\theta) + \left[\frac{\Delta\theta}{C_i} \right] \left\{ [q_x(\theta)]_i + [q_c(\theta)]_i + [q_r(\theta)]_i \right\} \quad 4-2$$

Thus, the temperature of surface i at time $\theta + \Delta\theta$ is expressed in terms of the temperature and net energy transfers at time θ . The variation of q_x with time is assumed to be known or imposed by external constraints upon the spacecraft. However, both conduction and radiation contain the temperature variable. The expression for q_c is

$$(q_c)_i = \sum_{k=1}^M \frac{T_k - T_i}{R_{ki}} \quad 4-3$$

The expression for q_r can be given by either the network method or by Hottel's "script F."* The equations which must be solved to obtain $(q_r)_i$ by the two methods is given in Section 4.1. They are

$$\text{Hottel: } (q_r)_i = \sum_{k=1}^M A_i \bar{F}_{ik} \sigma (T_k^4 - T_i^4) \quad 4-4$$

* The simple equivalence of Hottel (1) and Gebhart (2) methods (see Section 4.1) is such that for all practical purposes, they may be assumed to be identical.

Contrails

$$\text{Network: } (q_r)_i = A_i \begin{pmatrix} \epsilon_i \\ \rho_i \end{pmatrix} (\sigma T_i^4 - J_i) \quad 4-5$$

$$J_i = \epsilon_i \sigma T_i^4 + \rho_i \sum_{k=1}^M F_{ik} J_k \quad 4-6$$

or

$$(q_r)_i = A_i \epsilon_i \sigma T_i^4 - A_i \rho_i \sum_{k=1}^M F_{ik} J_k \quad 4-7$$

The difference between the two methods for radiation calculations becomes apparent by examining the above equations. At each time interval, the network method requires a new solution of the radiation problem; the "script F" technique requires the radiation problem to be solved once to determine the values of \bar{F}_{ik} . The determination of \bar{F}_{ik} does not need to be repeated unless the properties are changed. It should be noted that if the problem is not transient and no conduction is involved, neither method has any computational advantage over the other.

The procedure for obtaining the "script F" values for a given enclosure can be that described by Hottel (1) or from the network method (6). In both methods of securing \bar{F}_{ij} , one matrix inversion is required; if the two matrices are compared (see References 1 and 6), they differ only by the use of the areas of the surfaces in the diagonal of Hottel's matrix; i.e., no computational or accuracy advantage.

The inversion process and the time interval increments used in Equation 4-2 provides a quantitative means for determining the "cost" of solving Equation 4-2 by the radiosity method. A matrix of the coefficients of the various J's must be inverted once at the start of the entire problem and can be used again with the values of temperature obtained at subsequent times. Hottel's method for calculating "script F" requires a similar matrix inversion. In each case, after the matrix inversion, secondary calculations are required to determine the various \bar{F}_{ij} or the new radiosities. However, with "script F," this does not have to be repeated at each time interval. Hence, for N time intervals and M surface enclosure, the number of calculations using radiosities is:

$$NM^2 + \text{the matrix inversion}$$

The reciprocity relationship $A_i \bar{F}_{ij} = A_j \bar{F}_{ji}$ can be used in conjunction with the method given by Reference 6 to obtain \bar{F}_{ij} in a time corresponding to that given for the network method of:

$$1/2 (M)(M+1) + \text{the matrix inversion}$$

Consequently, the "script F" method is significantly more economical than the network method.

Contrails

The steady state case is also more readily solved by the "script F" method when radiation and conduction are both present. Equation 4-1 for the steady state case can be written with the aid of Equation 4-3 as:

$$T_i = T_i (1-\eta) + \eta \left[\frac{(q_x)_i + (q_r)_i + \sum_{k=1}^M \frac{T_k}{R_{ki}}}{\sum_{k=1}^M \frac{1}{R_{ki}}} \right] \quad 4-8$$

where η represents the convergence factor; i.e., $\eta \rightarrow 0$ with convergence. Equation 4-8 must be solved for all surfaces i , e.g., by iteration. If, for each iteration, a new solution for the values of $(q_r)_i$ is required, the number of calculations required is identical to the time interval problem. If however, $(q_r)_i$ is represented by Equation 4-4, the iteration process is independent of recalculation of the radiation problem.

This discussion of the relative merits of the network method and the "script F" method is not based upon the assumptions inherent in either procedure. Another technique based on less restrictive assumptions will be described in Section 4.2. It can be used in either a network or a "script F" form, and the same arguments will hold relative to the method of solution to be used.

The accuracy of any method can be separated into two parts. The first is that inherent in the assumptions; e.g., specular versus diffuse properties. The second part is the accuracy of computation. The assumptions of the analysis is the dominant factor in determining the degree to which a method approximates a real system.

4.1 COMPARISON OF THE ANALYTICAL METHODS OF HOTTEL (1), GEEHART (2), AND OPPENHEIM (3) FOR CALCULATION OF RADIATION HEAT TRANSFER

The calculation of radiation heat transfer is generally based upon several simplifying assumptions:

- (1) The thermal radiation properties of all surfaces involved in the heat transfer are diffuse (independent of angle), grey (independent of wavelength), not dependent upon temperature, and surfaces are opaque.
- (2) An "enclosure" can be constructed which contains and/or bounds all of the surfaces involved in the radiation exchange such that all radiation emitted and/or reflected from any one surface is reflected and/or absorbed by the other surfaces.
- (3) Any single surface used in the calculations is isothermal and uniformly irradiated; this may necessitate the subdivision of a large natural surface into several parts in order to approach this condition.
- (4) No effects occur as a result of polarization, diffraction or fluorescence.

Contrails

Three different methods of viewing the solution of this radiation exchange problem are available. These are generally known as the "script F" method (Hottel), Gebhart's method, and the network (Oppenheim). Intuitively, these methods must be identical since they are based upon the same physical assumptions and the conservation of energy. However, it is important that this equivalence be demonstrated. Sparrow (7) has recently shown this by developing the methods of Hottel and Gebhart from the network method. Since the "script F" method has been advocated as a more useful approach in complex transient radiation exchange, the "script F" method will be used here as the method of comparison.

Hottel's method is based upon the superposition of the radiant exchange within an enclosure. To do this, he assumed all of the surfaces except one within the enclosure to be at zero temperature; the remaining surface has an emission rate of unity, i.e., $\sigma T_i^4 = 1$. He then considers the quantity ${}_iR_j$, the power per unit area leaving surface j as a result of the power emitted by surface i; for surface i, the radiation leaving is $\epsilon_i + {}_iR_i$. The exchange between surfaces i and j are expressed as

$$Q_{ij} = A_i \bar{\bar{U}}_{ij} \sigma (T_i^4 - T_j^4) \quad 4-9$$

where the reciprocity relation has been used, i.e., $A_i \bar{\bar{U}}_{ij} = A_j \bar{\bar{U}}_{ji}$. The quantity ${}_iR_j$ is related to $\bar{\bar{U}}_{ij}$ by:

$$A_i \bar{\bar{U}}_{ij} = {}_iR_j A_j \left(\frac{\epsilon_j}{\rho_j} \right) \quad 4-10$$

Thus, the incident power per unit area (${}_iR_j/\rho_j$) is absorbed in the fraction ϵ_j . This absorbed power is a result of an emission from surface i of unity and must be increased by the factor σT_i^4 . Correspondingly, the absorbed power of surface i from emission by surface j must be increased by σT_j^4 . The "script F" is, therefore, a quantity which collects the interreflections within the enclosure and provides a measure of the radiant interchange between two surfaces by direct and reflected (from all surfaces) exchange.

The irradiation of surface j by surface i (${}_iR_j/\rho_j$) can be expressed for an M surface enclosure ($\sigma T_i^4 = 1$) as:

$$\frac{{}_iR_j}{\rho_j} = F_{ji} \epsilon_i + \sum_{k=1}^M F_{jk} {}_iR_k \quad 4-11$$

Contrails

Multiplying through by $\epsilon_j A_j / A_i$ gives

$$\frac{A_j \epsilon_j i R_j}{A_i \rho_j} = \frac{A_j F_{ji} \epsilon_i \epsilon_j}{A_i} + \sum_{k=1}^M \frac{\epsilon_j A_j F_{jk} i R_k}{A_i} \left(\frac{\rho_k}{\epsilon_k} \right) \left(\frac{\epsilon_k}{\epsilon_k} \right) \quad 4-12$$

With Equation 4-10 and noting $A_i F_{ij} = A_j F_{ji}$, this gives

$$\bar{U}_{ij} = \epsilon_i \epsilon_j F_{ij} + \sum_{k=1}^M (\epsilon_j F_{kj}) \frac{\rho_k}{\epsilon_k} \frac{A_k}{A_i} \frac{\epsilon_k}{\rho_k} i R_k$$

or

$$\bar{U}_{ij} = \epsilon_i \epsilon_j F_{ij} + \sum_{k=1}^M \epsilon_j F_{kj} \frac{\rho_k}{\epsilon_k} \bar{U}_{ik} \quad 4-13$$

Equation 4-13 will be developed by the network method in order to indicate the equivalence of the two techniques.

The Gebhart method is a variation of the "script F" phrased in different language. Gebhart utilized a quantity B_{ij} to represent the effects of interreflections within the enclosure. B_{ij} is the fraction of radiation emitted by surface i which is absorbed by surface j . The heat loss of a surface was expressed by Gebhart as:

$$q_j = \epsilon_j A_j \sigma T_j^4 - \sum_{i=1}^M B_{ij} \epsilon_i A_i \sigma T_i^4 \quad 4-14a$$

or

$$q_j = \epsilon_j A_j \sigma T_j^4 - \sum_{i=1}^M q_{ij} \quad 4-14b$$

The corresponding expression for Hottel's method is:

$$q_j = \sum_{i \neq j}^M A_j \bar{U}_{ji} \sigma T_j^4 - \sum_{i \neq j}^M A_i \bar{U}_{ij} \sigma T_i^4 \quad 4-15$$

The first term of Equation 4-15 simplifies by noting the total radiation leaving surface j is $\epsilon_j \sigma T_j^4$, i.e., $T_i = 0$

$$\sum_{i \neq j}^M \sigma T_j^4 \bar{U}_{ji} = \epsilon_j \sigma T_j^4 - \bar{U}_{jj} \sigma T_j^4$$

or

$$\sum_{i=1}^M \bar{U}_{ji} = \epsilon_j \quad 4-16$$

Equations 4-14 and 4-15 must represent the same net heat loss by surface j. Equating these two relations gives:

$$\sum_{i=1}^M A_i \bar{U}_{ij} \sigma T_i^4 = \sum_{i=1}^M B_{ij} \epsilon_i A_i \sigma T_i^4$$

This can only be true if:

$$\bar{U}_{ij} = \epsilon_i B_{ij} \quad 4-17$$

Consequently, Gebhart's B_{ij} is equal to Hottel's \bar{r}_{ij} divided by ϵ_i .

The equations representing the network method of solution utilize the radiosity* of a surface. The radiosity of a surface can be expressed as:

$$J_i = \epsilon_i \sigma T_i^4 + \sum_{k=1}^M \rho_i F_{ik} J_k \quad 4-18$$

The net heat flux leaving a surface is:

$$q_i = A_i \frac{\epsilon_i}{\rho_i} \left(\sigma T_i^4 - J_i \right) \quad 4-19$$

This can also be written as (since $\epsilon_i + \rho_i = 1$):

$$q_i = A_i J_i - A_i \sum_{k=1}^M F_{ik} J_k \quad 4-20$$

Now consider the case of an enclosure with all surfaces at zero temperature except surface i which has $\sigma T_i^4 = 1$.

$$J_j = \rho_j \sum_{k=1}^M F_{jk} J_k \quad 4-21$$

$$q_j = q_{ij} = A_j J_j - A_j \sum_{k=1}^M F_{jk} J_k \quad 4-22$$

or

$$q_{ij} = A_j J_j \left(1 - \frac{1}{\rho_j} \right) = - \left(\frac{\epsilon_j}{\rho_j} \right) A_j J_j \quad 4-23$$

*Radiosity is the sum of the emitted and reflected radiant power from a surface.

But by Equation 4-9 for the assumed constraints on surface temperatures

$$q_{ij} = -A_i \bar{u}_{ij} = -A_j \bar{u}_{ji}$$

Hence

$$\bar{u}_{ji} = \left(\frac{\epsilon_j}{\rho_j} \right) J_j \quad 4-24$$

Substitution of Equation 4-24 into Equation 4-20 yields

$$\bar{u}_{ij} = \epsilon_i \epsilon_j F_{ij} + \sum_{k=1}^M \epsilon_j F_{kj} \left(\frac{\rho_k}{\epsilon_k} \right) \bar{u}_{ik} \quad 4-25$$

This is identical to Equation 4-13.

SUMMARY

The method of Gebhart has been shown to be directly convertible to the "script F" of Hottel by the use of Equation 4-17. Similarly the network method has been shown to yield an expression for \bar{u}_{ij} identical to that obtained from Hottel's method (Equation 4-13 and 4-25). Therefore, there is no difference in the methods and by algebraic manipulation, one method can be expressed in the terms of either of the other two.

4.2 IMPROVED METHOD OF RADIATION ANALYSIS

The available methods for radiation heat transfer analysis have been restricted by the assumptions given in Section 4.1. Recently, a review of the problem has been made and a procedure is now available for eliminating the restriction to nondirectional diffuse properties (4). The use of non-grey thermal radiation properties can be used in the manner described by Bevans and Dunkle (8). Perfectly specular properties can be treated by the method of Eckert and Sparrow (9) but the properties must be considered to be nondirectional. The case of polarization can also be treated (10) but the practicality is limited to a few cases. The most practical new technique is believed to be that given by the second approximation described in Reference 4. The following discussion will describe the adaptation of this method to development of a "script F."

The second approximation of Reference 4 considers surfaces which have directionality and components of reflection which are diffuse and specular. The expression for the heat transfer to a surface within an enclosure under the assumptions of wavelength independent properties is: *

* This later restriction can be easily removed but is not pertinent to the ensuing discussion.

Contrails

$$\begin{aligned}
 q_k &= A_k \bar{\epsilon}_k \sigma_k^T \epsilon_k^4 - \sum_{j=1}^M A_k \alpha_{kj} F_{kj} \epsilon_{jk} \sigma_j^T \epsilon_j^4 \\
 &\quad - \sum_{j=1}^M \sum_{i=1}^M A_k \alpha_{kj} \rho_{ijk} \epsilon_{ij} F_{kj} F_{ji} \sigma_i^T \epsilon_i^4 \\
 &\quad - \pi \sum_{j=1}^M \sum_{i=1}^M A_k \alpha_{kj} \rho_{ijk} \rho_{ij} F_{kj} F_{ji} D_i
 \end{aligned}
 \tag{4-26}$$

This can be written as:

$$\begin{aligned}
 q_k &= A_k \bar{\epsilon}_k \sigma_k^T \epsilon_k^4 - \sum_{i=1}^M \sum_{j=1}^M A_k \alpha_{ki} (\epsilon_{ik} F_{ki} + \rho_{ijk} \epsilon_{ij} F_{kj} F_{ji}) \sigma_i^T \epsilon_i^4 \\
 &\quad - \pi \sum_{i=1}^M \sum_{j=1}^M A_k \alpha_{kj} \rho_{ijk} \rho_{ij} F_{kj} F_{ji} D_i
 \end{aligned}
 \tag{4-27}$$

In matrix notation this becomes:

$$\begin{aligned}
 \begin{bmatrix} q_1 \\ q_2 \\ \vdots \\ q_M \end{bmatrix} &= \begin{bmatrix} \epsilon_1 \sigma_1^T \epsilon_1^4 \\ \epsilon_2 \sigma_2^T \epsilon_2^4 \\ \vdots \\ \epsilon_M \sigma_M^T \epsilon_M^4 \end{bmatrix} + \begin{bmatrix} a_{11} & a_{12} & \dots & a_{1M} \\ a_{21} & a_{22} & \dots & a_{2M} \\ \vdots & \vdots & \ddots & \vdots \\ a_{M1} & a_{M2} & \dots & a_{MM} \end{bmatrix} \begin{bmatrix} \sigma_1^T \epsilon_1^4 \\ \sigma_2^T \epsilon_2^4 \\ \vdots \\ \sigma_M^T \epsilon_M^4 \end{bmatrix} \\
 &\quad - \begin{bmatrix} b_{11} & b_{12} & \dots & b_{1M} \\ b_{21} & b_{22} & \dots & b_{2M} \\ \vdots & \vdots & \ddots & \vdots \\ b_{M1} & b_{M2} & \dots & b_{MM} \end{bmatrix} \begin{bmatrix} D_1 \\ D_2 \\ \vdots \\ D_M \end{bmatrix}
 \end{aligned}
 \tag{4-28}$$

where

$$a_{xy} = - (A_x \alpha_{xy} \epsilon_{yx} F_{xy} + \sum_{z=1}^M A_x \alpha_{xy} \rho_{yzx} \epsilon_{yz} F_{xz} F_{zy})
 \tag{4-29}$$

$$b_{xy} = - \sum_{z=1}^M A_x \alpha_{xz} \rho_{yzx} F_{xz} F_{zy} \rho_{xz}
 \tag{4-30}$$

Contrails

The quantity D_k is given by:

$$\begin{aligned}
 D_k = & \frac{1}{\pi} \sum_{j=1}^M \epsilon_{jk} \sigma_{Tj}^4 F_{kj} + \frac{1}{\pi} \sum_{j=1}^M \sum_{i=1}^M \rho_{ijk} \epsilon_{ij} F_{kj} F_{ji} \sigma_{Ti}^4 \\
 & + \sum_{j=1}^M \sum_{i=1}^M \rho_{ijk} \rho_{ij} F_{kj} F_{ji} D_i
 \end{aligned} \tag{4-31}$$

In matrix notation, these equations can be written:

$$\begin{bmatrix} d_{11} & d_{12} & \dots & d_{1M} \\ d_{21} & d_{22} & \dots & \dots \\ \cdot & & \cdot & \\ \cdot & & \cdot & \\ \cdot & & \cdot & \\ d_{M1} & d_{M2} & \dots & d_{MM} \end{bmatrix} \begin{bmatrix} D_1 \\ D_2 \\ \cdot \\ \cdot \\ \cdot \\ D_M \end{bmatrix} = \begin{bmatrix} c_{11} & c_{12} & \dots & c_{1M} \\ c_{21} & c_{22} & \dots & c_{2M} \\ \cdot & & \cdot & \\ \cdot & & \cdot & \\ \cdot & & \cdot & \\ c_{M1} & c_{M2} & \dots & c_{MM} \end{bmatrix} \begin{bmatrix} \sigma_{T1}^4 \\ \sigma_{T2}^4 \\ \cdot \\ \cdot \\ \cdot \\ \sigma_{TM}^4 \end{bmatrix} \tag{4-32}$$

where

$$d_{xy} = \begin{cases} \sum_{z=1}^M \rho_{yzx} \rho_{yz} F_{xz} F_{zy} & (x \neq y) \\ 1 - \sum_{z=1}^M \rho_{xzx} \rho_{xz} F_{xz} F_{zx} & (x = y) \end{cases} \tag{4-33}$$

$$c_{xy} = \frac{1}{\pi} \epsilon_{yx} F_{xy} + \sum_{z=1}^M \rho_{yzx} \epsilon_{yz} F_{xz} F_{zy} \tag{4-34}$$

If Equation 4-32 is now solved for the quantities D, we have

$$\{D\} = [d]^{-1} [c] \{\sigma_{T^4}\} \tag{4-35*}$$

* The notation [] has been introduced to denote a square matrix, e.g., the d or c matrix of Equation 4-32; the { } denotes a column matrix such as the D or σ_{T^4} matrix of Equation 4-32; and []⁻¹ is the inverse of the indicated matrix

Contrails

Solution of Equation 4-35 yields the various D_k 's required in Equation 4-28. Equation 4-28 can then be expressed as:

$$\{q\} = \{\epsilon\sigma T^4\} + [a] \{\sigma T^4\} + [b] \{D\} \quad 4-36$$

A directional diffuse-specular "script F" can be obtained with Equations 4-35 and 4-36. Using Hottel's concept of a "script F," i.e., set all temperatures except one within the enclosure equal to zero and the remaining one equal to unity (say surface k), the heat flows (q) are then q_{kj} . With this condition:

$$\{q_{kj}\} = \{\epsilon_k^0\} + \{a_{jk}\} + [b] \{D_{jk}\} \quad 4-37^*$$

and

$$\{D_{kj}\} = [d]^{-1} \{c_{jk}\} \quad 4-38^*$$

The solution then proceeds as follows:

- (1) An index k is selected and the pertinent coefficients c_{kj} selected.
- (2) D_{jk} is computed for all j by Equation 4-38.
- (3) The values of a_{jk} are selected and the values of q_{kj} for all j are computed with Equation 4-37.
- (4) \bar{u}_{kj} is then computed with the definition:

$$\bar{u}_{jk} = \frac{q_{kj}}{A_j} \quad 4-39$$

- (5) The next value of k is selected, and the calculation continues until all M surfaces have been computed. The reciprocity relationship $A_j \bar{u}_{jk} = A_k \bar{u}_{kj}$ is used to reduce the number of computations.
- (6) \bar{u}_{jk} is used in the same manner as with Hottel's method and the solution of Equation 4-2 or 4-8.

*

$$\{q_{kj}\} = \begin{bmatrix} q_{k1} \\ q_{k2} \\ \vdots \\ q_{kM} \end{bmatrix} ; \{\epsilon_k^0\} = \begin{bmatrix} 0 \\ 0 \\ \vdots \\ \epsilon_k \\ \vdots \\ 0 \end{bmatrix} ; \{a_{jk}\} = \begin{bmatrix} a_{1k} \\ a_{2k} \\ \vdots \\ a_{Mk} \end{bmatrix} ; \{c_{jk}\} = \begin{bmatrix} c_{1k} \\ c_{2k} \\ \vdots \\ c_{Mk} \end{bmatrix}$$

Contrails

The equations presented in this section may appear to be more complicated and hence, more difficult than with the diffuse property assumption. Mathematically, this is not the case. The computations are more time consuming and require added computer time and storage space. This is only the penalty paid for more exact computations.

5. COMPUTER PROGRAM FOR DIRECTIONAL SPECULAR-DIFFUSE METHOD

The procedural steps required to calculate a "script F" (\bar{F}) from the equations for the directional specular-diffuse analysis have been described in Section 4.2. This method has been programmed for an IBM 7094 as a program separate from any general program for thermal analysis. The technical basis for selecting the \bar{F} procedure rather than the network approach have been discussed in the first portion of Section 4. For the reasons given there, most computer programs for thermal analysis have been written in terms of \bar{F} . Thus, the existing analysis programs could incorporate a directional specular-diffuse \bar{F} as an input quantity with a minimum of alteration. Furthermore, the directional specular-diffuse \bar{F} requires a much larger working computer storage than a diffuse \bar{F} . If an attempt was made to assemble a single \bar{F} and analysis program, the number of surfaces would have been seriously limited. It is for these technical and practical reasons that the \bar{F} calculation was programmed as a separate entity. The flow chart of the program is shown in Figure 8 and a complete printout in Appendix III. The symbols used are those of Section 4.2.

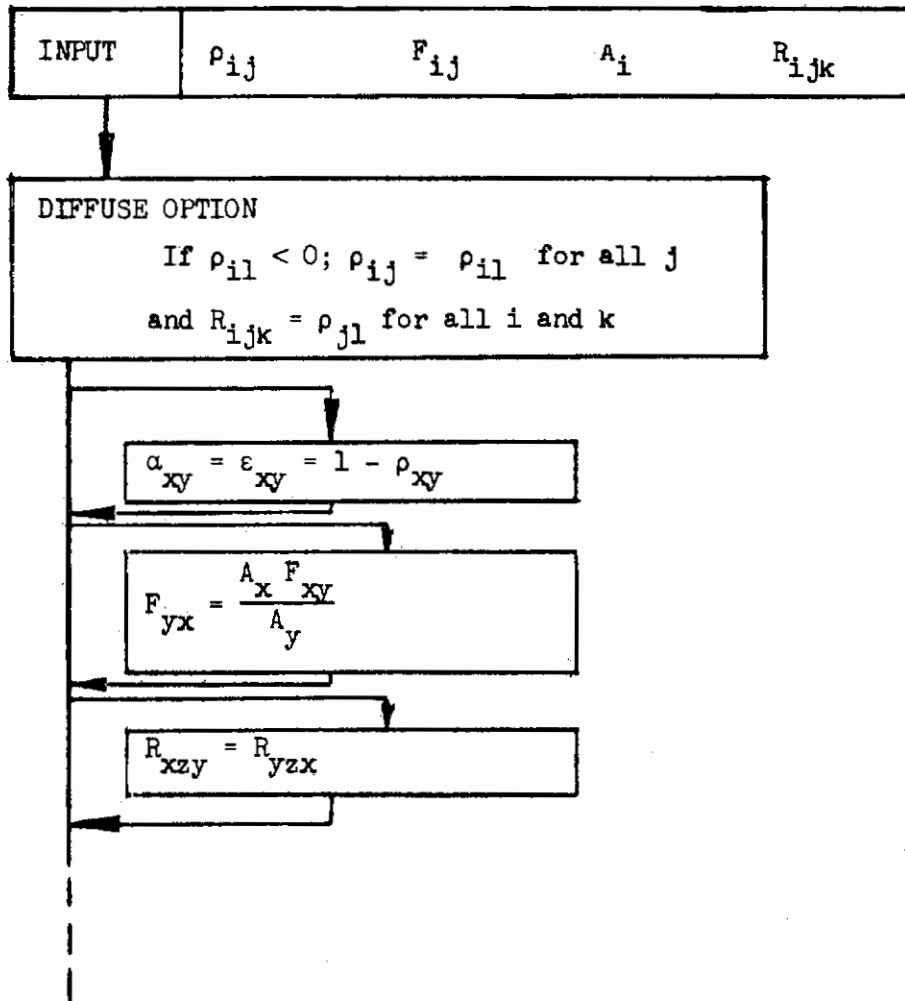
5.1 REQUIRED INPUT DATA

The physical factors which are required for the directional specular-diffuse \bar{F} are:

- (a) the areas of the surfaces involved ($A_i, i = 1, 2, 3 \dots$)
- (b) the number of surfaces used to subdivide the enclosure ($N; N \leq 20$)
- (c) the directional reflectance of surface i in the direction of surface j (ρ_{ij} of Reference 4; designated $RH\phi$ in machine language)
- (d) the geometrical bidirectional reflectance of surface j for radiation from surface i which is reflected to surface k by surface j (ρ_{ijk} of Reference 4; designated R_{ijk} in machine language)
- (e) the geometrical diffuse shape factors between surfaces (F_{ij})

The only quantities which are not used in conventional diffuse \bar{F} analysis are ρ_{ij} ($RH\phi$) and ρ_{ijk} (R_{ijk}). The use of the usual diffuse shape factors (F_{ij}) is made possible by assigning the deviations from diffuseness to the reflectances. This is described in greater detail in Reference 4 and leads to the concept of geometrical reflectances, i.e., a property which is weighted by the geometry and nondiffuseness of the surface. The directional emittance of a surface is incorporated in the program as: $1 - \rho_{ij}$. This introduces the gray radiation assumption, i.e., properties independent of wavelength. If desired, either a band energy or monochromatic analysis could be performed (see Reference 4).

Contrails



Continued on next page.

Figure 8. Computer Program Flow Chart

Contrails

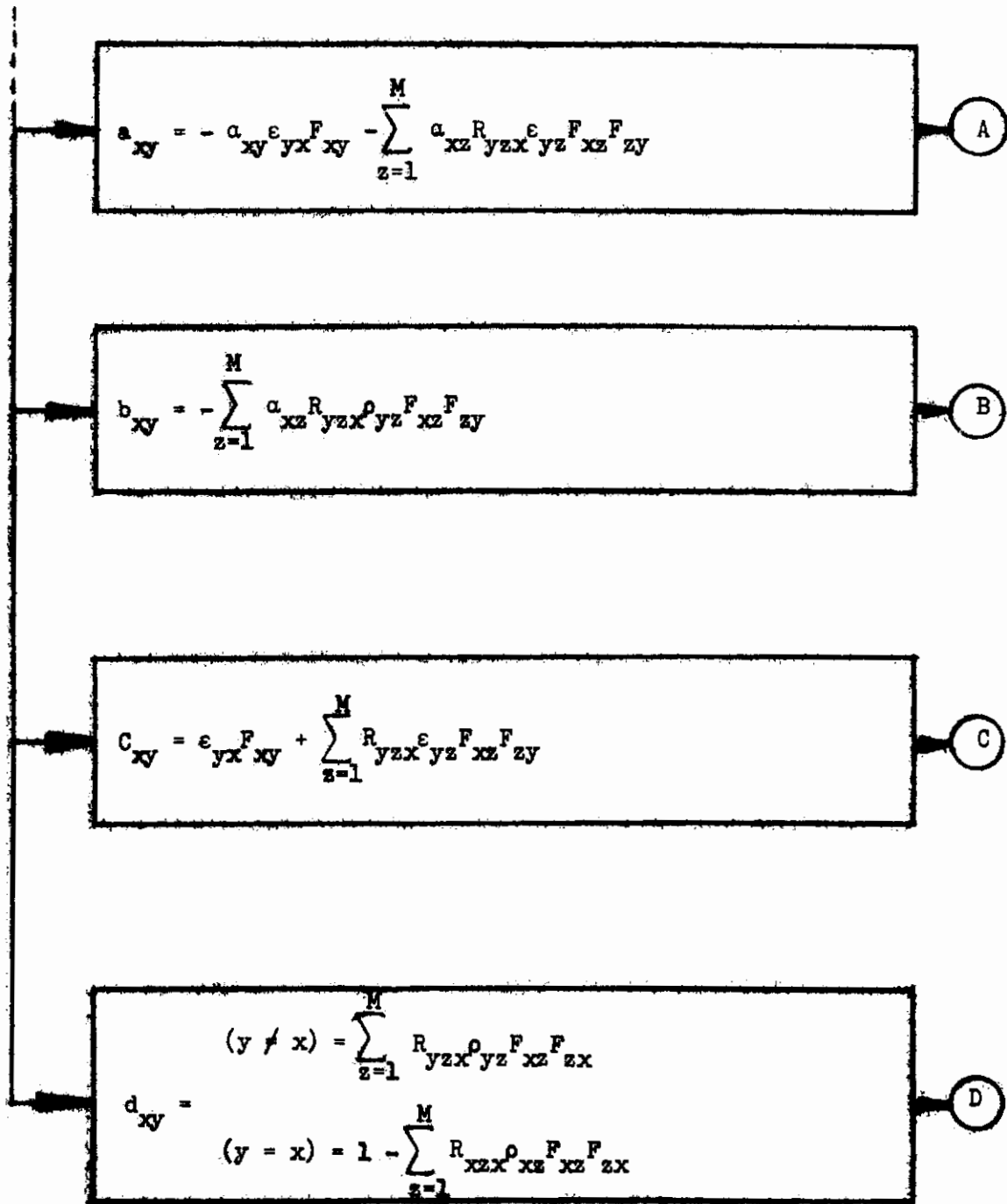


Figure 8. Computer Program Flow Chart (Cont.)

Contrails

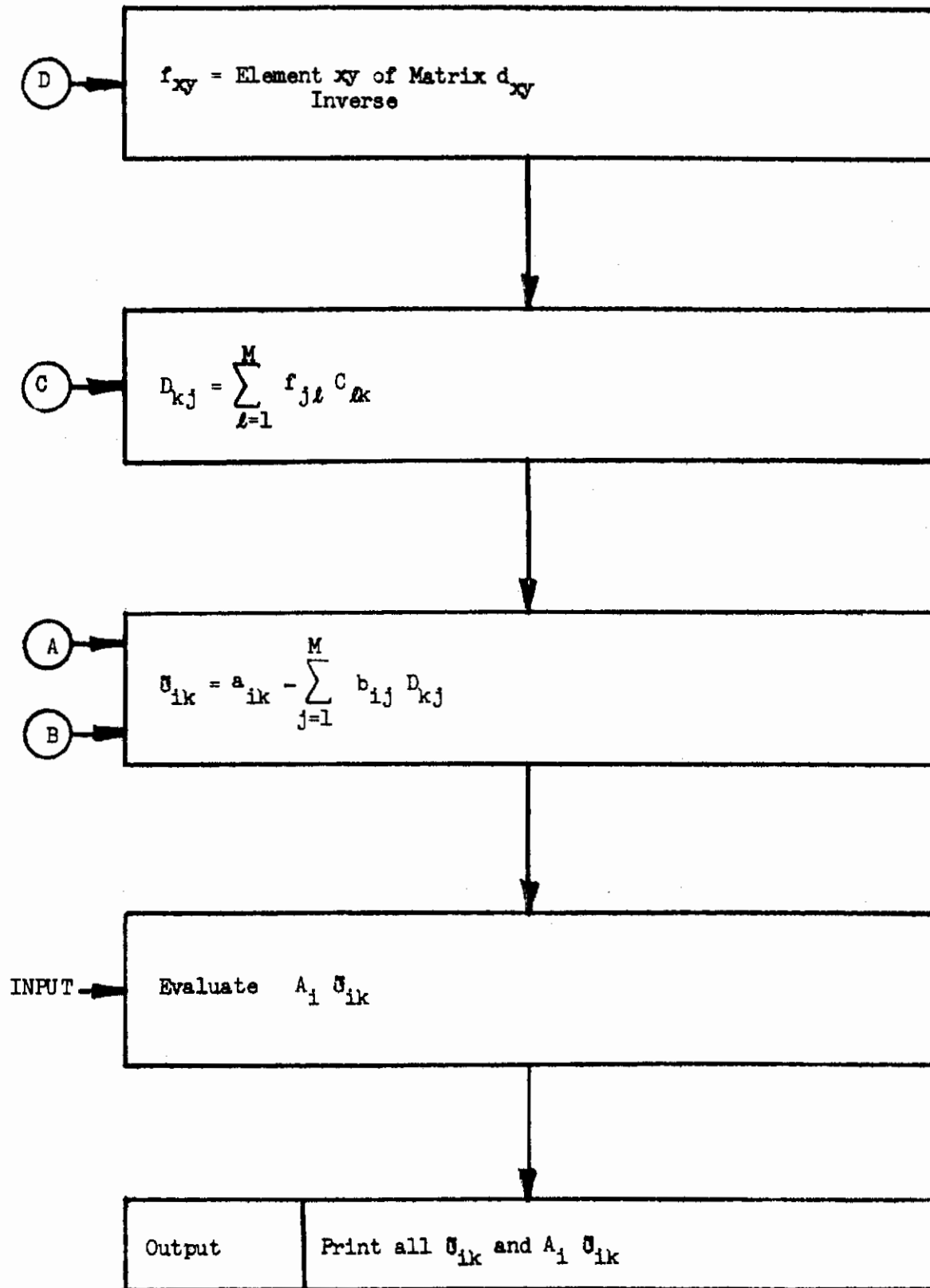


Figure 8. Computer Program Flow Chart (Cont.)

Contrails

Values of ρ_{ij} and ρ_{ijk} ($RH\phi$ and R_{ijk}) can be approximated with data obtained in many Thermophysics Laboratories (4). The methods suggested for this approximation will be illustrated in Section 5.3 and 6.2

5.2 INPUT PROCEDURE

The input format is shown in Figure 9. The quantities indicated are as follows:

- N = the number of surfaces within the enclosure to be examined.
The present program is storage limited to a maximum of 20 surfaces.
- CLR = a flag directing the program to clear itself of input information ($CLR = 1$), prior to proceeding to the next case, or instructing the program to retain input information ($CLR = 0$) for the following case. When CLR is set to zero, only those quantities that vary from case to case need be entered, all other information will be retained.
- L = a flag used in the column labeled "PRE" of the load sheet. The quantity L is used in conjunction with $CLR = 0$. An input matrix is not cleared of information if the quantity L is inserted in the column labeled "PRE."
- M = a flag used in the column labeled "PRE" of the load sheet. It instructs the program to clear the input matrix of information prior to storing data.
- ρ_{ij} = $RH\phi$ = the directional reflectivity of surface i in the direction of surface j . For program convenience, ρ_{i1} is set equal to the negative value of the hemispherical reflectance for a diffuse surface.
- F_{ij} = F = the shape factor of surface j as viewed by surface i . Only the lower triangular half of the shape factor matrix need be entered; that is: $F_{11}, F_{21}, F_{22}, F_{31}, F_{32}, F_{33}, \dots, F_{mn}$.
- R_{ijk} = Geometrical bidirectional reflectance of surface j for incident energy from surface i and reflected to surface k . Bidirectional reflectivities are inputted in block form as indicated by the sample load sheet. The block number corresponds to the third subscript k , and the other two subscripts are contained within the k 'th block. Only the upper triangular portion of the three dimensional R_{ijk} matrix need be entered. That is, R_{1j1} for $j = 1$ to n is entered for the first matrix, $K = 1$; R_{1j2} R_{2j2} , for $j = 1$ to n is entered for the second matrix, $K = 2$; $R_{1j3}, R_{2j3}, R_{3j3}$ for $j = 1$ to n is entered for the third matrix, $K = 3$; and so on until the full matrix is entered for $K = n$.
- A_i = A = surface area of node i .

Contrails

DATE _____		PAGE _____	OF _____
NAME _____		PRIORITY _____	
PROBLEM NO. _____		KEYPUNCHED BY _____	
NO. OF CARDS _____		VERIFIED BY _____	

1	7		73
H1	HEADERS - LIMITED TO 66 LINES EACH - USED		
H2	AS RUN DESCRIPTION ONLY		

IX

SYMBOL	1 2		7	17
	P	E		
		N		
		CLR		
	M	RH0	20, 20	
		01, 01		
		.		
		.		
		.		
		.		
	M	F	20, 20	
		01, 01		
		.		
		.		
		.		
	M	R1	20, 20	
		.		
		.		
		.		
	M	R2	20, 20	
		.		
		.		
		.		
	M	R3	20, 20	
		.		
		.		
		.		
	M	RN	20, 20	
		.		
		.		
		.		

IX

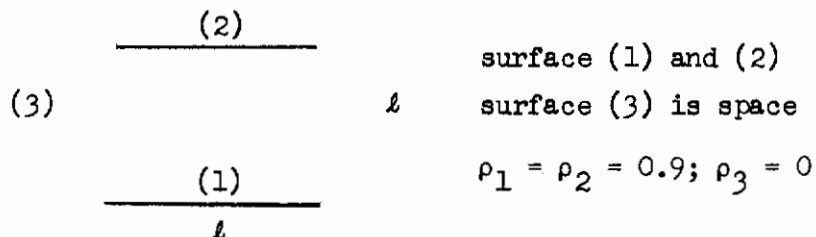
SYMBOL	1 2		7	17
	P	E		
		AREA		
		1		
		2		
		3		
		.		
		.		
		.		
		.		
		N		
		E ND		

Figure 9. Program Input Format

Contrails

An unlimited number of cases may be "stacked"; all that is required to run several cases together is an END card between cases. Output quantities \bar{U} and \bar{U} -area products, are printed out in matrix form.*

The following is a very simple problem which illustrates the input loading. Consider two infinite diffuse strips of unit width and separation, as shown below:



Input information:

(a) $\rho_{12} = \rho_{13} = \rho_{21} = \rho_{23} = 0.9$

$\rho_{31} = \rho_{32} = \rho_{33} = 0$

(b) $F_{12} = F_{21} = F_{33} = 0.414214$

$F_{13} = F_{23} = 0.585786$

(c) $R_{213} = R_{312} = R_{313} = R_{212} = \rho_1 = 0.9$

$R_{123} = R_{321} = R_{323} = R_{121} = \rho_2 = 0.9$

(d) $A_1 = A_2 = 1.0, A_3 = 2.0$

The load sheet for the above problem with diffuse surfaces can be found in Figure 10. The result of this computation is 0.0933965, which can be compared to the value given by Reference 9 of 0.09340.

It should be noted that in addition to comparing very favorably with the \bar{U} matrix evaluated by hand, using Hottel's techniques, the following holds

$$\bar{a}_k = \sum_{j=1}^M \bar{U}_{kj} = \text{hemispherical emittance}$$

as it should.

* It should be noted that all quantities should be left justified within their respective fields.

DATE _____ PAGE _____ OF _____
 NAME _____ PRIORITY _____
 PROBLEM NO. _____ KEYPUNCHED BY _____
 NO. OF CARDS _____ VERIFIED BY _____

1	7		73
H1	SAMPLE PROBLEM TWO PARALLEL INFINITE		
H2	DIFFUSE STRIPS OF UNIT WIDTH AND SEPARATION		
			IX

	<table border="1" style="width: 100%; border-collapse: collapse;"> <tr><td style="text-align: center;">1</td><td style="text-align: center;">2</td><td style="text-align: center;">7</td></tr> <tr><td style="text-align: center;">19</td><td style="text-align: center;">20</td><td style="text-align: center;">28</td></tr> <tr><td style="text-align: center;">37</td><td style="text-align: center;">38</td><td style="text-align: center;">43</td></tr> <tr><td style="text-align: center;">55</td><td style="text-align: center;">58</td><td style="text-align: center;">61</td></tr> </table>	1	2	7	19	20	28	37	38	43	55	58	61	LOC.	VALUE	<table border="1" style="width: 100%; border-collapse: collapse;"> <tr><td style="text-align: center;">17</td><td style="text-align: center;">38</td></tr> <tr><td style="text-align: center;">83</td><td style="text-align: center;">71</td></tr> </table>	17	38	83	71
1	2	7																		
19	20	28																		
37	38	43																		
55	58	61																		
17	38																			
83	71																			
SYMBOL	P R E	LOC.	VALUE	EXP.																
		N	3																	
		CLR	1																	
	M	RHØ	20, 20																	
		01, 01	-0.9																	
		02, 01	-0.9																	
		03, 01	-0.0																	
	M	F	20, 20																	
		02, 01	0.414214																	
		03, 01	0.292893																	
		03, 02	0.292893																	
		03, 03	0.414214																	
		AREA																		
		1	1.0																	
		2	1.0																	
		3	2.0																	
		E ND																		

	<table border="1" style="width: 100%; border-collapse: collapse;"> <tr><td style="text-align: center;">1</td><td style="text-align: center;">2</td><td style="text-align: center;">7</td></tr> <tr><td style="text-align: center;">19</td><td style="text-align: center;">20</td><td style="text-align: center;">28</td></tr> <tr><td style="text-align: center;">37</td><td style="text-align: center;">38</td><td style="text-align: center;">43</td></tr> <tr><td style="text-align: center;">55</td><td style="text-align: center;">58</td><td style="text-align: center;">61</td></tr> </table>	1	2	7	19	20	28	37	38	43	55	58	61	LOC.	VALUE	<table border="1" style="width: 100%; border-collapse: collapse;"> <tr><td style="text-align: center;">17</td><td style="text-align: center;">38</td></tr> <tr><td style="text-align: center;">83</td><td style="text-align: center;">71</td></tr> </table>	17	38	83	71
1	2	7																		
19	20	28																		
37	38	43																		
55	58	61																		
17	38																			
83	71																			
SYMBOL	P R E	LOC.	VALUE	EXP.																

IX

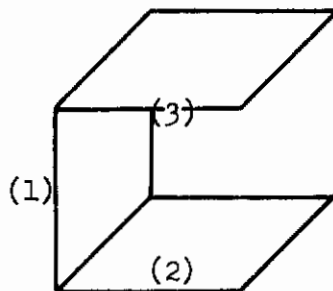
Figure 10. Load Sheet for Two Parallel Infinite Diffuse Strips of Unit Width and Separation

5.3 EXAMPLES OF INPUT FOR DIFFUSE, SPECULAR, AND SPECULAR-DIFFUSE

The following problem has been selected to illustrate the input required for the three cases of diffuse, specular and directional specular-diffuse. The \bar{U} computer program given here can treat these cases by manipulation of the quantity R_{ijk} (ρ_{ijk}). As discussed in Reference 4, this factor is approximated by:

$$\rho_{ijk} = (\rho_D)_j + (\rho_S)_j \left\{ \frac{F_{jk(j)}}{F_{kj} F_{ji}} \right\} \quad 5-1$$

If the perfectly diffuse assumption is to be made, the specular reflectance of surface j (ρ_S) is set equal to zero; if the perfectly specular assumption is made, the diffuse reflectance (ρ_D) is set equal to zero. The configuration to be used to illustrate the input is shown below:



Surface 1: $\rho_1 = 0.973$ (vacuum deposited aluminum)

Surface 2 $\rho_2 = \rho_3 = 0.116$ (3M black paint)
and 3:

Surface 4: $\rho_4 = 0$ (surrounding space)

$$F_{12} = F_{21} = F_{31} = F_{32} = F_{41} = F_{43} = 0.2$$

$$F_{44} = 0.4$$

$$A_1 = A_2 = A_3 = 1$$

$$A_4 = 3$$

The diffuse assumption input sheet is shown in Figure 11.

Contrails

DATE _____ PAGE _____ OF _____

NAME _____ PRIORITY _____

PROBLEM NO. _____ KEY PUNCHED BY _____

NO. OF CARDS _____ VERIFIED BY _____

1	7		73
H1	SAMPLE PROBLEM		
H2	DIFFUSE ASSUMPTION		

1	2	7	17
19	20	28	35
37	38	43	53
58	59	61	71

SYMBOL	P R E	LOC.	VALUE	EXP.
		N	4	
		CLR	1	
M		RHØ	20, 20	
		01, 01	-0.973	
		02, 01	-0.116	
		03, 01	-0.116	
		04, 01	-0.0	
	M	F	20,20	
		01, 02	0.2	
		02, 01	0.2	
		03, 01	0.2	
		03, 02	0.2	
		04, 01	0.2	
		04, 02	0.2	
		04, 03	0.2	
		04, 04	0.4	
		AREA		
		1	1.0	
		2	1.0	
		3	1.0	
		4	3.0	
		E N D		

SYMBOL	P R E	LOC.	VALUE	EXP.

Figure 11. Load Sheet for Sample Problem; Diffuse Assumption

Contrails

The specular assumption utilizes the same data as above, but the reflection is assumed to be perfectly specular. For this condition,

$$R_{213} = \rho_{12} \left\{ \frac{F_{23(1)}}{F_{21}F_{13}} \right\}$$
$$= 2.0897$$

The quantity R_{412} is obtained by noting for R_{ijk}

$$\rho_{jk} = \sum_{i=1}^n R_{ijk} F_{ji} \quad 5-2$$

i.e., conservation of energy. Thus,

$$R_{412} = \frac{\rho_{12} - R_{312}F_{13}}{F_{14}} = 0.9323$$

Use is made of reciprocity to find $R_{312} = R_{213}$, $R_{214} = R_{412}$, and $R_{412} = R_{413}$. The load sheet for this problem is shown in Figure 12.

The directional specular-diffuse procedure requires a knowledge of the directional properties of the surfaces. The greatest angle subtended by surface 3 as viewed from surface 2 is less than 55 degrees. For the black surface, the directional reflectance and hence directional emittance is very nearly equal to the near normal value. Therefore, the near normal value was used for ρ_{23} and ρ_{32} . To obtain ρ_{21} , a heat balance was used, i.e., for the general case of surface i

$$(\rho_H)_i = \frac{1}{A_i} \sum_{j=1}^n \rho_{ij} A_j F_{ij} \quad 5-3$$

where

$$(\rho_H)_i = \text{hemispherical reflectance of surface } i.$$

The value of ρ_{21} was obtained from:

$$\rho_{21} = \frac{(\rho_H)_2 - F_{23}\rho_{23}}{4 F_{21}}$$

or

$$\rho_{21} = 0.1275$$

Contrails

DATE _____ PAGE _____ OF _____

NAME _____ PRIORITY _____

PROBLEM NO. _____ KEYPUNCHED BY _____

NO. OF CARDS _____ VERIFIED BY _____

1		7		78
	H1		SAMPLE PROBLEM	
	H2		SPECULAR ASSUMPTION	
				IX

SYMBOL	1 2		7	17
	P	R		
		N	4	
		CLR	1	
M		RH0	20, 20	
		01, 02	0.9733	
		01, 03	0.9733	
		01, 04	0.9733	
		02, 01	-0.116	
		03, 01	-0.116	
		04, 01	-0.0	
M		F	20, 20	
		01, 02	0.2	
		02, 01	0.2	
		03, 01	0.2	
		03, 02	0.2	
		04, 01	0.2	
		04, 02	0.2	
		04, 03	0.2	
		04, 04	0.4	
		AREA		
		1	1.0	
		2	1.0	
		3	1.0	
		4	3.0	
M		R1	20, 20	
		01, 02	0.116	
		01, 03	0.116	
M		R2	20, 20	
		01, 03	0.116	
		02, 03	0.116	

SYMBOL	1 2		7	17
	P	R		
M		R3	20, 20	
		01, 02	0.116	
		02, 01	2.0897	
		03, 02	0.116	
M		R4	20, 20	
		01, 02	0.116	
		01, 03	0.116	
		02, 01	0.9323	
		02, 03	0.116	
		03, 01	0.9323	
		03, 02	1.0025	
		04, 02	0.116	
		04, 03	0.116	
		END		

STL FORM 1603 REV. 12/63

IX

Figure 12. Load Sheet for Sample Problem; Specular Assumption

Contrails

Reciprocity was utilized to obtain $\rho_{21} = \rho_{12}$, $\rho_{31} = \rho_{13}$, etc. Using the procedure described for ρ_{21} , the values of the other geometrical reflectances were:

$$\rho_{12} = \rho_{13} = 0.9716$$

$$\rho_{14} = 0.9744$$

$$\rho_{23} = \rho_{32} = 0.07$$

The load sheet for this problem is shown in Figure 13. The computer results for the above configuration will be found in Section 6.

Contrails

DATE _____ PAGE _____ OF _____

NAME _____ PRIORITY _____

PROBLEM NO. _____ KEYPUNCHED BY _____

NO. OF CARDS _____ VERIFIED BY _____

1	7	H1 SAMPLE PROBLEM	78
		H2 DIRECTIONAL SPECULAR-DIFFUSE ASSUMPTION	

IX

SYMBOL	1 2		7	17
	P	R		
		N	4	
		CLR	1	
M		RH0	20, 20	
		01, 02	0.9716	
		01, 03	0.9716	
		01, 04	0.9744	
		02, 01	0.1275	
		02, 03	0.07	
		02, 04	0.1275	
		03, 01	0.1275	
		03, 02	0.07	
		03, 04	0.1275	
M		F	20, 20	
		01, 02	0.2	
		02, 01	0.2	
		03, 01	0.2	
		03, 02	0.2	
		04, 01	0.2	
		04, 02	0.2	
		04, 03	0.2	
		04, 04	0.4	
		AREA		
		1	1.0	
		2	1.0	
		3	1.0	
		4	3.0	
M		R1	20, 20	
		01, 02	0.07	
		01, 03	0.07	

IX

SYMBOL	1 2		7	17
	P	R		
M		R2	20, 20	
		01, 03	0.07	
		02, 03	0.07	
M		R3	20, 20	
		01, 02	0.07	
		02, 01	2.086	
		03, 02	0.07	
M		R4	20, 20	
		01, 02	0.1658	
		01, 03	0.1658	
		02, 01	0.924	
		02, 03	0.07	
		03, 01	0.924	
		03, 02	0.07	
		04, 01	1.008	
		04, 02	0.1338	
		04, 03	0.1338	
		END		

Figure 13. Load Sheet for Sample Problem; Directional Specular-Diffuse Assumption

6. EXPERIMENTAL COMPARISON OF SPECULAR, DIFFUSE AND DIRECTIONAL SPECULAR-DIFFUSE ANALYSES

The purpose of this task was to obtain an experimental evaluation of the different analytical methods. Such a comparison must utilize an experimental system that is simple conceptually and physically. Otherwise the effects of geometry, conduction, convections, extraneous heat losses, etc., will not be controlled. The experimental configurations chosen are shown in Figure 14. A test consisted of placing the experiment within a cold wall vacuum chamber (to eliminate convection), insulating the non-radiative surfaces, supplying a known quantity of power to one of the surfaces and measuring the equilibrium temperatures of the other surface(s). The experimental results were then compared to the predicted values using the directional specular-diffuse analysis (4), the specular property assumption and the diffuse property assumption.

The following discussion will be divided into three parts: (1) the experimental test method, (2) the analytical results, and (3) a discussion of the comparison of experiment and analysis.

6.1 EXPERIMENTAL METHOD AND PROCEDURE

The configuration selected for test are shown in Figure 14. The test surfaces were six such squares of 1100 aluminum 0.0625 inches thick. In each case the lower surface was selected as the heat source and the remaining surface(s) allowed to reach an equilibrium condition with the environment. The heated surface had a heater of approximately 200 ohms cemented to its underside (the non-radiative side). This heater consisted of 40 gage constantan wire sandwiched between two sheets of 1 mil Mylar. Voltage leads were attached at the heater boundary and the four terminal resistance method used (see Section 3.1) to calculate power dissipation. The electrical measuring circuit was the same as shown in Figure 6 of Section 3 with a Leeds and Northrup 8686 substituted for the Type K 3.

Originally, the back of each surface was insulated with 20 layers of super insulation. However, the edge heat leak was found to be too large relative to the heat absorbed by the unheated surfaces. A guard heat system was found to be necessary. This was obtained by placing a heated plate on the outside of the insulation and adjusting the dissipation until the temperature difference across the insulation was zero, i.e., no heat flow through the insulation. The edges of the insulation, guard heater, and test surface were covered with 1/4 mil thick aluminized Mylar, aluminum side out. These steps reduced the edge and back heat "leak," i.e., uncontrolled loss, to approximately 1 Btu/hr for a test surface temperature of 70°F. This was satisfactory for all test surfaces except the surface coated with vacuum deposited aluminum. The radiative heat loss or gain from such a surface was the same order of magnitude as the edge loss. Hence, this test surface had to be used as a passive surface, i.e., a reflector, and no heat balance could be performed for it.

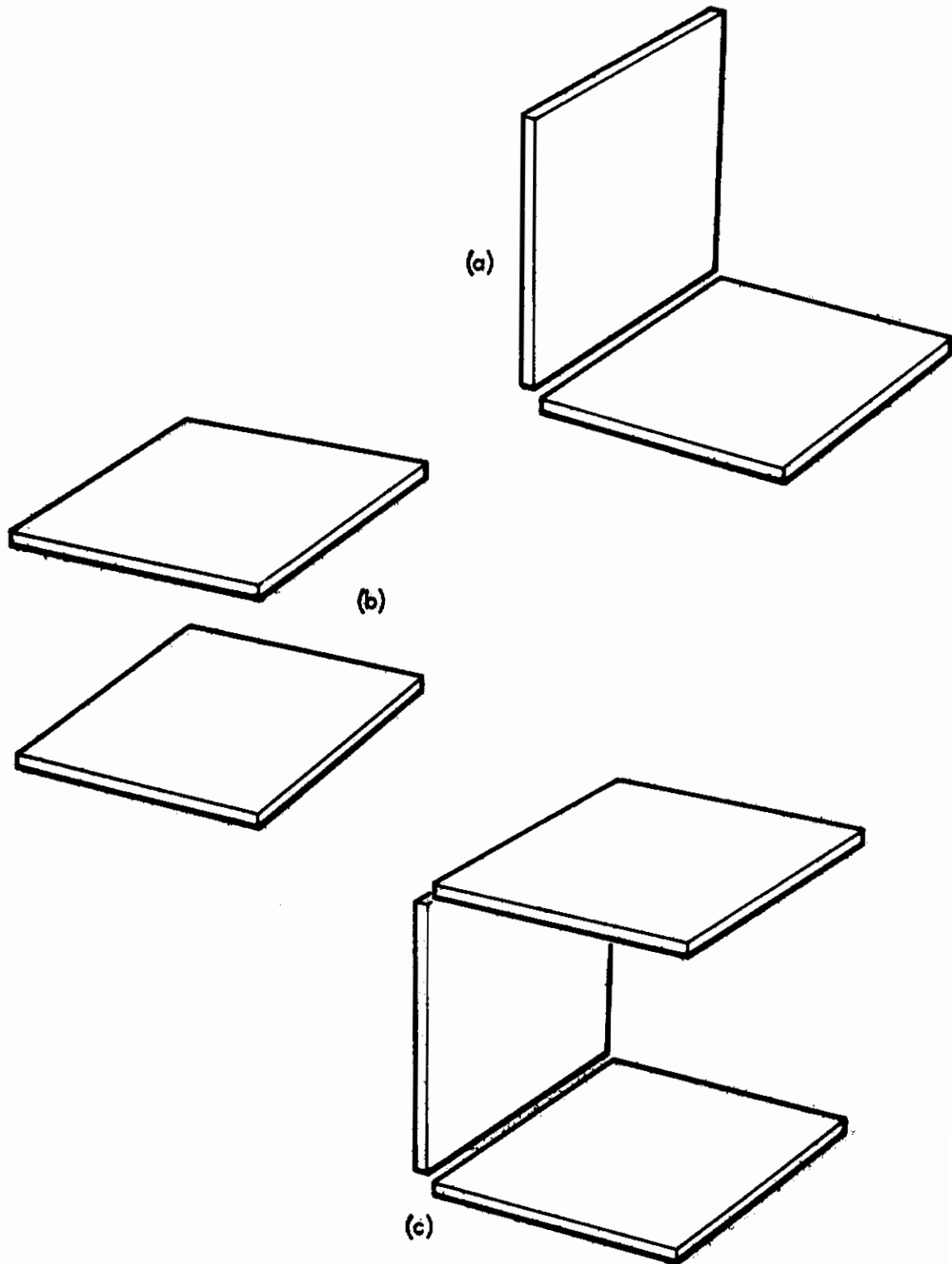


Figure 14. Configuration Used for Test of Radiation Analysis

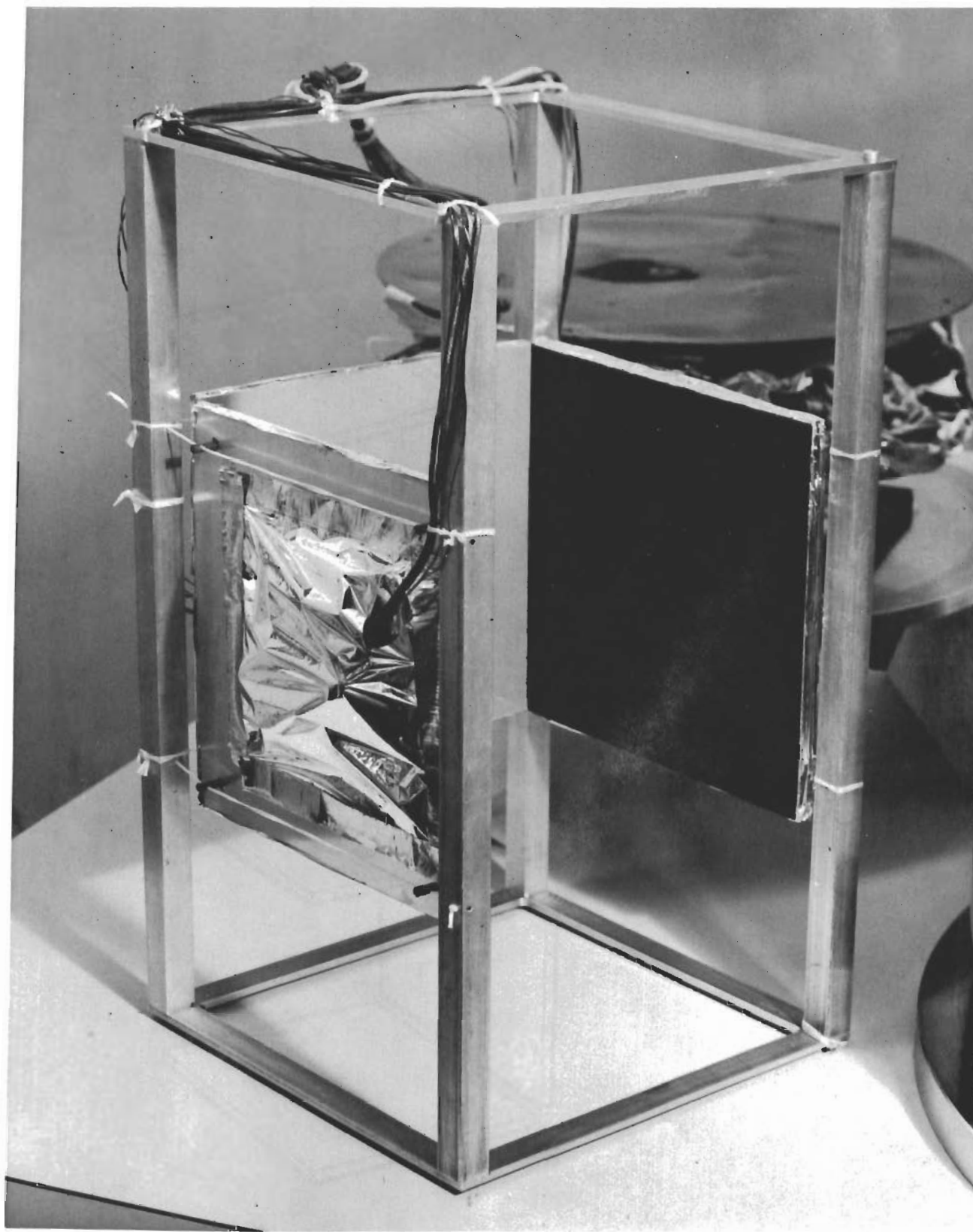


Figure 15. Test Configuration in Test Fixture

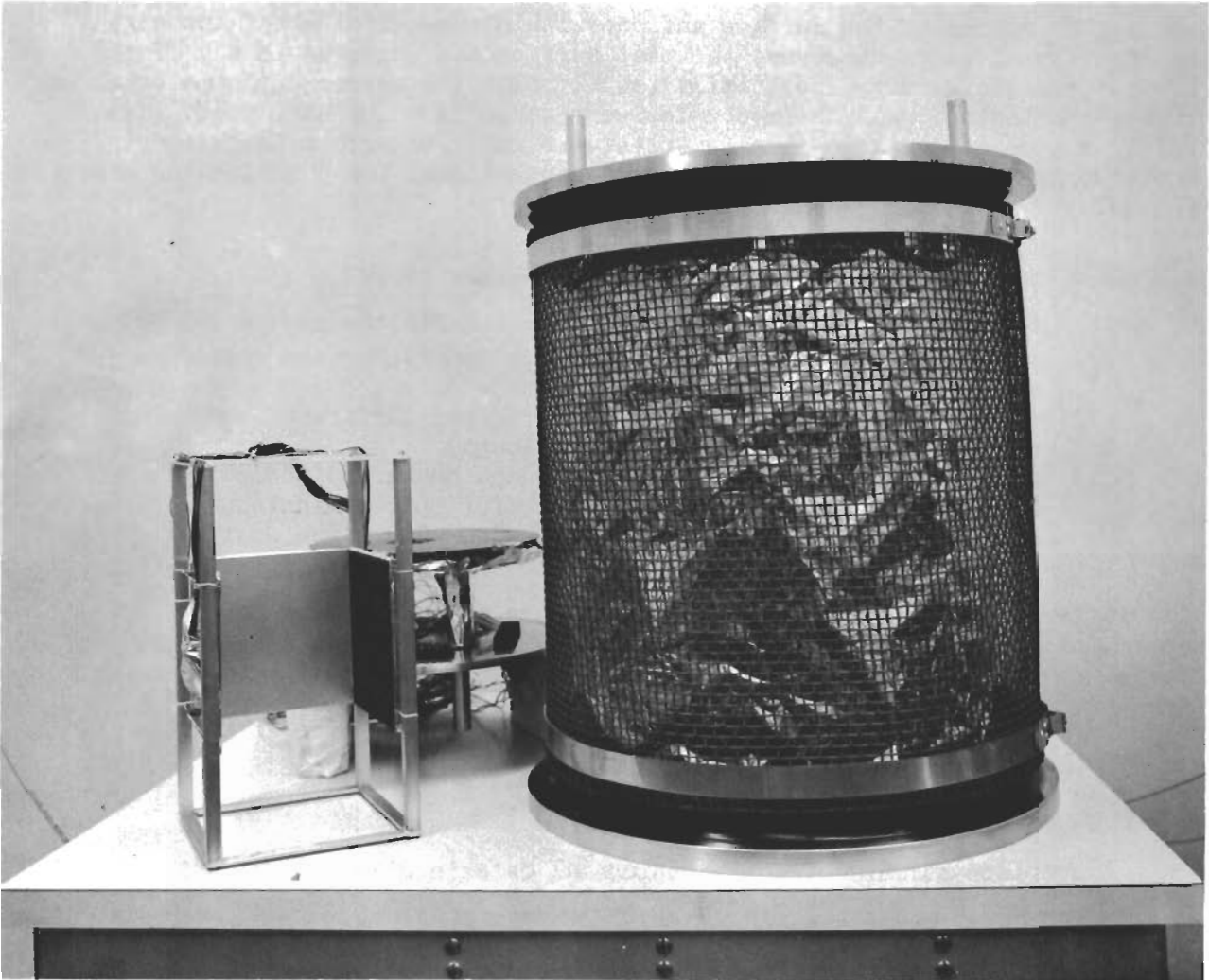


Figure 16. Test Configuration Ready for Testing

Contrails

Each test surface was supported within a framework by dacron cords attached to phenolic stand-off attachments. In this manner the test surfaces were isolated from the framework but properly positioned and restrained (see Figure 15). This framework was mounted within a LN₂ cooled baffled and the assembly placed within a vacuum system. A pressure of 10⁻⁵ torr or lower was obtained during the testing. The system is illustrated in Figure 16.

Thermocouples were placed on at least two points of each test surface; one at the center of the surface and one within one-half inch of the edge. No significant gradient across the test surface was observed in any of the tests; i.e., the surfaces were essentially isothermal. The thermocouple material was copper-constantan. All thermocouples were taken from the same roll. The voltages generated by the thermocouples were measured with a Leeds and Northrup Type 8686 potentiometer using a conventional ice junction compensation system.

The test procedure consisted of the following steps:

- (1) setting the predicted power dissipation for the source surface
- (2) setting estimated guard heat dissipation(s) for the receiving surface(s)
- (3) observing the temperature of the receiver surface(s) and adjusting the guard power dissipation(s)
- (4) when the receiver surface(s) and guard heater(s) indicated a negligible temperature difference for thirty minutes, at least two sets of data were recorded within the next thirty minutes.

The latter step insured that the surfaces were in equilibrium for approximately one hour. The accuracy of the measurements are estimated to be:

Temperature difference	+ 0.1 ^o F
Temperature	1 ^o F
Total power dissipated by the heat source	1.5%

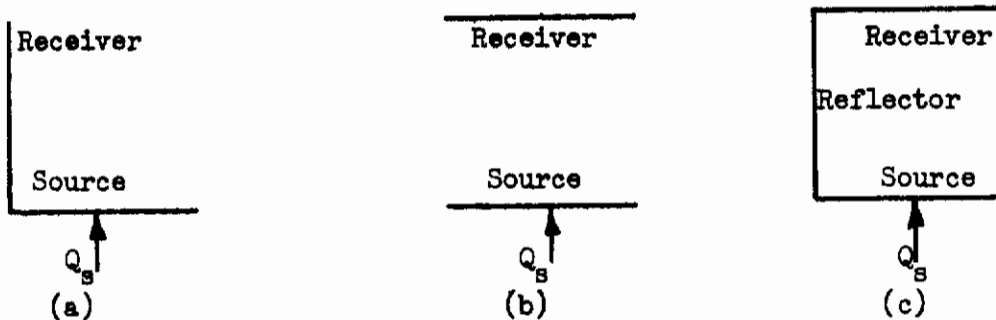
A complete summary of the experimental data is given in Appendix III.

6.2 ANALYTICAL PREDICTION

The radiative heat flow from the source surface and the temperature of the receiver surface were predicted by the analytical methods based upon the three different property assumptions: diffuse (1,2,3), specular (7), and the directional specular-diffuse (4). The prediction served to test the utility and practicality of the computer program developed for this study (Section 5) as well as provide a basis of comparison between theory and experiment.

The test configurations have been described in Section 6.1 and illustrated in Figure 14. These three configurations were combined with different surface coatings to give six different test systems. These systems are schematically represented in Figure 17. The directional

Contrails



Test	Surface Coatings			
	Source	Receiver	Reflector	Configuration
1.	"3M" Flat Black Paint	"3M" Flat Black Paint		(a)
2.	"3M" Flat Black Paint	"3M" Flat Black Paint		(b)
3.	"3M" Flat Black Paint	"3M" Flat Black Paint	Vacuum Deposited Aluminum	(c)
4.	"3M" Flat Black Paint	"3M" Flat Black Paint	Rinshed-Mason Leafing Aluminum Paint	(c)
5.	"3M" Flat Black Paint	Rinshed-Mason Leafing Aluminum Paint	Vacuum Deposited Aluminum	(c)
6.	"3M" Flat Black Paint	Rinshed-Mason Leafing Aluminum Paint	Anodized Aluminum	(c)

NOTE: The coating material descriptions are described in detail in Figures 18 through 21.

Figure 17. Experimental Matrix for Test of Radiation Analysis

reflectances of these coatings for a black body source at 540°R are shown in Figures 18 through 21. Included in these figures is the specular reflectance for the same radiation source. The specular reflectances were measured with a goniometric reflectometer shown in Figure 22. The directional reflectances were measured with a heated cavity reflectometer similar to that described in Reference 11.

The method of determining the various quantities and establishing the input for the computer program has been described in Section 5.3. The results of the computer calculations are shown in Table 7.

6.3 COMPARISON OF EXPERIMENTAL AND ANALYTICAL RESULTS

An examination of the results presented in Table 7 will quickly show one consistent fact: In every case, the experimentally measured temperature exceeded the value predicted by any of the analytical methods. A hasty conclusion would be that the experiments were in error in some manner. After re-examining the experimental technique for major errors, nothing sufficiently significant could be found. Conversely, many questions can be raised relative to the analytical predictions. The following discussion will be concerned with the errors of prediction. However, the possibility of an unrealized source of error in the experiments is not ruled out.

The difficulties with the predictions are believed to be centered about the thermal radiation properties used. The analyses are based upon the gray radiation assumption, i.e., wavelength independent properties. The source surface was operated at approximately 585°R whereas the receiver surfaces ranged between 340 and 415°R , i.e., a difference of 170 to 245°F . All properties used in the analysis assumed a material and source temperature of 585°R for emittance and reflectance. This "non-gray" error would be particularly noticeable with anodized aluminum and aluminum paint surfaces. To correct for this, the analyses would have to be performed on at least the band energy basis (4).

A second error was in the measurement of the properties. The heated cavity reflectometer is known to have an error due to sample heating (11). This error could be of the order of $.02$ -. 04 in directional reflectance (or emittance) and would affect the predicted temperatures slightly. It would have a more direct effect upon the predicted heat loss by the source surface. In only one case (Test 5), was the measured heat loss lower than predicted. In this instance, it was within experimental accuracy for the nearest prediction. The predicted temperatures and heat fluxes are too interrelated to separate them except as a first approximation. Thus, no firm conclusion can be drawn from this one case. However, the problem of sample emission is not considered to have been a major source of the discrepancies as judged from the spectral data.

Polarization of the energy with the monochromator of the heated cavity can also cause an error. For very highly reflective materials, e.g., vacuum deposited aluminum, or smooth dielectrics, polarization may cause an error as large as 10 to 20 percent in the reflectance at high angles.

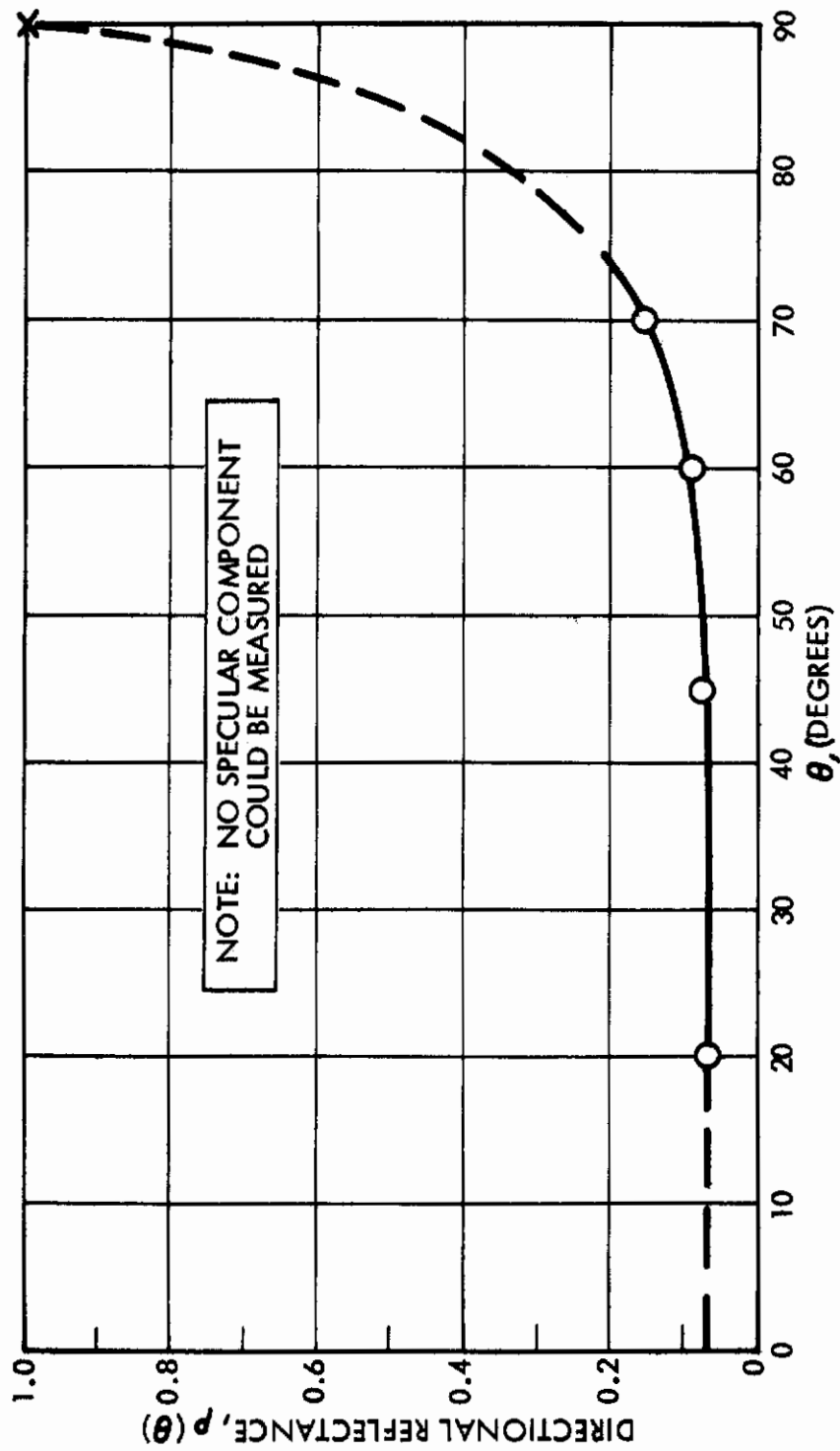


Figure 18. Directional Reflectance of 3M Flat Black Paint to a 540°R Black Body as a Function of Angle

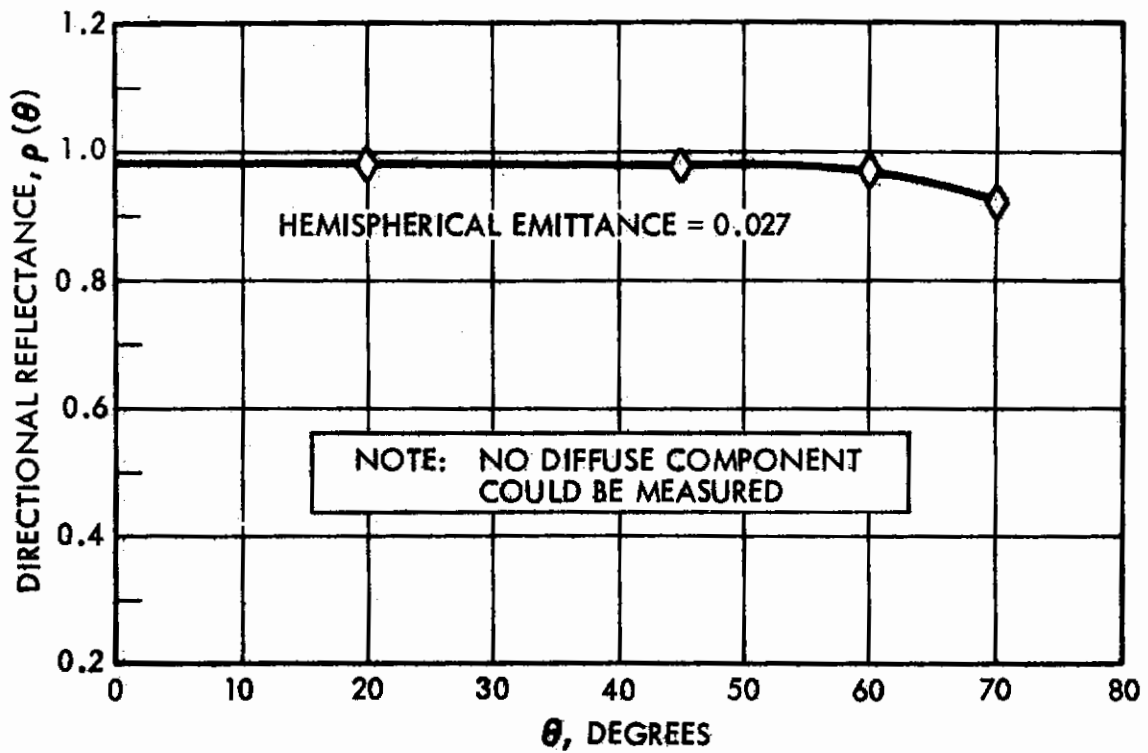


Figure 19. Directional Reflectance of Vacuum Deposited Aluminum to a 540° R Black Body as a Function of Angle

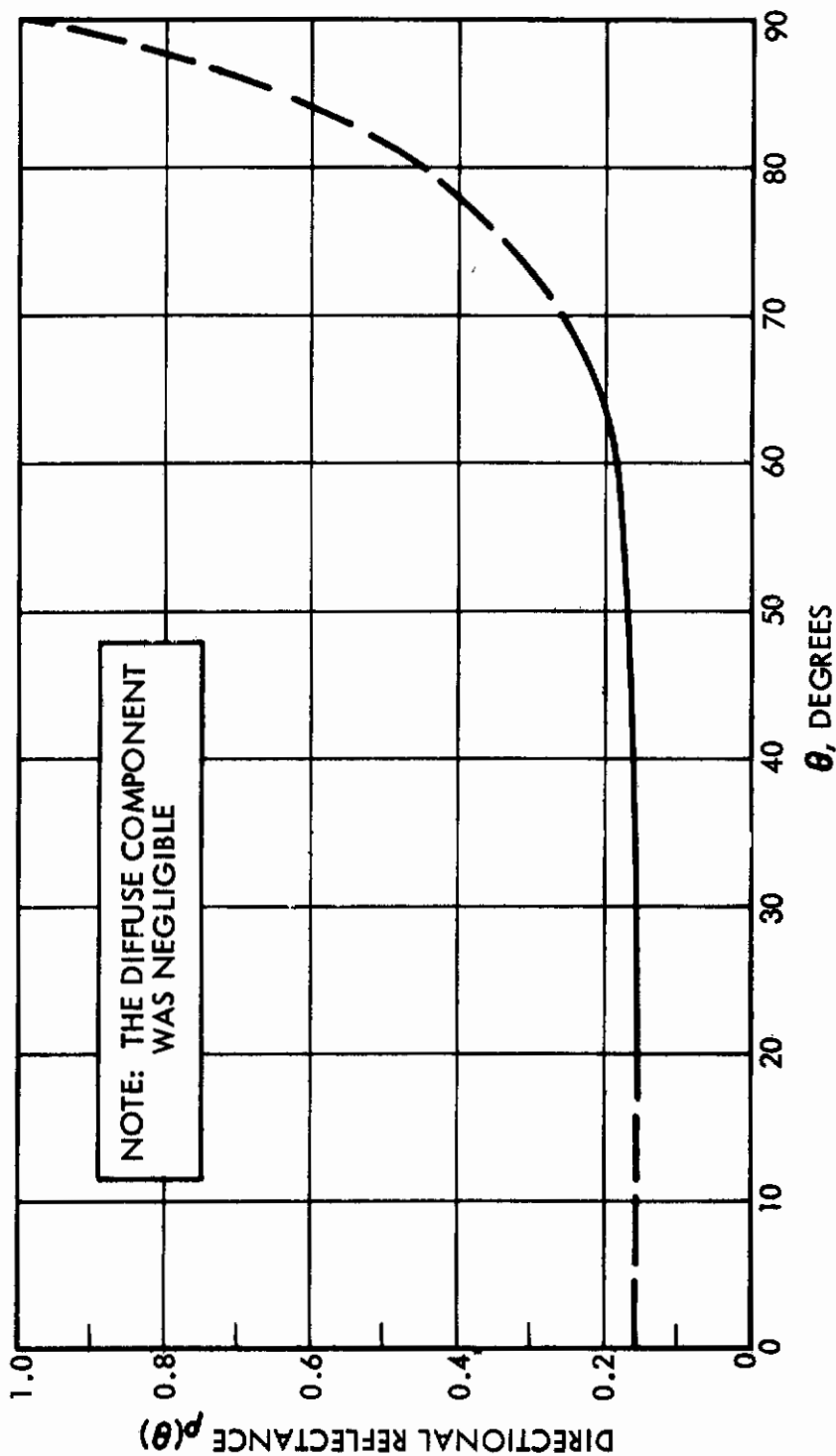


Figure 20. Directional Reflectance of Sulfuric Soft Anodized Aluminum (Type 1100), 0.0005 Inches Thick to a 540° R Black Body as a Function of Angle

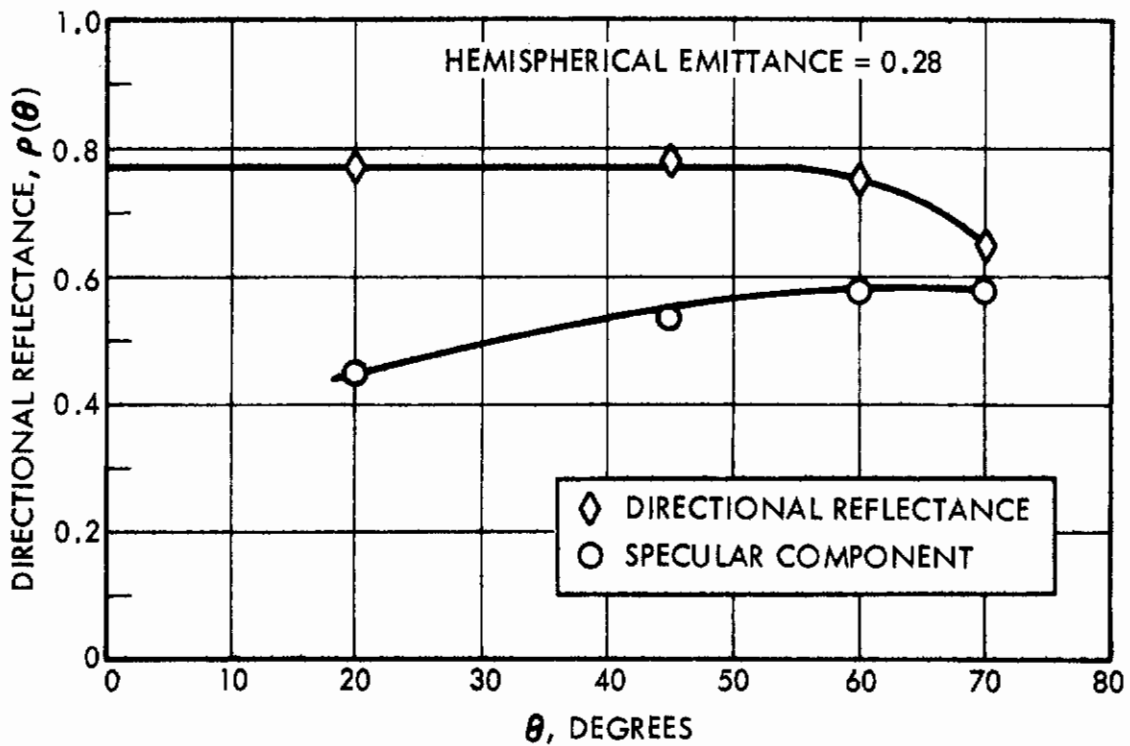


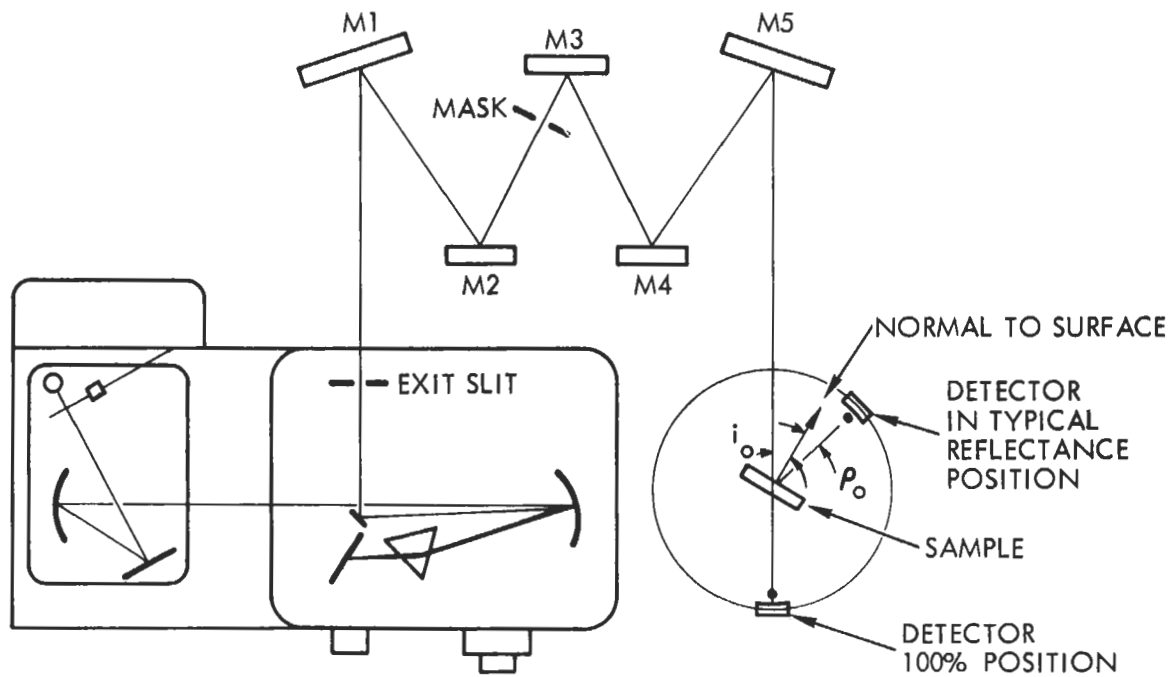
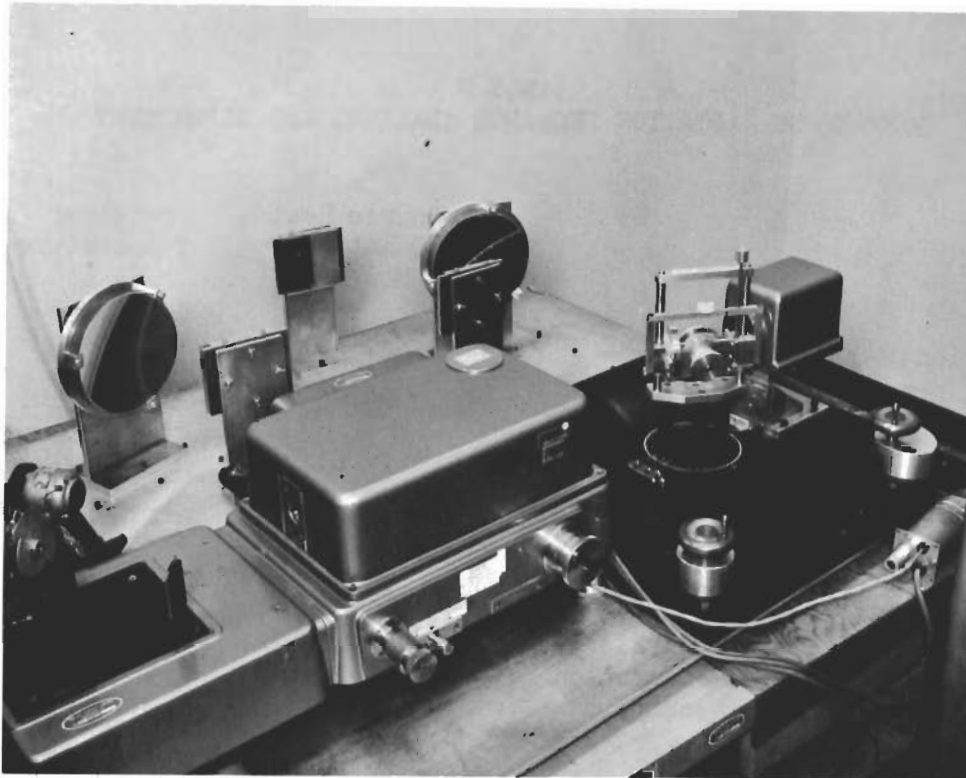
Figure 21. Directional Reflectance of Rinshed-Mason Leafing Aluminum Paint to a 540°R Black Body as a Function of Angle

Contrails

TABLE 7
SUMMARY OF RADIATION EXCHANGE ANALYSES AND EXPERIMENT

Configuration*		Q_s Source Heat Quantity Btu/hr	T_R Receiver Temperature $^{\circ}R$
1	Experimental	29.83	345.2
	Directional Specular- Diffuse Analysis	29.41	340.4
	Specular-Assumption	29.17	342.2
	Diffuse Assumption	29.17	342.2
2	Experimental	42.50	393.8
	Directional Specular- Diffuse Analysis	42.06	386
	Specular-Assumption	41.2	386.4
	Diffuse Assumption	41.2	386.4
3	Experimental	41.29	428.2
	Directional Specular- Diffuse Analysis	40.68	419.4
	Specular-Assumption	40.93	412.0
	Diffuse Assumption	39.69	393.8
4	Experimental	40.7	423.5
	Directional Specular- Diffuse Analysis	40.33	415.5
	Specular-Assumption	40.25	408.8
	Diffuse Assumption	40.54	397.4
5	Experimental	39.93	409.7
	Directional Specular- Diffuse Analysis	40.0	391.6
	Specular-Assumption	40.3	402.5
	Diffuse Assumption	40.2	383.8
6	Experimental	40.05	398.7
	Directional Specular- Diffuse Analysis	39.21	382.3
	Specular-Assumption	39.56	391.1
	Diffuse Assumption	40.19	387.9

*See Figures 14 and 17.



PERKIN-ELMER MODEL 12C

M1, M5 SPHERICAL MIRRORS 300 mm f.l.
M2, M3, M4 FLAT MIRRORS

Figure 22. STL Goniometric Reflectometer

Contrails

This source of error has also been recently recognized and the information required to assess this error is not yet available for the monochromator used. In the case of the tests described, only the 3M flat black paint will be free of this error.

A fourth source of error was the approximations used to obtain the geometrical reflectances; i.e., the interaction between spatial variation of reflectance and the shape factor integral. The methods used to approximate these properties have been described in Section 5.3. Until a spatial distribution of the reflectance property of a number of surfaces have been obtained and incorporated in the integration of a shape factor, the magnitude of this error will not be known. Simple analysis of an extreme case has shown this to be as large as 30 percent (4).

Considering all of these factors together, plus the probable experimental error, leads to the conclusion that the predicted temperatures should be re-examined. This would require the analyses to be performed on a band energy basis and with a more detailed evaluation of the properties.

The analytical results given in Table 7 also offer an opportunity to compare the different methods of analysis. The program described in Section 5 is based upon the method given in Reference 4. The technique is an admitted approximation to the integral equations describing the radiation exchange within an enclosure. The other two methods are also approximations in that an assumption is made relative to the radiation properties, i.e., nondirectional perfectly specular or perfectly diffuse. The approach programed to this study resulted in a set of equations which were very similar to those obtained in the diffuse approximation and could be solved with a slight increase in time. In contrast, an enclosure with perfectly specular surfaces can require extensive preliminary calculation to obtain the "specular interreflections."

The test configurations of Figure 17 are examples of very simple enclosures which are easily solved by any one of the three methods. They do not represent a complex enclosure and cannot adequately demonstrate the differences between the specular, diffuse and directional specular-diffuse methods. A trend can be inferred, however. For example, Test Configurations 1 and 2 should yield identical results for the specular and diffuse assumptions. The directional specular-diffuse analysis yields different results because the emission from source occurs at large angles from the normal. The predicted temperature of the receiver is higher for Test 1 and lower for Test 2 because of the angular effects of absorption. For Test 3, the specular analysis is suitable but does not account for the directional properties. The diffuse analysis does not account for specular reflection and radiation is "diffusely" reflected back to the source. The directional specular-diffuse result is between these two. Similar arguments hold for Test Configurations 4, 5, and 6. These geometries are more complicated by the use of the aluminum paint and anodized aluminum which have directional and/or specular components of reflection. In more complicated enclosures, such a simple explanation of possible differences is not practical. The only comment that can be made is that the directional specular-diffuse analysis is a more realistic approximation to physical fact.

7. CORRELATION OF COMPONENT JOINT EXPERIMENTAL RESULTS

At the request of the Technical Monitor, C. J. Feldmanis, an effort was made to correlate the experimentally measured values of joint conduction. This work was a substitute for the completion of the preliminary design task originally scheduled for the last portion of the program. This correlation effort has resulted in a simplified approach based on the conduction flow pattern to a circular cavity (region of the bolts) in the mating parts. For the thin plates in the component mounting joints, the conduction at the bolts was very high and the apparent contact area small. This led to the conclusion that macroscopic effects were of the greatest significance.

A review of the technical literature revealed little information that would be useful in predicting interface conductance for the bolted joints of this study. A subsequent study of the pressure distribution indicated that the apparent contact area occupies only to a small region near the bolts. This suggested that the predominant thermal resistance lies in the mating plates themselves. This correlation effort has resulted in a simplified expression for the interface conductance based on the heat flow pattern in a large circular region to a circular sink at the center. These comments apply specifically to the mounting plate configuration investigated in this study.

7.1 REVIEW OF LITERATURE

A review of technical literature reveals that the study of vacuum thermal contact resistance is of recent vintage. Past emphasis has been upon joints in a conducting fluid; e.g., air. This is not surprising since the need for information on the behavior of heat flow through connecting elements in a vacuum was not great until the advent of satellites. An excellent review of technical literature is contained in Reference 12 and a bibliography on contact conductance is contained in Reference 13; Appendix V list references that are not reported in Reference 13.

As background to the correlation to be presented, two well known methods that have been proposed will be cited. The applicability (or lack of it) to the type of joints considered in the present study will be indicated.

Fenech and Rohsenow (14) developed an expression for the thermal conductance of a mathematical model with contacting surfaces idealized as cylindrical contacts equally spaced in a triangular array. The thermal conductance was expressed in terms of the thermal conductivity of the metals and of the fluids of filling the voids, the real area in contact, the number of contact points per unit area, and the volume average thickness of the void gaps. A method of obtaining these physical properties of a contact is contained in Reference 15. The need for the profiles of the contacting surfaces precluded the examination of this method.

While most investigators were concerned with microscopic areas of contacts (those due to surface finish), Clausing and Chao (12) concluded that macroscopic resistances (that due to large scale waviness or non-flatness) was predominant over the microscopic resistance for a majority of engineering surfaces. The interface conductance was expressed in terms of the mean thermal conductivity of the two contacting materials, the radius of the macroscopic constriction ratio, the contact pressure, the macroscopic constriction ratio, the harmonic mean of the moduli of the two-contacting materials, and the total equivalent flatness deviation. This method requires the measurement of flatness deviation and surface finish; the latter is readily obtained, but the former is more difficult to measure. This method was not applied since subsequent studies showed that the apparent contact area (the region adjacent to the bolts) represents only a small percent of the total joint area. However, the concept of constrictive heat flow is employed in the present study, except that it is applied in a much larger, gross scale. The method is discussed below.

The two methods discussed above considered a physical system without a disruptive element such as a bolt. Intuitively, the influence of fasteners should be great. An attempt at correlating joint conductance data is reported in Reference 16, and the resultant expression is semi-empirical. The method employed in the present study is semi-analytical and the close correlation with experimental results strongly suggests that the governing resistance is centered in the plate itself; at least for the type of joints considered here. The analytical method is discussed below.

7.2 ANALYTICAL DEVELOPMENT

The correlation of joint conductance data was limited to the component joint configurations. An analytical model was postulated based on the work done by previous workers, experimental data and engineering judgement. The basic concept of the proposed method is that the controlling thermal resistance is the plate. It is postulated that the points of contact which contribute to the conductance are in the small region under and around the bolts. The problem is then to describe the heat flow in the plate to the bolt area. Two mathematical models were employed for this purpose.

7.2.1 ANALYTICAL MODEL I

The first model is shown in Figure 23(a). It is a disc with uniform heat flux over its surface and conduction to a central area at a constant temperature. The outside surface ($r = R$) is assumed to be insulated. This model is used to describe heat flow in a joint with only a few bolts in relation to the total area.

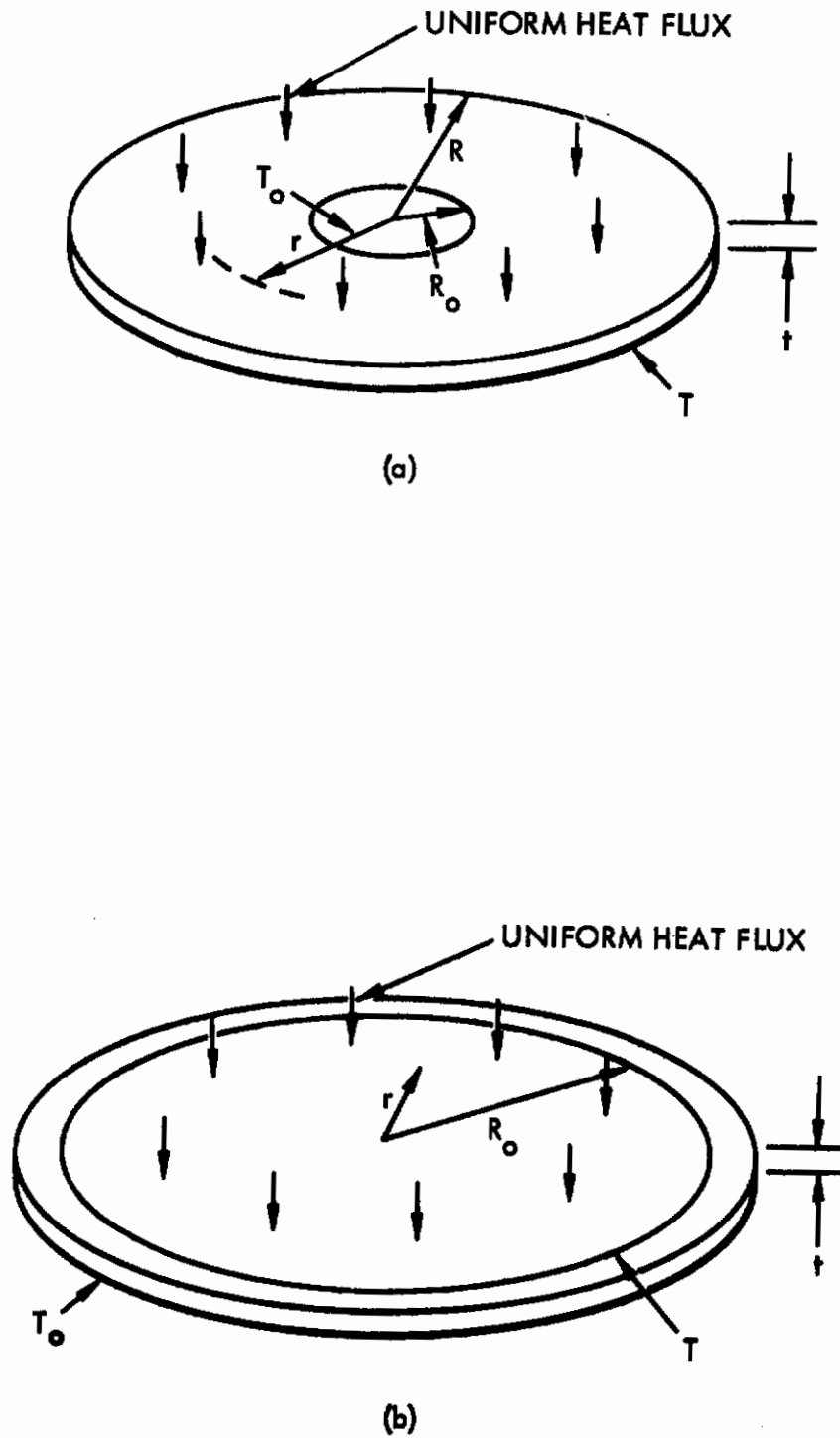
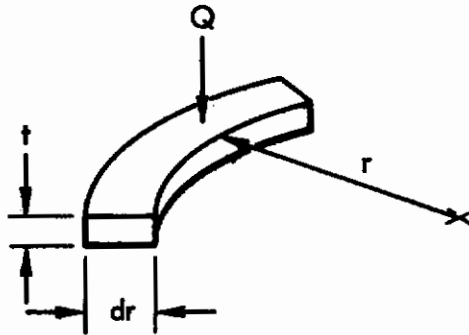


Figure 23. Analytical Models for Bolted Component Joint Correlation

Contrails

For an incremental volume at radius r , a heat balance yields,



$$Q - 2\pi r t \frac{dT}{dr} = -2\pi k t r \frac{dT}{dr} \Big|_{r+dr} + 2\pi k t r \frac{dT}{dr} \Big|_r \quad 7-1$$

or

$$Q = -\frac{kt}{r} \frac{d}{dr} \left(r \frac{dT}{dr} \right) \quad 7-2$$

with boundary conditions:

$$\text{at } r = R, \frac{dT}{dr} = 0 \text{ (insulated) and}$$

$$\text{at } r = R_o, T = T_o$$

$$\text{Hence, } T_o - T = \frac{Q}{Rt} \left[\frac{1}{4} (r^2 - R_o^2) + \frac{1}{2} R^2 \ln \frac{R_o}{r} \right] \quad 7-3$$

$$\text{Now let } \frac{r}{R} = \eta, \frac{R_o}{R} = \eta_o$$

$$\therefore T_o - T = \frac{QR^2}{kt} \left[\frac{1}{4} (\eta^2 - \eta_o^2) + \frac{1}{2} \ln \frac{\eta_o}{\eta} \right] = \Delta T \quad 7-4$$

The conductance of one plate is:

$$h = \frac{Q\pi R^2}{R \int_{R_o}^R (T - T_o) 2\pi r dr} \quad 7-5$$

Substituting ΔT from Equation 7-4 and changing the limits of integration gives:

$$h = \frac{Q\pi R^2}{1 \int_{\eta_0}^{\frac{QR}{kt}} \left[\frac{1}{4} (\eta_0^2 - \eta^2) + \frac{1}{2} \ln \frac{\eta}{\eta_0} \right] 2\pi\eta d\eta} \quad 7-6$$

Integrating and substituting the limits yields

$$h = \frac{2kt}{R^2} \left[\frac{1}{\eta_0^2 - \eta_0^4/4 - \ln \eta_0 - 3/4} \right] \quad 7-7$$

The bracketed term of Equation 7-7 is plotted in Figure 24 and the conductance versus radius for several effective contact radius values is shown in Figure 25.

7.2.2 ANALYTICAL MODEL II

The model which can be applied to a system having contact around the periphery is shown in Figure 23(b). The equation for this system is:

$$Q = - \frac{kt}{r} \frac{d}{dr} \left(r \frac{dt}{dr} \right) \quad 7-8$$

The boundary conditions are:

$$\begin{aligned} r = 0, & \quad T \text{ is finite} \\ r = R_0, & \quad T = T_0 \end{aligned}$$

Solution of Equation 7-8 yields,

$$T - T_0 = \frac{Q}{4kt} \left[R_0^2 - r^2 \right] \quad 7-9$$

The conductance of one plate is:

$$h = \frac{Q\pi R_0^2}{R_0 \int_0^{R_0} (T - T_0) 2\pi r dr} \quad 7-10$$

Substituting ΔT from Equation 7-9 and integrating gives:

$$h = \frac{8kt}{R_0^2} \quad 7-11$$

This equation is plotted in Figure 26.

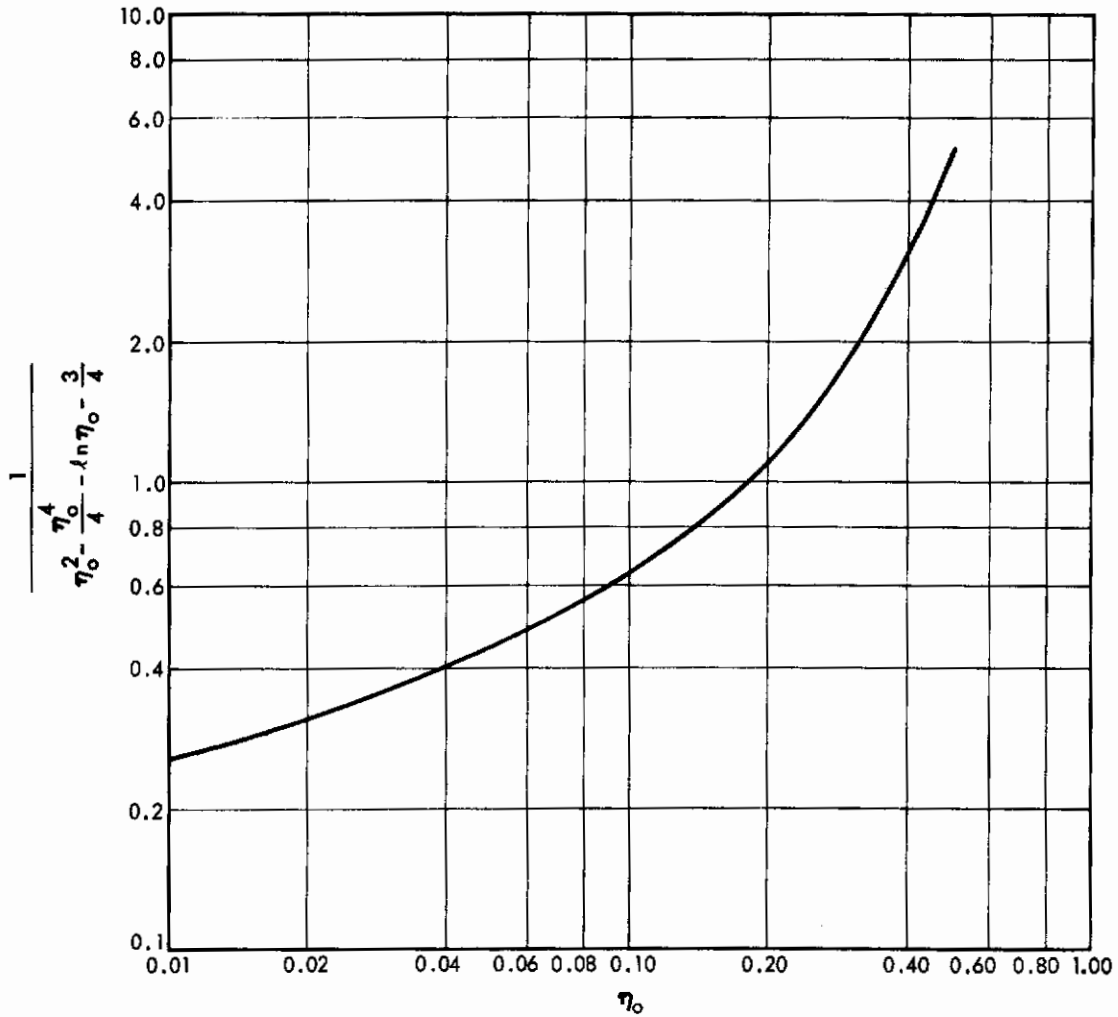


Figure 24. The Quantity $\left[\eta_0^2 - (\eta_0^4/4) - \ln \eta_0 - 3/4 \right]^{-1}$ as a Function of η_0

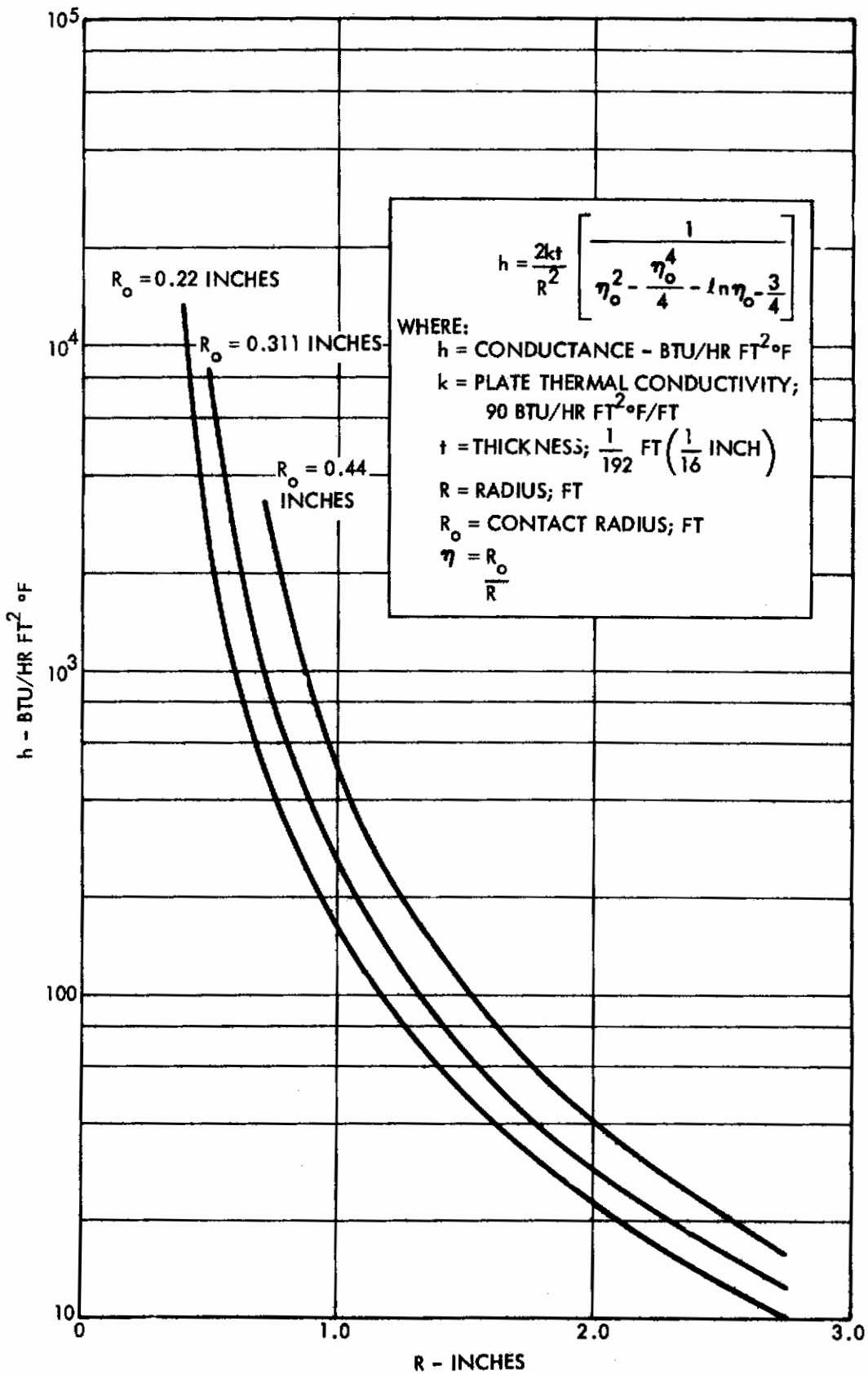


Figure 25. The Thermal Conductance of a Single Contact Junction as a Function of Contact Radius (R_o) for an Aluminum Plate 1/16th Inch Thick

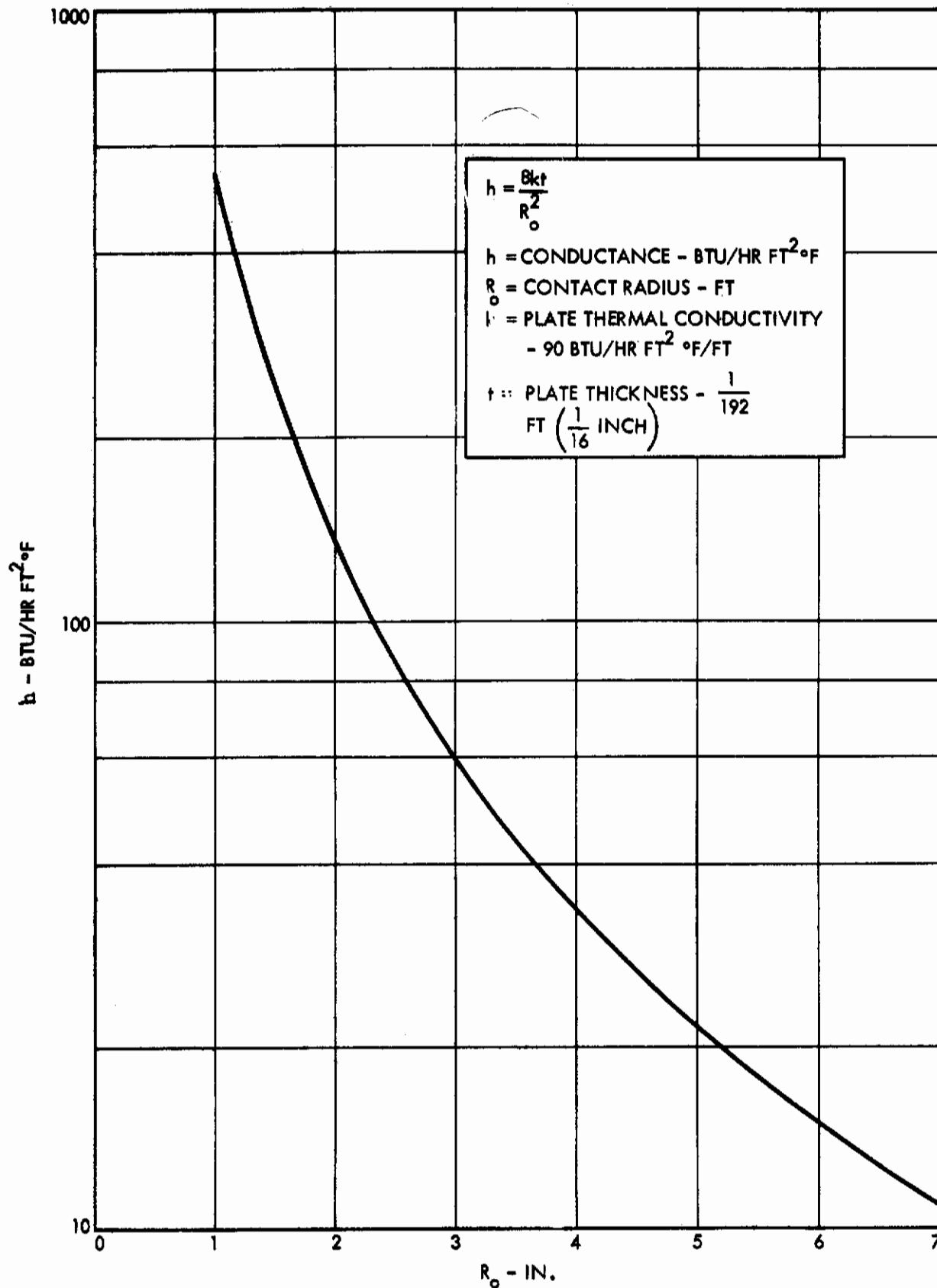


Figure 26. The Thermal Conductance of a Peripheral Contact Junction for an Aluminum Plate 1/16th Inch Thick

7.2.3 CONTACT REGION AROUND A BOLT

The contact area and conductance of a bolt is based on the deformation of the plates under bolt head. The method used to determine this quantity is that presented in reference (17). The analysis given by this reference assumes a uniform loading over the bolt area. The resultant stress distribution is shown in Figure 27 and can be expressed as (Equation 56, Reference 17):

$$\frac{\sigma_z}{\sigma_p} = 1 - \left(\frac{r}{c}\right) \left[\frac{2}{(c/a)^2 - 1} \right] \quad 7-12$$

The quantity c is dependent upon the bolt diameter, a , and the plate thickness, $\frac{b}{2}$. For a 1/16-inch plate in contact with a 1/8-inch plate, the effective contact radius, c , is given by Reference 17 as 1.35a.

The pressure under the bolt must be computed for use in the above expression. The tensile load in a bolt torqued to a preset value is determined from the approximate relation given in Reference 18.

$$T = 0.20 Fd. \quad 7-13$$

where

T = bolt torque, 24 in.-lb.

F = tensile load, lb.

d = major thread dia. = .190 in.

or

$$F = 630 \text{ lb.}$$

This value is conservative for the present application; that is, it yields a lower conductance than values given by other references. Aron and Colombo (16), for example, use a value of 800 lb. for 22 in.-lb. torque in the same size bolt.

The bolt (NAS 563) has a measured bearing diameter of 0.344 inches and the nut (NAS 671) has a measured bearing diameter of 0.312 inches. The area under the nut was used to obtain the pressure, assuming uniform loading ($\sigma_p = P$)

$$P = \frac{F}{A} = \frac{630 \text{ lb.}}{.0468 \text{ in}^2} = 13,450 \text{ lb/in}^2 \quad 7-14$$

This result was used with Equation 7-12 to obtain the pressure distribution and conductance at the bolt. The solution of Equation 7-12 for σ_z , using the results of Equation 7-14, are plotted in Figure 28. The pressure distribution was used by dividing the area into annular zones and evaluating each zone to estimate its conductance. The numerical values were obtained from the conductance versus pressure plot given in

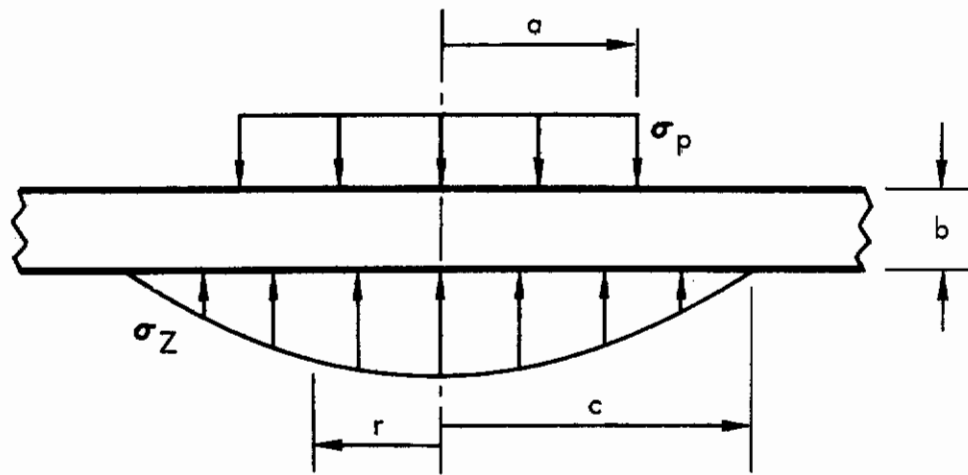


Figure 27. Stress Distribution in a Bolted Plate for Uniform Bolt Pressure

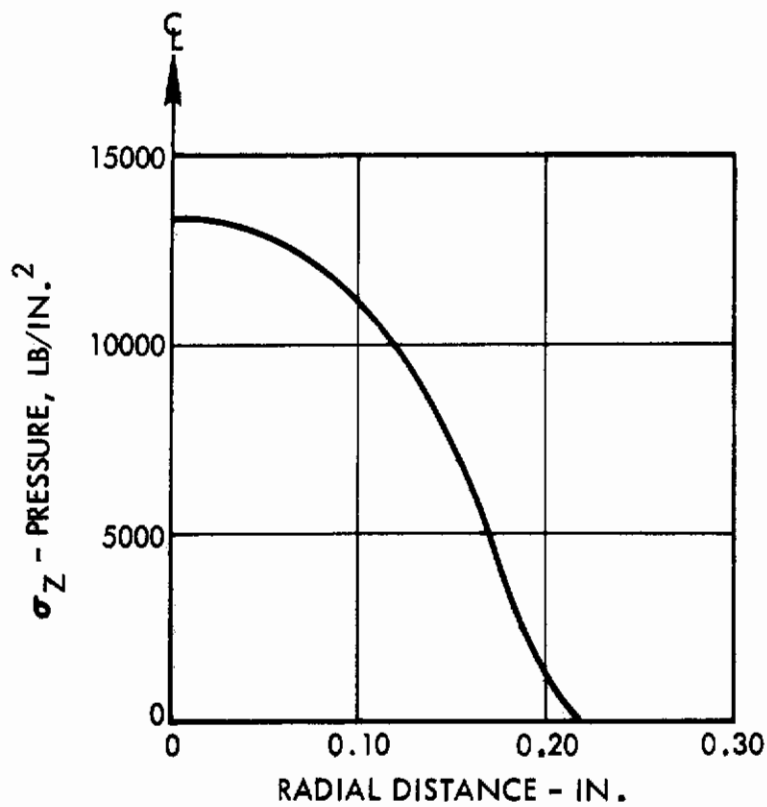


Figure 28. The Pressure Distribution Under the Nut of a Bolted Plate According to Equation 7-12

Figure 6-3 of Reference 19, labeled "Best line through most of the Aluminum (II) Data-Vacuum." The results of this calculation yield a conductance through the bolt of 21,000 Btu/hr ft² °F. This can be compared to the value of 10,000 Btu/hr ft² °F calculated in Reference 19 for a No. 10 bolt tightened to 22 in.-lb₂ torque. The area under the bolt in Reference 19 is given as 0.33 inches² (a washer was used in Reference 19). The contact area under the bolt in the present study was 0.12 in.². Thus, the thermal resistance of the two bolts can be compared:

Present Study:

$$R = \frac{1}{hA} = .0575 \frac{^{\circ}\text{F hr}}{\text{BTU}}$$

Reference (3)

$$R = \frac{1}{hA} = .044 \frac{^{\circ}\text{F hr}}{\text{BTU}}$$

7.3 APPLICATION TO TEST CONFIGURATIONS

Three component test configurations were run with fewer than the normal 12 bolts to evaluate bolt spacing effectiveness. These tests were in addition to those reported in Section 3.1. These configurations are shown in Figure 29 (a, b, and c). The sample size was 6 inches by 6 inches, the upper plate thickness was 1/16 inch, and the mounting plate was 1/8 inch thick. The bolt torque was 24 in. lb. for all cases.

Configuration 29-a was divided into four equal areas for purposes of analytical correlation. Each triangular section was assumed to be deformed into a semicircular shape of the same area and having a contact region at the center. The radius of the segment is then 2.38 in., and the bolt contact area, now semicircular, has an effective radius of 0.311 in. These dimensions were substituted in the equations described in Section 7.2.1. The resulting conductance of the upper plate was found to be: $h_1 = 18.3$ Btu/hr ft² °F.

The conductance of the lower plate will be computed using the same analytical procedure. Since the heat removal from the lower plate is not as uniform as heat supplied to the upper plate, the analytical model is now a poorer approximation of the real system. The results were used as an approximation since an analytical solution of the real heat flow in this plate would be a lengthy task. Applying this method to the lower plate, which has a thickness twice that of the upper plate, results in

$h_2 = 36.6$ Btu/hr ft² °F. These two plate thermal conductances must be combined with the bolt thermal conductance. The thermal circuit for this system is:

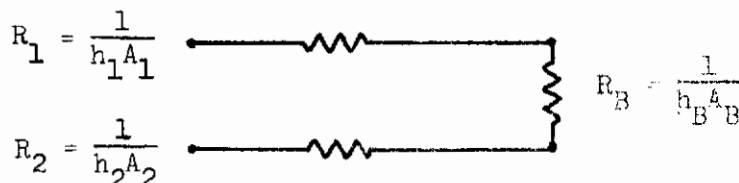


Figure 30. Thermal Circuit for Calculating Overall Thermal Conductance

Contrails

The overall conductance is given by:

$$\frac{1}{hA} = \frac{1}{h_1 A_1} + \frac{1}{h_B A_B} + \frac{1}{h_2 A_2}$$

Substituting the values gives:

$$\frac{1}{hA} = \frac{1}{18.3 \left(\frac{9}{144}\right)} + \frac{1}{21,000 \left(\frac{.12}{144}\right)} + \frac{1}{36.6 \left(\frac{9}{144}\right)}$$

$$\frac{1}{hA} = .874 + .057 + .437$$

or

$$h = \frac{1}{1.368 \left(\frac{9}{144}\right)} = 11.7 \text{ Btu/hr ft}^2 \text{ } ^\circ\text{F}$$

Applying this technique to Configuration 29-b, the corner bolts were close together and were lumped together to form a quarter circular area having an effective radius of 0.622 inches. The analytical method of Section 7.2.1 and thermal circuit substitutions yield an overall conductance of $h = 8.0 \text{ Btu/hr ft}^2 \text{ } ^\circ\text{F}$.

Configuration 29-c was divided by allotting to each corner bolt a hemicircular area of 4 in.^2 and each center bolt a quarter circle of 5 in.^2 . Using the same technique as above, the thermal circuit gave:

$$h = 22.0 \text{ Btu/hr ft}^2 \text{ } ^\circ\text{F}.$$

The twelve-bolt configuration was analyzed in the same manner by dividing this area into eight equal area segments as shown in Figure 29-d. The result was:

$$h = 26.7 \text{ Btu/hr ft}^2 \text{ } ^\circ\text{F}.$$

The 6 inch by 12 inch component configuration can be approached using the same technique by dividing the area into eight hemicircular sectors and four quarter circular sectors each with an effective area of 6 in.^2 . Similarly the 12 by 12 configuration was divided into twelve hemicircles and four quarter circles of equal area, 9 in.^2 . The results for these six configurations are shown in Table 8.

The 6 inch by 6 inch, 12 bolt and 12 inch by 12 inch, 24 bolt configurations can also be predicted using the method described in Section 7.2.2. An effective radius based on the plate area was used in Equation 7-11. The results are also given in Table 8. The results of these correlation attempts are compared to the measured values in Table 8. The agreement is adequate in all cases except 29-b where the predicted value is a little more than half of the measured conductance. In spite of this, the success of the technique is quite satisfactory. Further exploitation should be made of the approach described here. The results have been restricted to a bolted thin plate without a filler material.

Contrails
 EXPERIMENTAL SYSTEMS
 AND
 ANALYTICAL APPROXIMATIONS

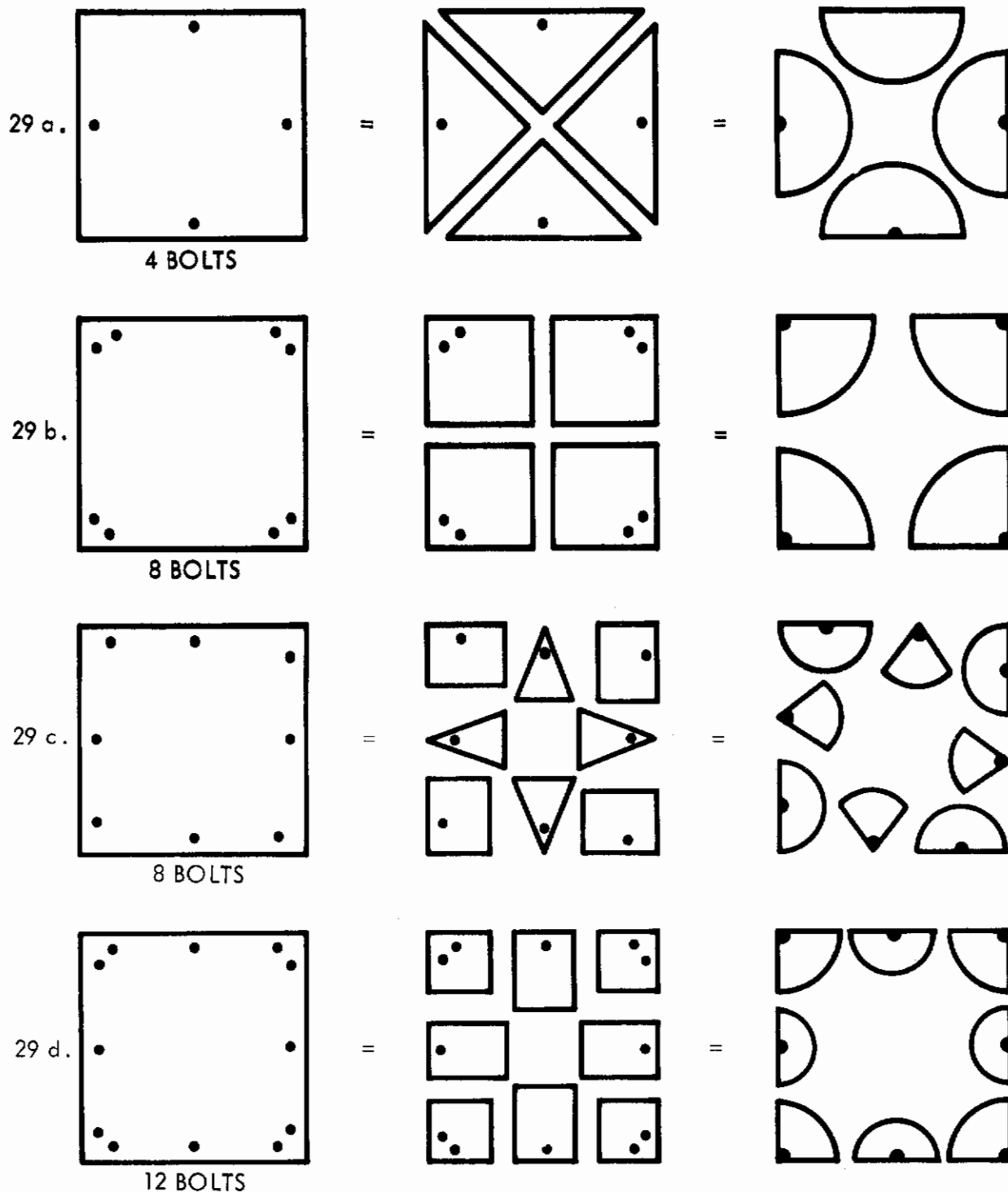


Figure 29. Method of Subdividing the Test Configurations to Predict Overall Thermal Conductance

TABLE 8
COMPARISON OF PREDICTED AND MEASURED COMPONENT JOINT CONDUCTANCES

Configuration	Experimental h, BTU/hr ft ² °F	Method I (Sec. 7.2.1) h, BTU/hr ft ² °F	Method II (Sec. 7.2.2) h, BTU/hr ft ² °F
29-a	13.4	11.7	
29-b	13.7	8.0	
29-c	22.0	22.0	
29-d			
6 x 6, 12 bolts	26.3	26.7	29
6 x 12, 18 bolts	18.5	18.1	
12 x 12, 24 bolts	8.3	10.5	7.8

Contrails

An attempt should be made to extend this to thick plates with and without a filler and to thin plates with a filler.

8. CONCLUSIONS AND RECOMMENDATIONS

This report presents the results of the first phase of a program designed to improve the prediction of spacecraft thermal performance. The information necessary for the comparison of prediction and test of a spacecraft model has been gathered. The continuation of the program to this natural conclusion is the second phase of the study. There has been no decrease in the practical needs for this continuation and it is important to complete this program.

There have been several developments within this program which warrant further study. The first is the extension of the joint conductance testing to include a larger number of joint types. The techniques which have been developed in this program for experimentally measuring the conductance of practical joints have proven to be very simple and inexpensive. The accuracy which is obtained is adequate for such joints and is a satisfactory compromise with the cost of such experimentation. The joints for this additional work should not be chosen on the basis of a thermal test model but selected for the frequency with which they are used in actual practice, e.g., riveted joints, low conductance joints, etc.

The practical correlation of joint conductances should also be continued. The correlation for the thin plate unfilled component joints was obtained by assuming the primary resistance to heat flow was in the thin plates. This primary resistance was found to be adequately described by radial in the region surrounding each bolt fastener. The success with which the component joints were correlated by this procedure was very encouraging. The limitations of time and resources did not allow a similar attempt to be made to correlate filled joints or structural joints. However, such a correlation is believed to be feasible. This work could be included in the second phase of the program; correlation of other test joints would be performed as part of the experimental work described above or as a separate study. Regardless of the mechanism chosen for performing this correlation, this work should be continued and extended.

The application of the directional specular-diffuse method of analysis has indicated a major gap in our knowledge of thermal radiation properties. A critical part of this method is the separation of the thermal radiation properties into the diffuse and specular components. Additional experimental and analytical work is required to develop a basis for this separation from measurements of the directional and specular reflectances. Such a study should include an examination of the geometrical reflectances (and emittances) relative to the distribution of reflected (and emitted) radiation.

Although the comparisons of predicted and experimental radiation exchange in the simple geometries were close, further refinement of the predictions are desired. This problem is related in part to the separation of the diffuse and specular components discussed above. The effect of non-gray radiation properties is probably of equal or greater importance. Further study is needed for the improvement of the predicted temperatures and heat fluxes, e.g., a prediction using the band energy method.

Contrails

In conclusion, the objectives of the first phase of the program have been satisfied; i.e., the data and methods required to compare the predicted and test thermal performance of a model spacecraft have been developed. Other areas for further study have also been found:

- (1) practical joint conductance measurements
- (2) correlation of measured joint conductances
- (3) the separation of radiation properties into diffuse and specular components for the directional specular-diffuse analysis
- (4) the importance of the non-gray property assumption

The development of additional problems is to be expected in a study of this nature. The second phase of the program should be expected to raise its own share of new problems.

Contrails

REFERENCES

1. H. C. Hottel, "Radiant Heat Transmission," Chapter 4 of Heat Transmission, 3rd Ed., W. H. McAdams, McGraw-Hill Book Co., New York, 1954.
2. B. Gebhart, "Unified Treatment for Thermal Radiation Transfer Processes," Paper No. 57-A-34, Winter Meeting ASME, Dec. 1959.
3. A. K. Oppenheim, Trans. ASME 78:725-735 (1956).
4. J. T. Bevens and D. K. Edwards, "Radiation Exchange in an Enclosure with Directional Wall Properties," presented at the ASME Winter Meeting, Dec. 1965, Paper No. 64WA/HT-52, published in the August issue of the Journal of Heat Transfer 87:388-396 (1965).
5. C. D. Coulbert and Chien Liu, WADC TN 53-50 June 1953.
6. T. Ishimoto and J. T. Bevens, AIAA Journal 1:1428-9 (1963).
7. E. M. Sparrow, "On the Calculation of Radiant Interchange Between Surfaces," pp 181-212, W. Ibele editor Academic Press, New York, 1963.
8. J. T. Bevens and R. V. Dunkle, Trans. ASME, Series C 82:1-19 (1960).
9. E. M. Sparrow, et al., Trans. ASME, Series C 84:294-299 (1962).
10. D. K. Edwards and J. T. Bevens, "Effect of Polarization on Spacecraft Radiation Heat Transfer," to be published in the July issue of the AIAA Journal, 1965.
11. R. V. Dunkle, et al., "Heated Cavity Reflectometer for Angular Reflectance Measurements," Prog. in Intl. Research on Thermodynamics and Transport Properties Am. Soc. Mech. Engrs., pp 541-562 (1962).
12. A. M. Clausing and B. T. Chao, "Thermal Contact Resistance in a Vacuum Environment," University of Illinois Experimental Station Report, ME-TN-242-1, August 1963.
13. H. Atkins, "Bibliography on Thermal Metallic Contact Conductance," NASA TM X-53227, April 15, 1965, Marshall Space Flight Center.
14. H. Fenech and W. M. Rohsenow, "Prediction of Thermal Conductance of Metallic Surfaces in Contact," (Paper No. 62-HT-32) J. Heat Transfer, Vol. 85, pp 15-24, Feb.
15. J. J. Henry and H. Fenech, "The Use of Analogue Computers for Determining Surface Parameters Required for Prediction of Thermal Contact Conductance," ASME Paper 63-WA-104, 1963; also J. of Heat Transfer Transaction of ASME, Vol. 86, Series C, No. 4, Nov. 1964.
16. W. K. Aron and G. Colombo, "Controlling Factors of Thermal Conductance Across Bolted Joints in a Vacuum," ASME Paper 63-W-196.
17. K. G. Lindh, et al., "Studies in Heat Transfer in Aircraft Structure Joints," UCLA Report 57-50, May 1957.
18. J. E. Shigley, Machine Design, McGraw-Hill Book Co., Inc. New York, 1956.
19. M. F. Bloom, "Thermal Contact Conductance in a Vacuum Environment," Douglas Aircraft Report SM-47700, Dec. 1964.

APPENDICES

- I. Experimental Data—Component Joints
- II. Structural Joint Tests
- III. Script F Computer Program Print Out
- IV. Experimental Data—Radiation Exchange Experiment
- V. Bibliography for Joint Thermal Conductance
- VI. Component Joint Test Data used for Correlation Task

APPENDIX I
EXPERIMENTAL DATA—COMPONENT JOINTS

Contrails

The experimental data for the 6 x 6 component joint is listed in Table 9 of this appendix. The thermocouple locations are shown on the full size drawing of Figure 31. In addition to these thermocouples, thermocouples were placed in the cooling water inlet and outlet lines. These are absolute thermocouples No. 3 and 4 respectively. The approximate cooling water flow rate was also recorded, but varied as the water pressure fluctuated. The heater voltage and current are also recorded.

Figure 31 also illustrates the zones which were used in computing the area weighted temperature difference. A sample calculation for run No. 1 is as follows:

$$\overline{\Delta T}_{\textcircled{1}} = \frac{1.02 + 1.04 + 0.80 + 0.77}{4} = 0.91^{\circ}\text{F}$$

$$\overline{\Delta T}_{\textcircled{2}} = 1.98^{\circ}\text{F}$$

$$\overline{\Delta T}_{\textcircled{3}} = \frac{2.50 + 4.11 + 2.57}{3} = 3.06^{\circ}\text{F}$$

$$\overline{\Delta T}_{\textcircled{4}} = \frac{6.29 + 6.53}{2} = 6.41^{\circ}\text{F}$$

These average ΔT 's are for each zone, obtained by averaging the differential thermocouple readings in each zone. The overall ΔT is now computed by area weighting these values.

$$\Delta T_M = \Delta T_{\textcircled{1}} \frac{A_{\textcircled{1}}}{A_T} + \Delta T_{\textcircled{2}} \frac{A_{\textcircled{2}}}{A_T} + \Delta T_{\textcircled{3}} \frac{A_{\textcircled{3}}}{A_T} + \Delta T_{\textcircled{4}} \frac{A_{\textcircled{4}}}{A_T}$$

$$\Delta T_M = \frac{9.05}{36} (0.91) + \frac{7.50}{36} (1.98) + \frac{13.2}{36} (3.06) + \frac{6.25}{36} (6.41)$$

$$\Delta T_M = 0.229 + 0.412 + 1.121 + 1.11$$

$$\Delta T_M = 2.872^{\circ}\text{F}$$

$$Q_{IN} = 3.702 (0.1314) = 4.864 \text{ watts}$$

$$= 16.6 \text{ Btu/hr}$$

Contrails

$$\begin{aligned}h &= \frac{Q}{A\Delta T_M} \\ &= \frac{16.6 \text{ Btu/hr}}{1/4 \text{ ft}^2 \cdot 2.872^\circ\text{F}} \\ h &= 23.1 \text{ Btu/hr ft}^2 \text{ }^\circ\text{F}\end{aligned}$$

The experimental data for the 6 inch x 12 inch and 12 inch x 12 inch component joints are given in Tables 10 and 11, respectively, of this appendix. The thermocouple locations and temperature weighting zones are shown in Figures 32 and 33 for these two experimental configurations.

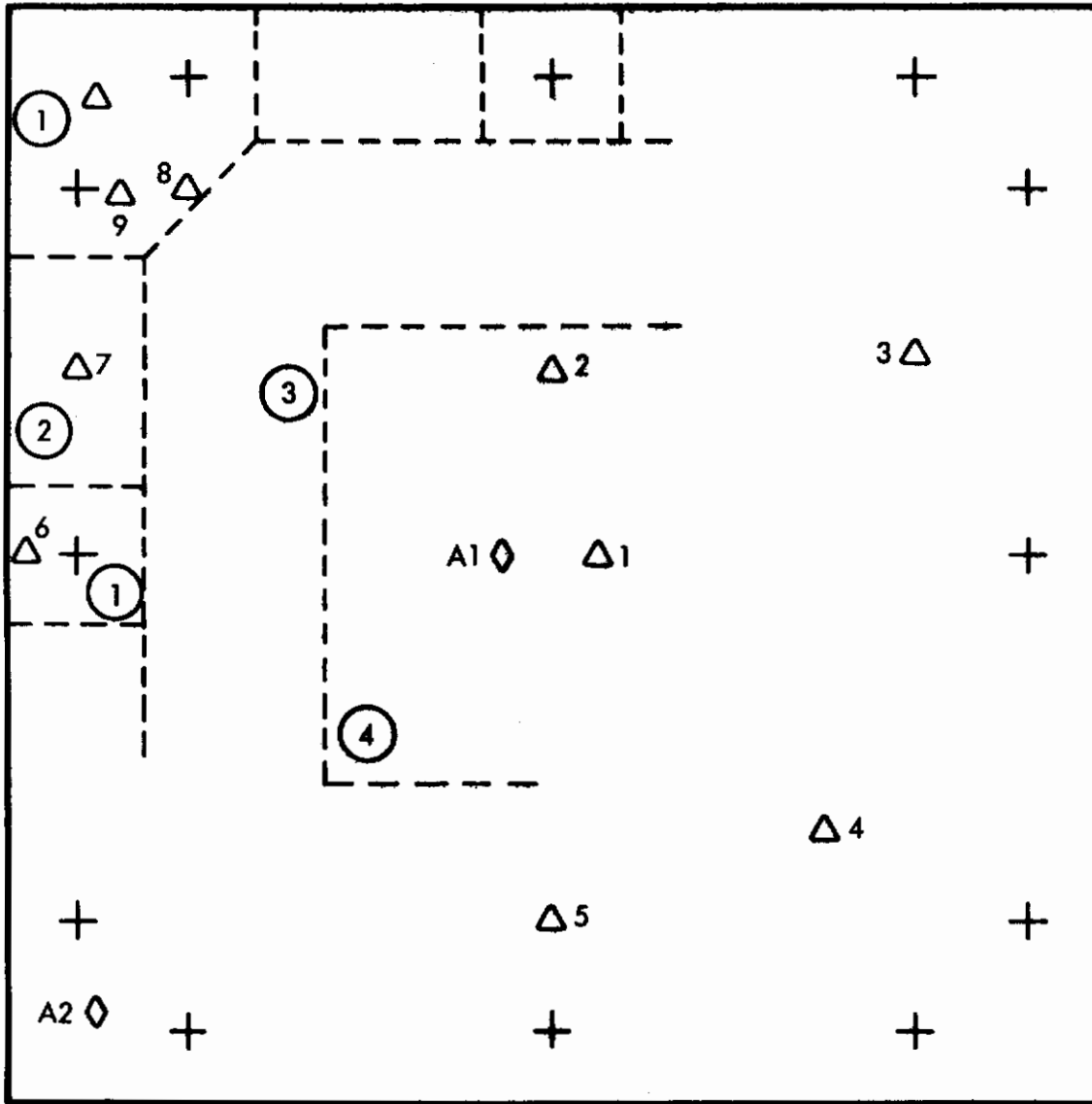
Differential thermocouples are located at the same (x, y) coordinates on the back of the mounting plate and the component plate at the locations shown on Figures 31, 32 and 33.

The conductance is calculated using the following equation:

$$h = \frac{Q}{A\Delta T}$$

The area used in this calculation is the contact area of the mating parts. For the structural joints, this was the overlap area between the angle bracket and the panel. The ΔT is an area weighted average which is determined by the method explained in above.

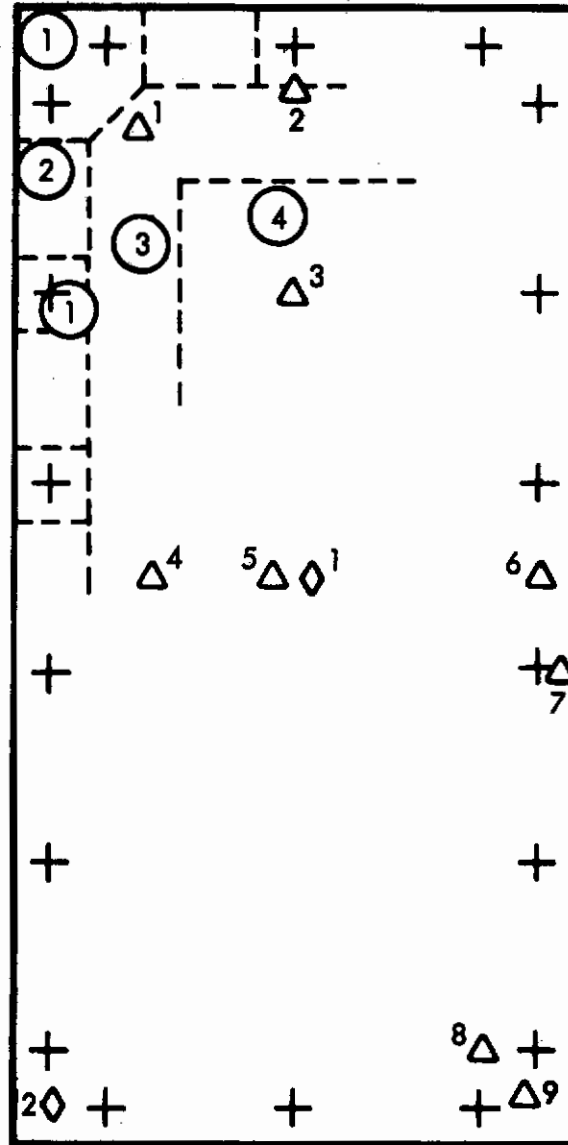
6" x 6" COMPONENT THERMOCOUPLE LOCATION



- | | | | |
|---|---------------------------------------|---|---|
| ① | ZONE 1, AREA = 9.05 IN. ² | △ | DIFFERENTIAL THERMOCOUPLES |
| ② | ZONE 2, AREA = 7.50 IN. ² | ◇ | ABSOLUTE THERMOCOUPLES |
| ③ | ZONE 3, AREA = 13.20 IN. ² | + | BOLT LOCATION |
| ④ | ZONE 4, AREA = 6.25 IN. ² | ○ | ZONE AREAS USED TO CALCULATE AVERAGE ΔT |

Figure 31. 6" x 6" Component Joint Thermocouple Location

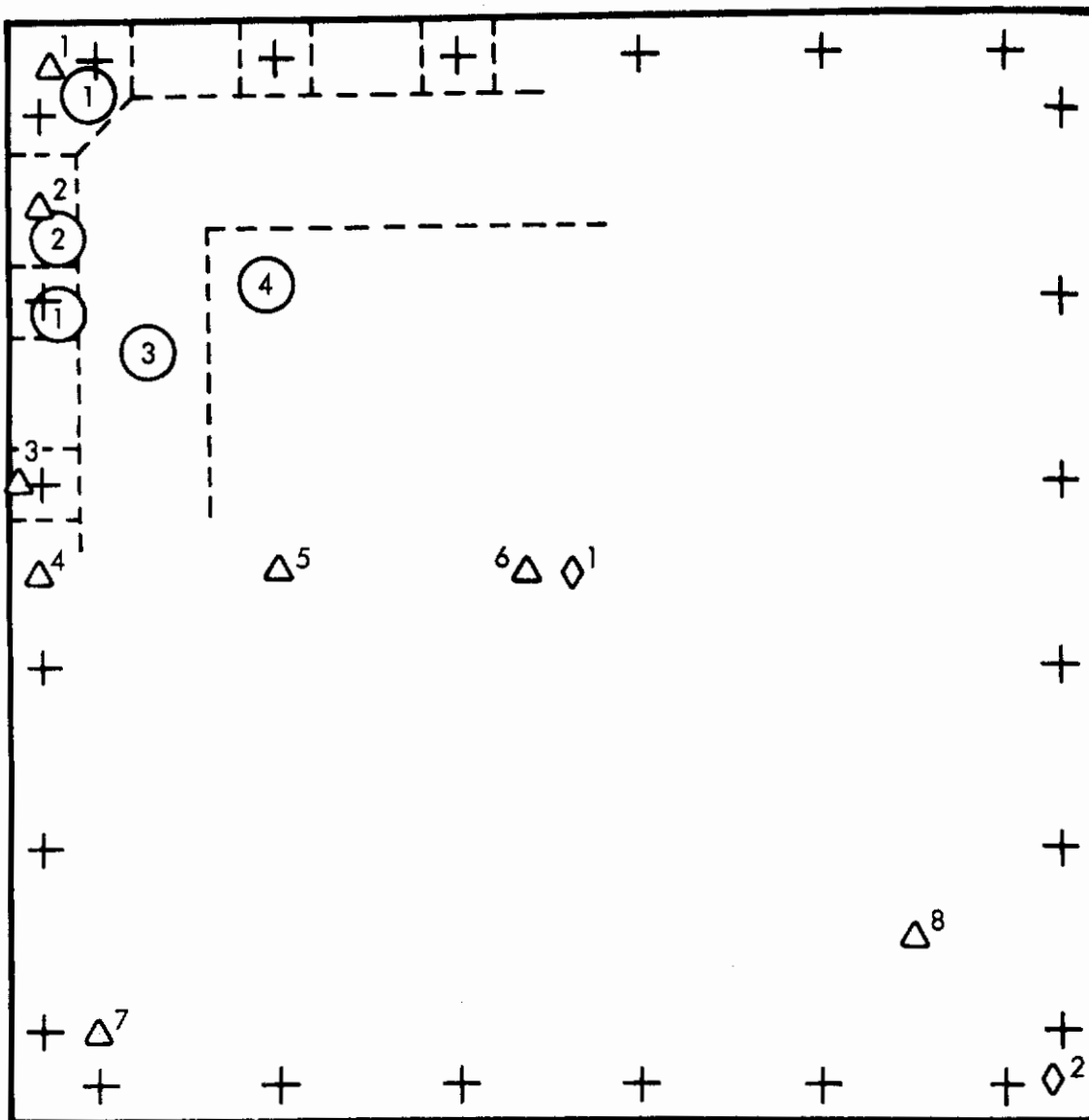
6" x 12" COMPONENT THERMOCOUPLE LOCATION



- | | | | |
|---|--------------------------------|---|---|
| ① | ZONE 1, 12.40 IN. ² | △ | DIFFERENTIAL THERMOCOUPLES |
| ② | ZONE 2, 13.15 IN. ² | ◇ | ABSOLUTE THERMOCOUPLES |
| ③ | ZONE 3, 25.20 IN. ² | + | BOLT LOCATION |
| ④ | ZONE 4, 21.25 IN. ² | ○ | ZONE AREAS USED TO CALCULATE AVERAGE ΔT |

Figure 32. 6" x 12" Component Joint Thermocouple Location

12" x 12" COMPONENT THERMOCOUPLE LOCATION



- | | | | |
|---|--------------------------------|---|---|
| ① | ZONE 1, 15.78 IN. ² | △ | DIFFERENTIAL THERMOCOUPLES |
| ② | ZONE 2, 18.75 IN. ² | ◇ | ABSOLUTE THERMOCOUPLES |
| ③ | ZONE 3, 53.22 IN. ² | + | BOLT LOCATION |
| ④ | ZONE 4, 56.25 IN. ² | ○ | ZONE AREAS USED TO CALCULATE AVERAGE ΔT |

Figure 33. 12" x 12" Component Joint Thermocouple Location

Contrails

Table 9. Experimental Data—6 by 6 Inch Component Joints

Run No.	1	2	3	4	5
Date	10/26/64	10/26/64	10/26/64	10/26/64	10/27/64
Pressure, Torr	6×10^{-7}	6×10^{-7}	6×10^{-7}	6×10^{-7}	5×10^{-7}
Absolute T. C.					
1 - °F	85.7	95.3	107.1	119.0	85.3
2 - °F	80.2	85.6	91.6	97.8	79.8
3 - °F	74.0	74.5	74.5	74.3	73.8
4 - °F	74.1	74.8	75.0	75.0	74.0
Differential T. C.					
1 - °F	6.53	11.78	18.28	24.72	6.72
2 - °F	6.29	11.38	17.60	23.78	6.48
3 - °F	2.50	4.56	7.25	9.85	2.52
4 - °F	4.11	7.06	10.95	14.90	4.05
5 - °F	2.57	4.64	7.25	9.81	2.63
6 - °F	1.02	1.81	2.81	3.81	1.02
7 - °F	1.98	3.52	5.46	7.40	2.00
8 - °F	1.04	1.88	2.92	3.96	1.07
9 - °F	0.80	1.41	2.19	2.97	0.81
10 - °F	0.77	1.31	2.04	2.77	0.74
Voltage, volts	37.02	49.31	61.54	72.04	36.99
Current, amps	0.1314	0.1750	0.2185	0.2560	0.1313
Water Flow, ml/min	725	650	650	650	575
Bolt Torque, in-lb	24	24	24	24	24
Filler	None	None	None	None	None
Sample Number	1	1	1	1	1
Number of Bolts	12	12	12	12	12
h, Btu/hr ft ² °F	23.1	22.9	23.0	22.3	22.8

Contrails

Table 9. Experimental Data—6 by 6 Inch Component Joints (Continued)

Run Number	6	7	8	9	10
Date	10/27/64	10/27/64	10/27/64	10/28/64	10/28/64
Pressure, Torr	5×10^{-7}	5×10^{-7}	5×10^{-7}	6×10^{-7}	7×10^{-7}
Absolute T. C.					
1 - °F	95.1	107.5	118.5	105.5	117.5
2 - °F	85.2	92.3	97.3	89.9	102.3
3 - °F	74.1	74.3	73.3	73.2	74.7
4 - °F	74.5	75.0	74.1	73.6	89.1
Differential T. C.					
1 - °F	11.78	18.30	24.72	18.27	18.68
2 - °F	11.31	17.65	23.89	17.68	17.82
3 - °F	4.48	7.25	9.85	7.22	7.95
4 - °F	7.03	10.95	14.88	10.90	11.32
5 - °F	4.60	7.50	9.79	7.19	7.44
6 - °F	1.78	2.77	3.77	2.78	2.53
7 - °F	3.50	5.45	7.37	5.50	5.04
8 - °F	1.86	2.92	3.96	2.94	2.87
9 - °F	1.40	2.16	2.94	2.19	2.00
10 - °F	1.30	2.00	2.71	2.02	1.82
Voltage, volts	49.33	61.54	72.02	61.53	61.52
Current, amps	0.1751	0.2185	0.2559	0.2185	0.2185
Water Flow, ml/min	525	525	525	1175	21
Bolt Torque, in-lb	24	24	24	24	24
Filler	None	None	None	None	None
Sample Number	1	1	1	1	1
Number of Bolts	12	12	12	12	12
h, Btu/hr ft ² °F	23.2	22.9	23.1	23.0	22.8

Contrails

Table 9. Experimental Data—6 by 6 Inch Component Joints (Continued)

Run Number	11	12	13	14	15
Date	10/29/64	10/29/64	10/29/64	10/29/64	10/30/64
Pressure, Torr	7×10^{-7}	7×10^{-7}	7×10^{-7}	7×10^{-7}	5×10^{-7}
Absolute T. C.					
1 - °F	85.0	94.2	105.7	117.8	84.8
2 - °F	79.8	84.9	91.9	97.5	79.5
3 - °F	73.8	73.9	73.7	73.6	73.6
4 - °F	74.0	74.3	74.3	74.4	73.6
Differential T. C.					
1 - °F	6.22	10.90	17.20	23.37	6.27
2 - °F	5.88	10.29	16.30	22.10	5.93
3 - °F	2.23	4.02	6.62	9.10	2.90
4 - °F	3.88	6.74	10.52	14.31	3.90
5 - °F	2.45	4.30	6.80	9.30	2.55
6 - °F	0.62	1.10	1.73	2.32	0.68
7 - °F	1.83	3.21	5.04	6.81	1.84
8 - °F	0.91	1.61	2.57	3.50	0.95
9 - °F	0.66	1.19	1.87	2.53	0.70
10 - °F	0.74	1.31	2.04	2.73	0.79
Voltage, volts	37.00	49.32	61.54	72.02	37.0
Current, amps	0.1313	0.1751	0.2185	0.2559	0.1313
Water Flow, ml/min	525	550	550	550	500
Bolt Torque, in-lb	30	30	30	30	18
Filler	None	None	None	None	None
Sample Number	1	1	1	1	1
Number of Bolts	12	12	12	12	12
h, Btu/hr ft ² °F	25.0	25.2	24.8	25.0	23.9

Contrails

Table 9. Experimental Data—6 by 6 Inch Component Joints (Continued)

Run Number	16	17	18	19	20
Date	10/30/64	11/2/64	11/2/64	11/2/64	11/2/64
Pressure, Torr	5×10^{-7}	6×10^{-7}	6×10^{-7}	6×10^{-7}	6×10^{-7}
Absolute T. C.					
1 - °F	94.1	81.5	88.4	96.1	104.5
2 - °F	84.8	78.9	84.0	88.9	94.7
3 - °F	73.7	73.2	73.6	73.4	0.891
4 - °F	74.1	73.4	73.9	73.9	
Differential T. C.					
1 - °F	10.99	2.20	3.76	5.76	7.83
2 - °F	10.34	2.25	3.87	5.94	8.05
3 - °F	4.10	0.50	0.83	1.27	1.73
4 - °F	6.76	1.49	2.50	3.90	5.27
5 - °F	4.46	0.43	0.72	1.11	1.52
6 - °F	1.19	0.27	0.47	0.71	0.98
7 - °F	3.21	0.52	0.83	1.26	1.71
8 - °F	1.67	0.15	0.25	0.38	0.53
9 - °F	1.24	0.28	0.44	0.67	0.91
10 - °F	1.38	0.45	0.73	1.11	1.49
Voltage, volts	49.30	37.00	49.34	61.50	72.04
Current, amps	0.1750	0.1313	0.1751	0.2183	0.2558
Water Flow, ml/min	525	600	600	600	600
Bolt Torque, in-lb	18	24	24	24	24
Filler	None	RTV 11	RTV 11	RTV 11	RTV 11
Sample Number	1	1	1	1	1
Number of Bolts	12	12	12	12	12
h , Btu/hr ft ² °F	24.8	76.9	81.5	82.5	83.2

Table 9. Experimental Data—6 by 6 Inch Component Joints (Continued)

Run Number	21	22	23	24	25
Date	11/6/64	11/6/64	11/9/64	11/9/64	11/9/64
Pressure, Torr.	8×10^{-7}	8×10^{-7}	9×10^{-7}	9×10^{-7}	9×10^{-7}
Absolute T. C.					
1 - °F	81.4	91.0	83.7	86.8	95.5
2 - °F	76.0	80.2	74.2	77.5	80.9
3 - °F	73.3	73.8	70.9	71.7	72.1
4 - °F	73.4	74.1	71.1	72.1	72.5
Differential T. C.					
1 - °F	5.76	11.60	5.69	9.82	15.25
2 - °F	5.11	10.29	5.06	8.71	13.56
3 - °F	2.88	5.85	2.87	4.92	7.65
4 - °F	2.29	4.62	2.23	3.82	5.96
5 - °F	0.65	1.32	0.45	0.76	1.18
6 - °F	1.36	2.76	1.26	2.17	3.38
7 - °F	0.95	1.97	0.91	1.55	2.44
8 - °F	0.48	1.02	0.44	0.74	1.17
9 - °F					
10 - °F					
Voltage, volts	37.03	53.01	37.01	49.33	61.53
Current, amps	0.1315	0.1883	0.1314	0.1752	0.2186
Water Flow, ml/min	1300	675	575	575	575
Bolt Torque, in-lb	12	12	24	24	24
Filler	None	None	None	None	None
Sample Number	2	2	2	2	2
Number of Bolts	12	12	12	12	12
h, Btu/hr ft ² °F	24.7	28.5	29.1	30.1	30.1

Contrails

Table 9. Experimental Data—6 by 6 Inch Component Joints (Continued)

Run Number	26	27	28	29	30
Date	11/9/64	11/10/64	11/13/64	11/17/64	11/17/64
Pressure, Torr.	9×10^{-7}	1×10^{-6}	1×10^{-6}	1×10^{-6}	1×10^{-6}
Absolute T. C.					
1 - °F	104.7	88.2	81.2	71.6	75.7
2 - °F	84.5	77.4	75.4	69.0	70.9
3 - °F	72.1	70.8	69.9	66.0	70.9
4 - °F	73.0	71.3	70.4	66.4	66.5
Differential T. C.					
1 - °F	20.93	11.30	3.78	1.80	3.08
2 - °F	18.57	10.09	3.38	1.61	2.76
3 - °F	10.51	5.74	1.38	0.63	1.11
4 - °F	8.19	4.50	0.72	0.31	0.58
5 - °F	1.63	0.84	0.29	0.21	0.36
6 - °F	4.62	2.54	0.20	0.091	0.20
7 - °F	3.34	1.78	0.26	0.095	0.20
8 - °F	1.63	0.89	0.26	0.091	0.27
9 - °F					
10 - °F					
Voltage, volts	72.03	53.01	53.03	37.02	49.31
Current, amps	0.2560	0.1883	0.1883	0.1314	0.1751
Water Flow, ml/min	575	575	575	625	600
Bolt Torque, in-lb	24	30	12	24	24
Filler	None	None	RTV 11	RTV 11	RTV 11
Sample Number	2	2	2	2	2
Number of Bolts	12	12	12	12	12
h, Btu/hr ft ² °F	30.1	30.0	123.0	128.1	127.0

Contrails

Table 9. Experimental Data—6 by 6 Inch Component Joints (Continued)

Run Number	31	32	33	34	35
Date	11/17/64	11/17/64	11/19/64	11/20/64	11/23/64
Pressure, Torr	1×10^{-6}	1×10^{-6}	7×10^{-7}	1×10^{-6}	1×10^{-6}
Absolute T. C.					
1 - °F	81.7	87.0	78.8	80.6	72.1
2 - °F	74.2	76.5	73.4	72.5	68.2
3 - °F	66.2	66.1	67.7	66.7	65.2
4 - °F	67.0	67.0	68.2	67.1	65.4
Differential T. C.					
1 - °F	4.72	6.39	3.39	7.25	3.62
2 - °F	4.25	5.77	3.04	6.20	1.29
3 - °F	1.73	2.35	1.12	3.12	1.57
4 - °F	0.89	1.24	0.54	2.22	1.07
5 - °F	0.51	0.67	0.31	0.37	0.19
6 - °F	0.30	0.41	0.17	0.93	0.45
7 - °F	0.29	0.37	0.17	0.53	0.23
8 - °F	0.44	0.65	0.30	0.42	0.15
9 - °F					
10 - °F					
Voltage, volts	61.51	72.05	53.01	52.99	37.00
Current Amps	0.2185	0.2560	0.1883	0.1879	0.1312
Water Flow, ml/min	600	600	600	600	460
Bolt Torque, in-lb	24	24	30	12	24
Filler	RTV 11	RTV 11	RTV 11	G 683	G 683
Sample Number	2	2	2	2	2
Number of Bolts	12	12	12	12	12
h, Btu/hr ft ² °F	129.0	130.0	142.0	55.5	63.0

Contrails

Table 9. Experimental Data—6 by 6 Inch Component Joints (Continued)

Run Number	36	37	38	39	40
Date	11/23/64	11/23/64	11/23/64	11/23/64	11/24/64
Pressure, Torr	1×10^{-6}	1×10^{-6}	1×10^{-6}	1×10^{-6}	5×10^{-7}
Absolute T. C.					
1 - °F	78.3	85.7	92.4	79.9	88.1
2 - °F	71.4	74.7	77.4	71.7	73.9
3 - °F	66.0	66.7	66.5	65.9	66.7
4 - °F	66.5	67.4	67.5	66.4	67.1
Differential T. C.					
1 - °F	6.20	9.46	12.83	7.15	13.58
2 - °F	2.07	3.11	4.15	6.15	13.37
3 - °F	2.72	4.17	5.63	2.99	6.59
4 - °F	1.86	2.88	3.89	2.37	4.72
5 - °F	0.33	0.52	0.67	0.33	1.07
6 - °F	0.77	1.17	1.56	0.72	3.35
7 - °F	0.42	0.66	0.87	0.44	2.22
8 - °F	0.34	0.56	0.77	0.34	1.18
9 - °F					
10 - °F					
Voltage, volts	49.31	61.53	72.04	52.96	52.96
Current, amps	0.1749	0.2183	0.2556	0.1878	0.1880
Water Flow, ml/min	460	460	460	475	560
Bolt Torque, in-lb	24	24	24	30	12
Filler	G 683	G 683	G 683	G 683	None
Sample Number	2	2	2	2	3
Number of Bolts	12	12	12	12	12
h, Btu/hr ft ² °F	65.0	66.1	67.1	57.0	24.8

Contrails

Table 9. Experimental Data—6 by 6 Inch Component Joints (Continued)

Run Number	41	42	43	44	45
Date	11/24/64	11/25/64	11/25/64	11/25/64	11/25/64
Pressure, Torr	5×10^{-7}	5×10^{-6}	5×10^{-6}	5×10^{-7}	5×10^{-7}
Absolute T. C.					
1 - °F	92.6	88.4	92.7	77.5	85.0
2 - °F	81.8	74.9	75.0	70.7	72.9
3 - °F	66.6	65.9	66.4	66.8	66.2
4 - °F	67.0	66.4	66.9	67.0	66.7
Differential T. C.					
1 - °F	17.64	14.32	18.42	6.70	11.50
2 - °F	17.70	13.93	18.45	6.65	11.44
3 - °F	11.94	7.36	10.19	3.17	5.45
4 - °F	7.46	4.97	10.59	2.26	3.92
5 - °F	1.80	1.11	9.44	4.78	0.80
6 - °F	7.80	4.26	7.95	1.57	2.67
7 - °F	10.18	3.26	3.64	0.93	1.65
8 - °F	10.40	2.53	1.61	0.49	0.92
9 - °F					
10 - °F					
Voltage, volts	52.96	52.95	52.95	37.01	49.32
Current, amps	0.1880	0.1880	0.1880	0.1313	0.1751
Water Flow, ml/min	700	575	550	625	625
Bolt Torque, in-lb	24	24	24	24	24
Filler	None	None	None	None	None
Sample Number	3	3	3	3	3
Number of Bolts	4*	8*	8*	12	12
h, Btu/hr ft ² °F	13.4	22.0	13.7	22.1	25.9

*See Appendix VI.

Contrails

Table 9. Experimental Data—6 by 6 Inch Component Joints (Continued)

Run Number	46	47	48	49	50
Date	11/27/64	11/27/64	11/30/64	12/3/64	12/3/64
Pressure, Torr	5×10^{-7}	5×10^{-7}	6×10^{-7}	4×10^{-7}	4×10^{-7}
Absolute T. C.					
1 - °F	94.6	105.5	81.8	73.0	79.1
2 - °F	75.7	79.6	72.7	68.8	71.5
3 - °F	65.4	65.5	66.0	65.3	65.8
4 - °F	66.0	66.4	66.5	65.6	66.3
Differential T. C.					
1 - °F	17.67	23.95	5.63	2.63	4.54
2 - °F	17.59	23.80	6.21	3.00	5.14
3 - °F	8.36	11.31	1.81	0.76	1.32
4 - °F	6.02	8.20	0.75	0.27	0.45
5 - °F	1.26	1.69	0.24	0.14	0.21
6 - °F	4.14	5.60	0.24	0.13	0.20
7 - °F	2.59	3.54	0.24	0.12	0.23
8 - °F	1.49	2.02	0.37	0.05	0.23
9 - °F					
10 - °F					
Voltage, volts	61.52	72.06	53.01	37.00	49.34
Current, amps	0.2184	0.2560	0.1881	0.1313	0.1751
Water Flow, ml/min	600	600	600	550	550
Bolt Torque, in-lb	24	24	12	24	24
Filler	None	None	RTV 11	RTV 11	RTV 11
Sample Number	3	3	3	3	3
Number of Bolts	12	12	12	12	12
h , Btu/hr ft ² °F	26.2	26.6	84.1	91.0	93.5

Contrails

Table 9. Experimental Data—6 by 6 Inch Component Joints (Continued)

Run Number	51	52	53	54
Date	12/3/64	12/3/64	12/4/64	12/4/64
Pressure, Torr	4×10^{-7}	4×10^{-7}	5×10^{-7}	2×10^{-6}
Absolute T. C.				
1 - °F	86.8	94.9	83.5	75.6
2 - °F	74.8	78.5	72.2	70.0
3 - °F	66.2	66.2	65.6	66.7
4 - °F	66.9	67.1	66.0	67.0
Differential T. C.				
1 - °F	6.95	9.44	8.95	4.52
2 - °F	7.86	10.62	9.19	4.48
3 - °F	2.03	2.77	3.22	1.59
4 - °F	0.70	0.96	2.25	1.09
5 - °F	0.30	0.40	0.26	0.12
6 - °F	0.29	0.40	0.92	0.42
7 - °F	0.37	0.52	0.70	0.28
8 - °F	0.44	0.67	0.42	0.11
9 - °F				
10 - °F				
Voltage, volts	61.54	72.05	53.01	37.05
Current, amps	0.2184	0.2558	0.1878	0.1312
Water Flow, ml/min	550	550	650	600
Bolt Torque, in-lb	24	24	12	24
Filler	RTV 11	RTV 11	G 683	G 683
Sample Number	3	3	3	3
Number of Bolts	12	12	12	12
h, Btu/hr ft ² °F	94.8	95.4	47.0	47.3

Table 9. Experimental Data—6 by 6 Inch Component Joints (Continued)

Run Number	55	56	57	58
Date	12/4/64	12/7/64	12/7/64	12/8/64
Pressure, Torr	5×10^{-8}	1×10^{-6}	1×10^{-6}	5×10^{-7}
Absolute T. C.				
1 - °F	81.9	88.0	97.1	71.0
2 - °F	72.9	72.9	76.4	66.3
3 - °F	63.5	63.5	63.8	63.1
4 - °F	64.3	63.4	64.7	63.5
Differential T. C.				
1 - °F	7.70	11.80	15.93	3.12
2 - °F	7.74	11.88	16.05	3.25
3 - °F	2.76	4.25	5.74	0.85
4 - °F	1.91	2.98	4.02	0.48
5 - °F	0.22	0.36	0.48	0.15
6 - °F	0.74	1.09	1.48	0.18
7 - °F	0.54	0.81	1.10	0.73
8 - °F	0.33	0.51	0.76	0.
9 - °F				
10 - °F				
Voltage, volts	49.36	61.52	72.04	37.02
Current, amps	0.1748	0.2180	0.2554	0.1311
Water Flow, ml/min	600	500	500	525
Bolt Torque, in-lb	24	24	24	24
Filler	G 683	G 683	G 683	G 641
Sample Number	3	3	3	3
Number of Bolts	12	12	12	12
h, Btu/hr ft ² °F	48.2	48.8	49.5	77.5

Contrails

Table 9. Experimental Data—6 by 6 Inch Component Joints (Continued)

Run Number	59	60	61
Date	12/8/64	12/8/64	12/8/64
Pressure, Torr	5×10^{-7}	5×10^{-7}	5×10^{-7}
Absolute T. C.			
1 - °F	77.8	85.8	93.8
2 - °F	69.7	73.2	76.8
3 - °F	63.9	64.5	64.8
4 - °F	64.4	65.2	65.8
Differential T. C.			
1 - °F	5.36	8.20	11.10
2 - °F	5.58	8.56	11.56
3 - °F	1.47	2.27	3.07
4 - °F	0.85	1.34	1.81
5 - °F	0.22	0.32	0.40
6 - °F	0.33	0.51	0.70
7 - °F	0.20	0.37	0.54
8 - °F	0.19	0.45	0.69
9 - °F			
10 - °F			
Voltage, volts	49.35	61.52	72.02
Current, amps	0.1748	0.2180	0.2553
Water Flow, ml/min	525	525	525
Bolt Torque, in-lb	24	24	24
Filler	G 641	G 641	G641
Sample Number	3	3	3
Number of Bolts	12	12	12
h, Btu/hr ft ² °F	79.0	79.0	79.5

Table 10. Experimental Data—6 by 12 Inch Component Joints

Run Number	62	63	64	65	66
Date	12/9/64	12/9/64	12/9/64	12/10/64	12/10/64
Pressure, Torr	3×10^{-7}	3×10^{-7}	3×10^{-7}	5×10^{-7}	5×10^{-7}
Absolute T. C.					
1 - °F	74.4	84.9	106.0	74.9	70.0
2 - °F	67.7	71.6	79.0	68.1	66.7
3 - °F	63.8	63.9	63.5	64.0	64.5
4 - °F	64.3	64.8	65.2	64.6	64.9
Differential T. C.					
1 - °F	2.43	5.93	8.94	3.02	1.35
2 - °F	1.94	3.87	7.90	1.96	0.98
3 - °F	5.83	11.57	23.50	5.87	2.94
4 - °F	5.22	10.40	22.02	5.17	2.59
5 - °F	3.15	11.71	29.30	7.22	3.64
6 - °F	2.49	4.95	10.20	2.47	1.24
7 - °F	0.73	1.43	2.85	0.75	0.39
8 - °F	1.33	2.61	5.37	1.31	0.66
9 - °F	0.50	1.00	2.09	0.51	0.25
Voltage, volts	35.48	50.00	70.70	35.47	25.00
Currents, amps	0.2837	0.4000	0.5667	0.2840	0.2001
Water Flow, ml/min	575	600	600	550	550
Bolt Torque, in-lb	24	24	24	24	24
Filler	None	None	None	None	None
Sample Number	1	1	1	1	1
Number of Bolts	18	18	18	18	18
h, Btu/hr ft ² °F	22.7	19.5	18.5	18.5	18.5

Contrails

Table 10. Experimental Data—6 by 12 Inch Component Joints

Run Number	67	68	69	70	71
Date	12/10/64	12/14/64	12/14/64	12/14/64	12/17/64
Pressure, Torr.	5×10^{-7}	4×10^{-7}	4×10^{-7}	4×10^{-7}	6×10^{-7}
Absolute T. C.					
1 - °F	86.5	70.4	76.0	88.3	68.6
2 - °F	73.3	67.9	70.8	77.6	65.2
3 - °F	65.2	64.6	65.0	66.5	62.0
4 - °F	66.2	65.1	65.9	67.7	62.6
Differential T. C.					
1 - °F	4.72	0.32	0.66	1.68	0.64
2 - °F	3.86	0.22	0.44	0.95	0.28
3 - °F	11.60	1.25	2.52	5.26	1.27
4 - °F	10.37	1.06	2.09	4.24	1.05
5 - °F	14.36	1.55	3.06	6.15	1.42
6 - °F	4.95	0.22	0.48	1.02	0.15
7 - °F	1.46	0.19	0.37	0.80	0.08
8 - °F	2.60	0.18	0.41	0.91	0.04
9 - °F	1.02	0.12	0.29	0.61	
Voltage, volts	50.00	35.47	50.00	70.73	35.49
Current, amps	0.4005	0.2839	0.4004	0.5669	0.2822
Water Flow, ml/min	550	625	625	625	575
Bolt Torque, in-lb	24	24	24	24	24
Filler	None	RTV 11	RTV 11	RTV 11	RTV 11
Sample Number	1	1	1	1	2
Number of Bolts	18	18	18	18	18
h, Btr/hr ft ² °F	18.9	103.0	101.5	98.0	103.0

Contrails

Table 10. Experimental Data—6 by 12 Inch Component Joints (Continued)

Run Number	72	73	74	75	76
Date	12/17/64	12/17/64	12/21/64	12/21/64	12/21/64
Pressure, Torr.	6×10^{-7}	6×10^{-7}	6×10^{-7}	6×10^{-7}	6×10^{-7}
Absolute T. C.					
1 - °F	75.5	88.5	67.5	73.5	86.2
2 - °F	68.8	75.0	64.2	67.0	73.4
3 - °F	62.6	62.8	61.1	61.1	61.6
4 - °F	63.6	64.8	61.6	61.9	63.3
Differential T. C.					
1 - °F	1.37	2.85	0.71	1.41	2.88
2 - °F	0.59	1.21	0.27	0.52	1.05
3 - °F	2.52	5.50	1.26	2.48	5.02
4 - °F	2.13	4.30	1.21	2.37	4.74
5 - °F	2.86	5.76	1.79	3.51	7.05
6 - °F	0.33	0.71	0.17	0.30	0.57
7 - °F	0.12	0.23	0.11	0.20	0.36
8 - °F	0.11	0.26	0.16	0.30	0.61
9 - °F		0	0.08	0.17	0.38
Voltage, volts	50.02	70.64	35.48	50.01	70.71
Current, amps	0.3980	0.5628	0.2834	0.3995	0.5651
Water Flow, ml/min	575	575	650	650	650
Bolt Torque, in-lb	24	24	24	24	24
Filler	RTV 11	RTV 11	RTV 11	RTV 11	RTV 11
Sample Number	2	2	3	3	3
Number of Bolts	18	18	18	18	18
h, Btu/hr ft ² °F	101.0	97.0	90.0	92.0	92.0

Table 11. Experimental Data—12 by 12 Inch Component Joint

Run	77	78	79	80
Date	12/22/64	12/22/64	12/22/64	12/28/64
Pressure, Torr	4×10^{-7}	4×10^{-7}	4×10^{-7}	6×10^{-7}
Absolute T. C.				
1 - °F	80.5	100.2	138.6	69.9
2 - °F	66.3	71.6	82.3	65.6
3 - °F	61.1	60.9	61.4	61.8
4 - °F	62.0	62.8	65.2	62.8
Differential T. C.				
1 - °F	0.58	0.92	1.64	0.51
2 - °F	1.89	3.85	7.73	0.28
3 - °F	1.35	2.75	5.19	0.18
4 - °F	3.29	6.75	13.40	0.10
5 - °F	12.10	24.50	48.60	1.49
6 - °F	16.42	33.20	65.80	3.14
7 - °F	1.30	2.69	5.36	0.12
8 - °F	5.78	11.59	22.90	0.70
Voltage, volts	29.60	41.90	59.20	29.61
Current, amps	0.6753	0.9543	1.3437	0.6748
Water Flow, ml/min	550	550	550	600
Bolt Torque, in-lb	24	24	24	24
Filler	None	None	None	RTV 11
Sample Number	1	1	1	1
Number of Bolts	24	24	24	24
h, Btu/hr ft ² °F	8.36	8.32	8.34	56.6

Table 11. Experimental Data—12 by 12 Inch Component Joint (Continued)

Run	81	82	83	84
Date	12/28/64	12/28/64	1/5/65	1/5/65
Pressure, Torr	6×10^{-7}	6×10^{-7}	8×10^{-8}	8×10^{-7}
Absolute T. C.				
1 - °F	77.7	93.3	68.7	77.3
2 - °F	69.0	76.0	64.5	69.5
3 - °F	61.5	61.7	60.5	61.4
4 - °F	63.4	65.3	61.7	63.5
Differential T. C.				
1 - °F	0.72	0.98	0.31	0.53
2 - °F	0.53	1.04	0.20	0.37
3 - °F	0.37	0.68	0.20	0.35
4 - °F	0.22	0.48	0.12	0.20
5 - °F	2.95	5.91	1.74	3.39
6 - °F	6.25	12.41	2.76	5.42
7 - °F	0.27	0.55	0.14	0.25
8 - °F	1.48	2.94	1.06	2.10
Voltage, volts	41.83	59.22	29.59	41.84
Current, amps	0.9527	1.3460	0.6747	0.9521
Water Flow, ml/min	600	600	550	550
Bolt Torque, in-lb	24	24	24	24
Filler	RTV 11	RTV 11	RTV 11	RTV 11
Sample Number	1	1	2	2
Number of Bolts	24	24	24	24
h, Btu/hr ft ² °F	55.8	56.1	51.7	52.8

Table 11. Experimental Data—12 by 12 Inch Component Joint (Continued)

Run	85	86	87	88
Date	1/5/65	1/7/65	1/7/65	1/8/65
Pressure, Torr	8×10^{-7}	8×10^{-7}	8×10^{-7}	5×10^{-7}
Absolute T. C.				
1 - °F	95.6	69.0	76.9	92.7
2 - °F	79.2	64.8	68.3	75.7
3 - °F	63.4	60.6	60.4	59.1
4 - °F	67.1	61.6	62.3	63.3
Differential T. C.				
1 - °F	1.06	0.42	0.57	0.87
2 - °F	0.77	0.17	0.32	0.66
3 - °F	0.65	0.13	0.28	0.60
4 - °F	0.37	-	-	-
5 - °F	6.80	1.89	3.76	7.54
6 - °F	10.80	2.91	5.72	11.40
7 - °F	0.63	0.14	0.30	0.64
8 - °F	4.64	0.93	1.85	3.58
Voltage, volts	59.26	29.65	41.85	59.25
Current, amps	1.3436	0.6750	0.9518	1.3440
Water Flow, ml/min	550	550	550	500
Bolt Torque, in-lb	24	24	24	24
Filler	RTV 11	RTV 11	RTV 11	RTV 11
Sample Number	2	3	3	3
Number of Bolts	24	24	24	24
h, Btu/hr ft ² °F	51.0	51.4	51.9	52.4

APPENDIX II
STRUCTURAL JOINT TESTS

Contrails

The experimental data for structural joint configuration No. 1 (Figure 3 of main report) is given in Table 12 of this appendix. The location of thermocouples is shown in Figures 34 and 35. The average ΔT for each joint, called "a" and "b," was obtained by dividing the joint area into zones. Two zones were used, a one inch square zone at each bolt, with the bolt in the center, and the remaining area as the other zone. The water flow rate and temperatures were monitored as in the component joints, and absolute thermocouples 2 and 3 measure inlet and outlet temperatures respectively. For run number 1, the conductance calculation for joint "a" is as follows:

$$\overline{\Delta T}_{\textcircled{1}} = 3.56^{\circ}\text{F}$$

$$\overline{\Delta T}_{\textcircled{2}} = \frac{6.10 + 8.17}{2} = 7.13^{\circ}\text{F}$$

$$\overline{\Delta T}_M = \frac{A_1}{A_T} \overline{\Delta T}_1 + \frac{A_2}{A_T} \overline{\Delta T}_2$$

$$\overline{\Delta T}_M = \frac{2}{6} (3.56) + \frac{4}{6} (7.13)$$

$$\overline{\Delta T}_M = 5.95^{\circ}\text{F}$$

$$Q_{\text{IN}} = 22.05(0.2310) = 5.099 \text{ watts}$$

$$= 17.4 \text{ Btu/hr}$$

$$h_a = \frac{Q}{A \overline{\Delta T}_M}$$

$$h_a = \frac{17.4}{\frac{6}{144} \times 5.95} = 70.3 \text{ Btu/hr ft}^2 \text{ }^{\circ}\text{F}$$

Thermocouples 1, 2, and 3 are used to calculate the conductance of joint "a," h_a , and thermocouples 6, 7, and 8 to calculate the conductance of joint "b," h_b .

Contrails

Table 13 lists the experimental data for structural joint configuration 2. The thermocouple locations are shown in Figures 34 and 35. This configuration utilizes nut plates on one joint, called joint "b" in Table 13.

The results for configuration 3 are shown in Table 14, and the thermocouple locations in Figures 36 and 37. Differential thermocouples are located at the same (x, y) coordinates on the back of the angle brackets and panels at the locations shown on Figures 34, 35, 36, and 37.

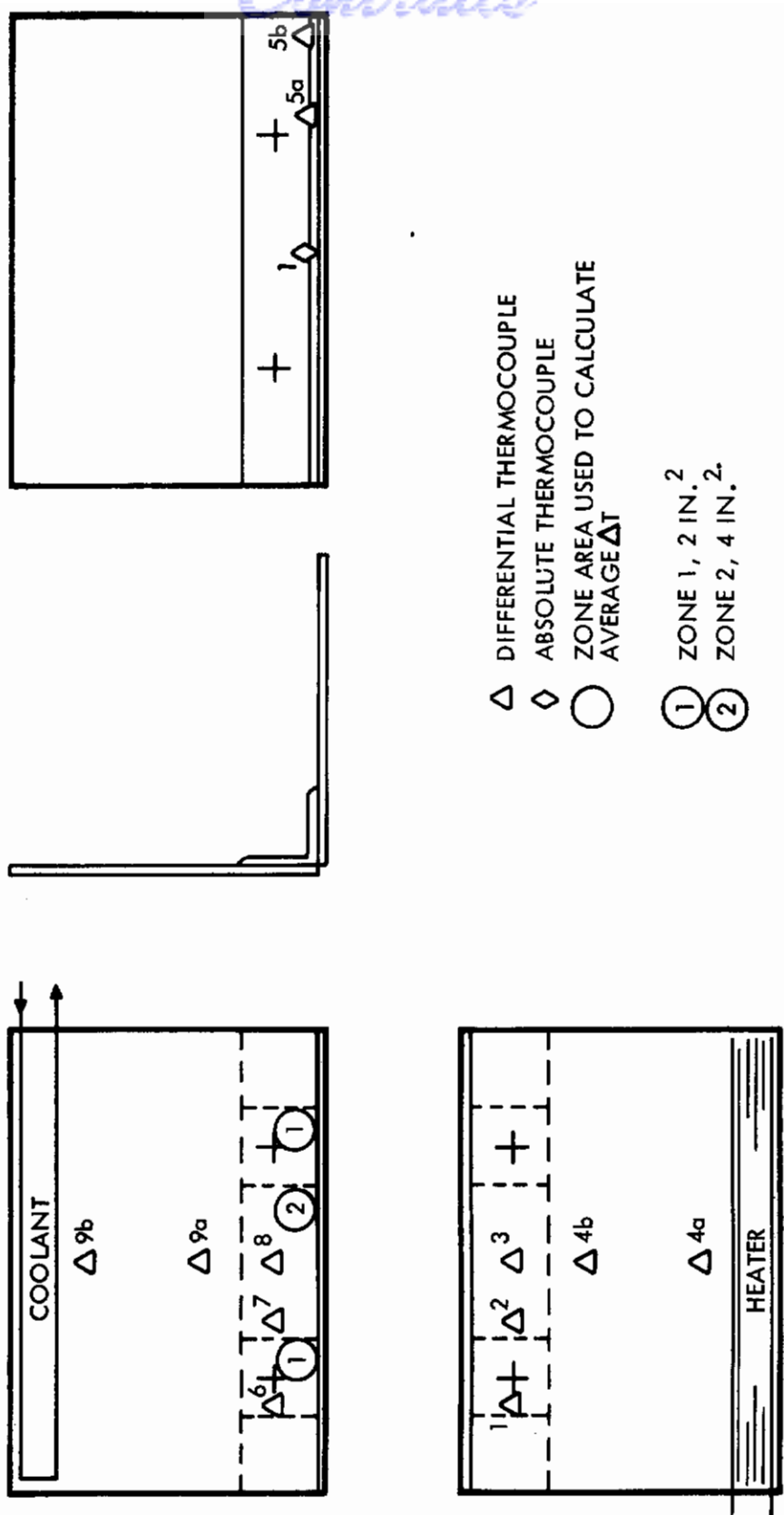
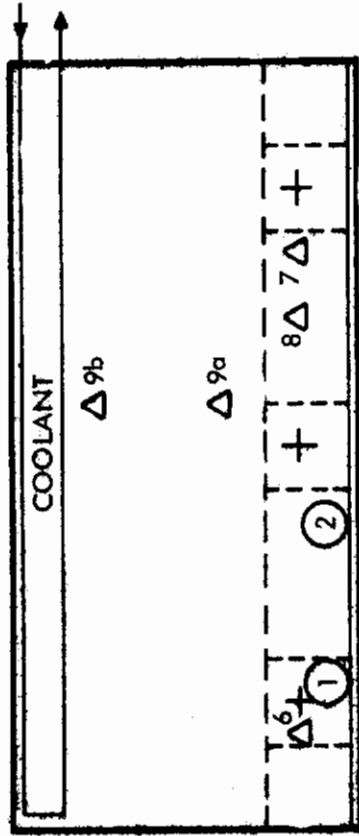
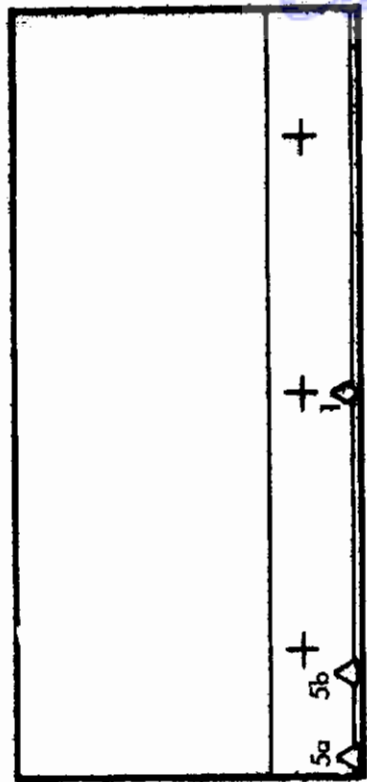


Figure 34. 6 Inch Structural Joint, Configurations 1 and 2, Thermocouple Locations



- Δ DIFFERENTIAL THERMOCOUPLE
- ◇ ABSOLUTE THERMOCOUPLE
- ZONE AREA USED TO CALCULATE AVERAGE ΔT
- ① ZONE 1, 3 IN.²
- ② ZONE 2, 6 IN.²

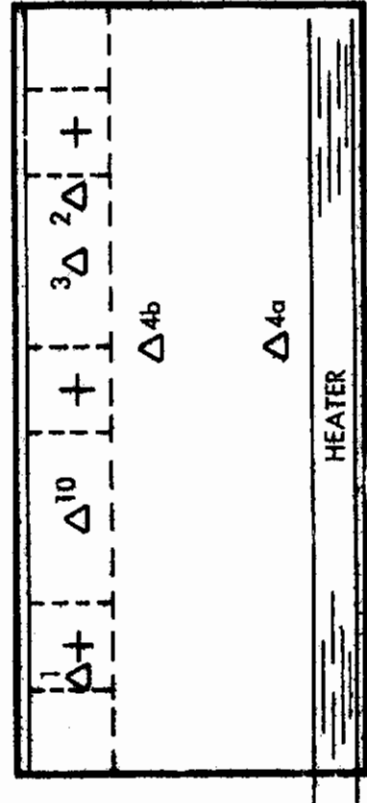


Figure 35. 9 Inch Structural Joint, Configurations 1 and 2, Thermocouple Locations

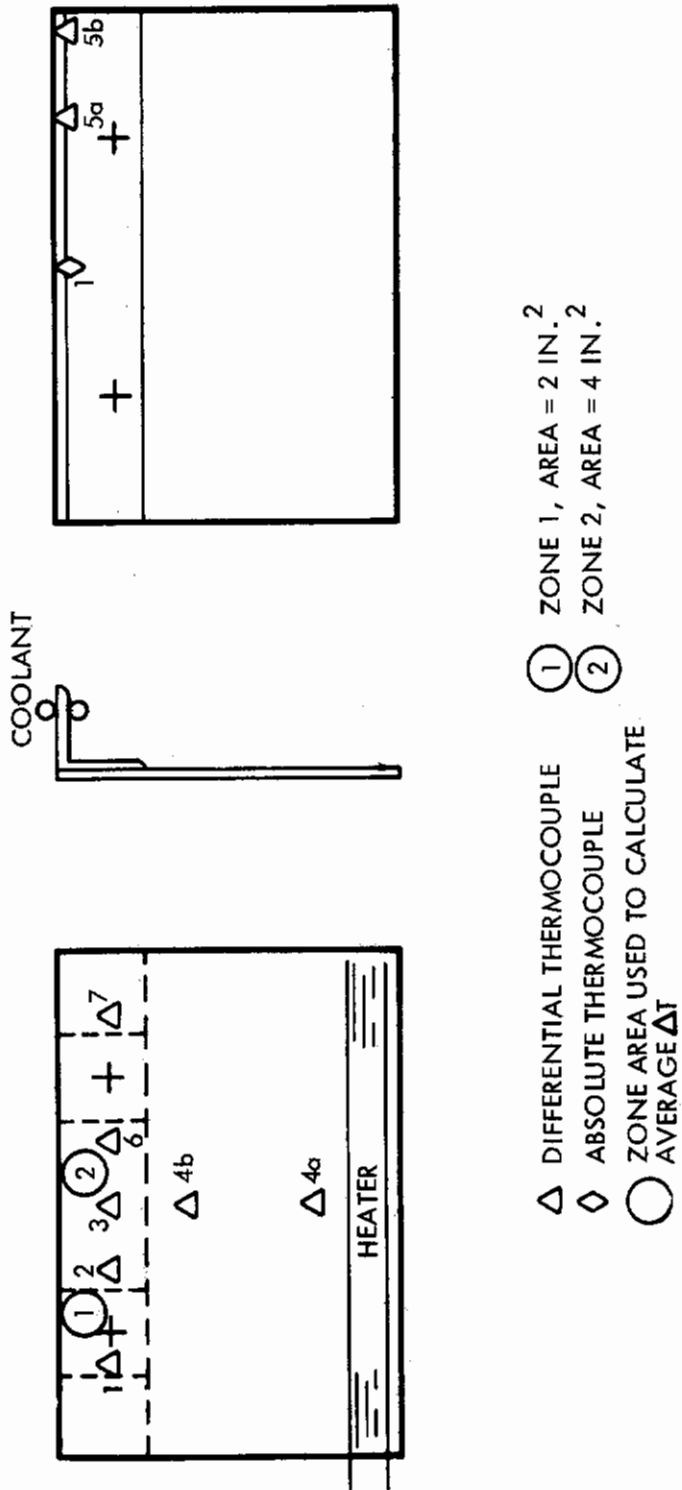


Figure 36. 6 Inch Structural Joint, Configuration 3, Thermocouple Locations

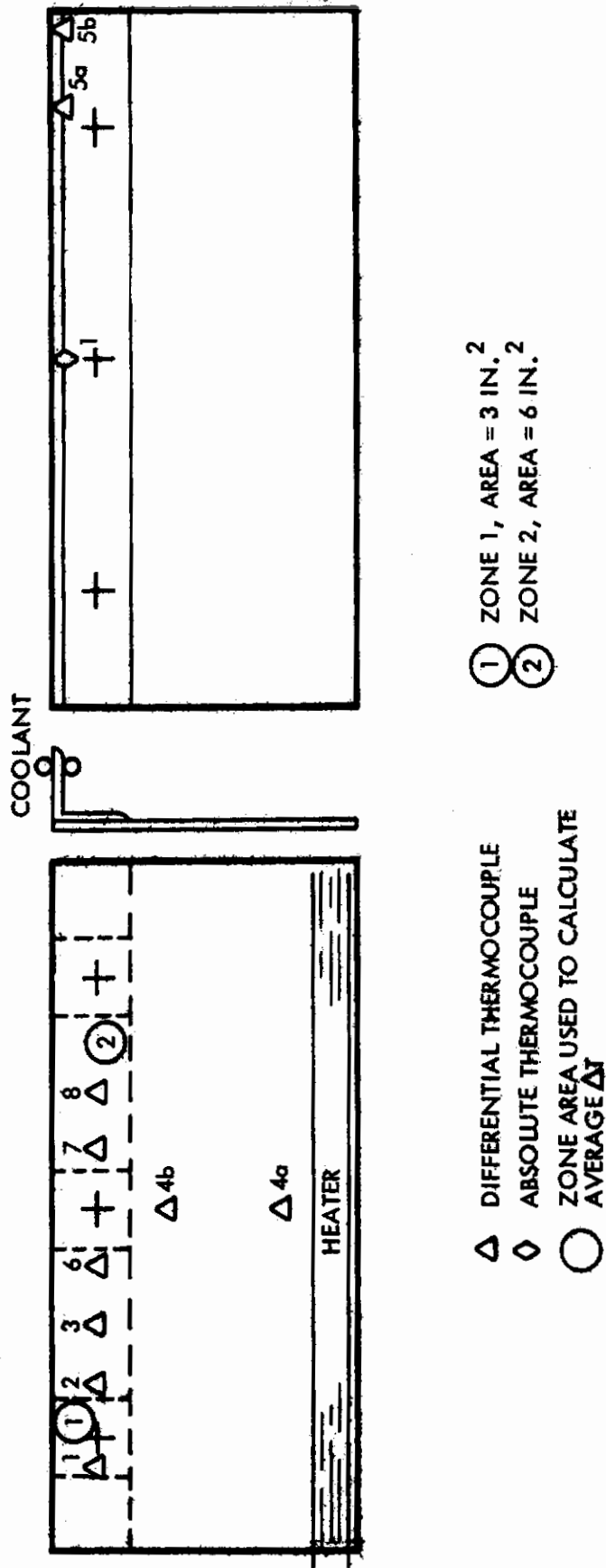


Figure 37. 9 Inch Structural Joint, Configuration 3, Thermocouple Locations

Table 12. Experimental Data—Structural Joint Configuration 1

Run Number	1	2	3	4	5
Date	2/16/65	2/16/65	2/16/65	2/17/65	3/1/65
Pressure, Torr	2×10^{-6}	2×10^{-6}	2×10^{-6}	1×10^{-6}	1×10^{-6}
Absolute T. C.					
1 - °F	93.0	126.2	158.4	196.7	88.0
2 - °F	63.5	63.8	63.0	60.2	63.1
3 - °F	63.9	64.4	63.9	61.4	63.5
Differential T. C.					
1 - °F	3.56	7.46	11.32	16.00	0.22
2 - °F	6.10	12.48	18.32	25.55	0.54
3 - °F	8.17	17.05	26.55	37.70	0.45
4 - °F	7.89	16.82	26.30	36.95	7.95
5 - °F	0.50	0.97	1.51	2.13	0.06
6 - °F	3.30	7.00	10.72	14.90	0.20
7 - °F	5.11	11.47	17.60	23.93	0.33
8 - °F	7.24	14.72	23.28	31.60	0.65
9 - °F	6.72	13.88	21.44	30.10	7.30
10 - °F					
Voltage, volts	22.05	32.21	40.17	48.17	22.00
Current, amps	0.2310	0.3376	0.4216	0.5061	0.2306
Water Flow, ml/min	750	750	750	550	700
Bolt Torque, in-lb	24	24	24	24	24
Filler	None	None	None	None	RTV 11
Sample Number	1	1	1	1	1
Joint Length, in.	6	6	6	6	6
Number of Bolts	2	2	2	2	2
h_a , Btu/hr ft ² °F	70.3	72.0	74.2	75.7	1042
h_b , Btu/hr ft ² °F	80.5	80.6	80.6	85.3	1042

Table 12. Experimental Data—Structural Joint Configuration 1 (Continued)

Run Number	6	7	8	9	10
Date	3/1/65	3/1/65	2/19/65	2/19/65	2/19/65
Pressure, Torr	1×10^{-6}	1×10^{-6}	1×10^{-6}	1×10^{-6}	1×10^{-6}
Absolute T. C.					
1 - °F	141.0	176.6	88.4	149.8	184.9
2 - °F	62.8	62.6	61.1	62.3	61.3
3 - °F	63.6	63.7	61.6	63.1	62.5
Differential T. C.					
1 - °F	0.88	2.30	2.58	8.25	11.31
2 - °F	1.95	3.36	4.08	14.20	20.52
3 - °F	1.61	2.77	5.44	18.88	27.42
4 - °F	25.10	38.60	8.06	26.22	37.95
5 - °F	0.33	2.75	0	0.04	0.13
6 - °F	0.68	0.82	3.50	11.24	15.88
7 - °F	1.08	2.05	4.50	14.80	19.80
8 - °F	2.28	3.89	6.17	19.93	26.08
9 - °F	22.58	33.75	7.82	24.17	34.85
10 - °F					
Voltage, volts	39.52	48.40	22.01	39.99	47.92
Current, amps	0.4149	0.5085	0.2319	0.4223	0.5067
Water Flow, ml/min	700	700	650	650	650
Bolt Torque, in-lb	24	24	24	24	24
Filler	RTV 11	RTV 11	None	None	None
Sample Number	1	1	2	2	2
Joint Length, in.	6	6	6	6	6
Number of Bolts	2	2	2	2	2
h_a , Btu/hr ft ² °F	906	715	103.5	100.1	100.9
h_b , Btu/hr ft ² °F	995	895	88.5	90	96.5

Contrails

Table 12. Experimental Data — Structural Joint Configuration 1 (Continued)

Run Number	11	12	13	14	15
Date	3/5/65	3/5/65	3/8/65	3/9/65	3/9/65
Pressure, Torr	2×10^{-6}	2×10^{-6}	1×10^{-6}	8×10^{-7}	8×10^{-7}
Absolute T. C.					
1 - °F	90.5	142.5	192.1	87.7	134.7
2 - °F	63.5	63.4	62.9	62.8	62.5
3 - °F	63.9	64.1	64.0	63.1	63.1
Differential T. C.					
1 - °F	7.12	21.30	35.8	0.50	1.50
2 - °F	5.98	18.07	30.82	0.75	2.44
3 - °F	2.61	7.99	13.70	0.77	2.27
4 - °F	7.21	21.42	36.0	7.92	23.70
5 - °F	1.74	4.96	7.85	0.35	1.02
6 - °F	7.21	21.05	32.65	0	0.07
7 - °F	5.87	17.37	28.5	0.65	2.08
8 - °F	2.84	8.36	14.4	1.16	3.53
9 - °F	6.98	20.05	33.15	6.98	20.47
10 - °F	1.37	3.84	5.49		
Voltage, volts	21.58	37.50	48.22	21.83	37.83
Current, amps	0.2327	0.4050	0.5217	0.2289	0.3972
Water Flow, ml/min	675	675	700	750	750
Bolt Torque, in-lb	24	24	24	24	24
Filler	None	None	None	G 683	G 683
Sample Number	3	3	3	1	1
Joint Length, in.	6	6	6	6	6
Number of Bolts	2	2	2	2	2
h_a , Btu/hr ft ² °F	78.5	79.4	77.0	602	595
h_b , Btu/hr ft ² °F	77.5	79.8	81.8	681	652

Contrails

Table 12. Experimental Data — Structural Joint Configuration 1 (Continued)

Run Number	16	17	18	19
Date	3/9/65	3/15/65	3/16/65	3/16/65
Pressure, Torr	8×10^{-7}	8×10^{-7}	6×10^{-7}	6×10^{-7}
Absolute T. C.				
1 - °F	176.5	88.5	138.9	189.1
2 - °F	62.7	62.5	62.2	62.6
3 - °F	63.8	63.0	63.3	64.2
Differential T. C.				
1 - °F	2.48	1.96	7.85	12.53
2 - °F	4.59	4.05	13.85	22.80
3 - °F	3.82	4.59	15.75	25.65
4 - °F	37.45	8.62	26.40	43.30
5 - °F	1.66	1.21	4.55	7.48
6 - °F	0.21	3.64	11.28	18.70
7 - °F	3.26	6.02	18.05	28.85
8 - °F	5.71	6.57	19.58	31.45
9 - °F	31.90	7.70	23.25	37.20
10 - °F		3.86	13.80	21.77
Voltage, volts	47.80	19.44	33.73	43.55
Current, amps	0.5024	0.3841	0.6672	0.8623
Water Flow, ml/min	750	700	625	625
Bolt Torque, in-lb	24	24	24	24
Filler	G 683	None	None	None
Sample Number	1	1	1	1
Joint Length, in.	6	9	9	9
Number of Bolts	2	3	3	3
h_a , Btu/hr ft ² °F	542	116	98.5	100.8
h_b , Btu/hr ft ² °F	645	74	75.3	77.9

Table 13. Experimental Data—Structural Joint Configuration 2

Run Number	20	21	22	23	24
Date	3/23/65	3/23/65	3/23/65	3/25/65	3/25/65
Pressure, Torr	5×10^{-7}	5×10^{-7}	5×10^{-7}	7×10^{-7}	7×10^{-7}
Absolute T. C.					
1 - °F	87.8	134.5	178.8	89.3	140.4
2 - °F	63.7	64.4	64.0	63.5	64.2
3 - °F	64.0	65.0	65.0	63.9	64.9
Differential T. C.					
1 - °F	2.61	8.02	12.75	2.14	6.53
2 - °F	5.20	16.10	25.80	3.93	12.42
3 - °F	6.79	20.95	33.75	5.55	17.25
4 - °F	8.03	24.35	38.65	7.37	21.60
5 - °F	-0.11	-0.23	0.05	0.35	0.94
6 - °F	3.32	9.70	15.35	3.53	10.44
7 - °F	3.75	10.81	16.33	5.25	15.20
8 - °F	5.35	15.91	24.62	6.72	19.88
9 - °F	7.24	21.40	34.10	7.07	20.22
10 - °F					
Voltage, volts	21.89	37.85	48.97	21.88	37.99
Current, amps	0.2284	0.3956	0.5126	0.2279	0.3964
Water Flow, ml/min	775	775	775	625	625
Bolt Torque, in-lb	24	24	24	24	24
Filler	None	None	None	None	None
Sample Number	1	1	1	2	2
Joint Length, in.	6	6	6	6	6
Number of Bolts	2	2	2	2	2
h_a , Btu/hr ft ² °F	84.2	81.5	85.0	105.5	102.0
h_b , Btu/hr ft ² °F	99.0	100.8	110.3	82.4	81.4

Table 13. Experimental Data—Structural Joint Configuration 2 (Continued)

Run Number	25	26	27	28
Date	3/25/65	3/26/65	3/26/65	3/29/65
Pressure, Torr	7×10^{-7}	3×10^{-6}	3×10^{-6}	2×10^{-6}
Absolute T. C.				
1 - °F	188.6	94.0	149.7	206.2
2 - °F	63.8	64.7	64.5	64.8
3 - °F	65.1	65.0	65.2	65.8
Differential T. C.				
1 - °F	11.05	2.54	8.00	12.35
2 - °F	20.80	4.89	14.73	23.78
3 - °F	29.35	6.41	19.12	31.00
4 - °F	34.70	7.35	21.92	37.80
5 - °F	1.53	1.02	2.50	3.65
6 - °F	17.48	3.69	10.81	17.25
7 - °F	24.20	4.31	11.94	18.55
8 - °F	32.45	5.24	14.55	23.10
9 - °F	32.80	6.91	19.87	32.10
10 - °F				
Voltage, volts	49.00	21.86	37.75	48.88
Current, amps	0.5121	0.2308	0.3993	0.5179
Water Flow, ml/min	550	700	700	650
Bolt Torque, in-lb	24	24	24	24
Filler	None	None	None	None
Sample Number	2	3	3	3
Joint Length, in.	6	6	6	6
Number of Bolts	2	2	2	2
h_a , Btu/hr ft ² °F	100.8	89.5	88.5	92.6
h_b , Btu/hr ft ² °F	83.2	93.5	99.3	105.2

Contrails

Table 13. Experimental Data — Structural Joint Configuration 2 (Continued)

Run Number	29	30	31	32
Date	3/31/65	3/31/65	3/31/65	4/1/65
Pressure, Torr	7×10^{-7}	7×10^{-7}	7×10^{-7}	1×10^{-6}
Absolute T. C.				
1 - °F	84.2	124.7	165.0	84.0
2 - °F	63.3	63.5	63.5	62.7
3 - °F	63.6	64.1	64.7	63.0
Differential T. C.				
1 - °F	0.70	2.51	4.46	0.95
2 - °F	0.07	0.08	0.34	0.67
3 - °F	0.09	0.40	1.05	1.17
4 - °F	7.73	22.85	37.85	7.53
5 - °F	0.33	0.91	1.37	0.20
6 - °F	0.48	1.50	2.19	0.54
7 - °F	0.64	1.96	3.70	0.80
8 - °F	1.24	3.72	6.65	2.24
9 - °F	7.42	21.50	34.75	7.49
10 - °F				
Voltage, volts	21.93	37.87	48.93	21.83
Current, amps	0.2289	0.3958	0.5120	0.2279
Water Flow, ml/min	650	650	650	575
Bolt Torque, in-lb	24	24	24	24
Filler	RTV 11	RTV 11	RTV 11	G 683
Sample Number	1	1	1	1
Joint Length, in.	6	6	6	6
Number of Bolts	2	2	2	2
h_a , Btu/hr ft ² °F	1427	1227	1050	438
h_b , Btu/hr ft ² °F	520	514	490	341

Table 13. Experimental Data—Structural Joint Configuration 2 (Continued)

Run Number	33	34	35	36
Date	4/1/65	4/2/65	4/5/65	4/5/65
Pressure, Torr	1×10^{-6}	7×10^{-7}	1×10^{-6}	1×10^{-6}
Absolute T. C.				
1 - °F	126.0	167.2	88.8	137.0
2 - °F	62.9	63.1	64.2	65.1
3 - °F	63.8	64.5	64.6	66.0
Differential T. C.				
1 - °F	3.54	6.13	2.78	8.04
2 - °F	1.89	3.10	4.03	11.92
3 - °F	3.33	5.44	6.31	18.92
4 - °F	22.40	36.95	8.51	26.80
5 - °F	0.50	0.91	0.25	0.74
6 - °F	1.73	2.66	2.76	8.35
7 - °F	2.44	3.74	5.23	15.50
8 - °F	6.53	10.03	6.21	18.28
9 - °F	21.75	35.15	7.97	23.00
10 - °F			5.13	14.95
Voltage, volts	37.96	48.96	19.43	33.66
Current, amps	0.3967	0.5124	0.3865	0.6710
Water Flow, ml/min	575	550	600	600
Bolt Torque, in-lb	24	24	24	24
Filler	G 683	G 683	None	None
Sample Number	1	1	1	1
Joint Length, in.	6	6	9	9
Number of Bolts	2	2	3	3
h_a , Btu/hr ft ² °F	425	420	93.5	95.2
h_b , Btu/hr ft ² °F	345	375	84.1	87.8

Table 13. Experimental Data — Structural Joint Configuration 2 (Continued)

Run	37	38	39	40
Date	4/5/65	4/6/65	4/6/65	4/6/65
Pressure, Torr	1×10^{-6}	8×10^{-7}	8×10^{-7}	8×10^{-7}
Absolute T. C.				
1 - °F	182.2	85.1	126.0	162.2
2 - °F	64.6	64.0	64.4	64.0
3 - °F	66.2	64.4	65.1	65.0
Differential T. C.				
1 - °F	12.58	0.16	0.60	1.26
2 - °F	20.59	0.39	1.44	2.99
3 - °F	32.44	0.83	2.61	4.95
4 - °F	45.32	7.33	22.00	36.10
5 - °F	1.28	0.35	1.05	1.87
6 - °F	12.05	0.17	0.65	3.43
7 - °F	23.56	0.13	0.51	1.44
8 - °F	27.59	0.35	1.36	2.86
9 - °F	36.90	7.41	21.60	35.02
10 - °F	25.22			
Voltage, volts	43.44	21.89	37.99	48.99
Current, amps	0.8674	0.2281	0.3960	0.5119
Water Flow, ml/min	600	625	625	625
Bolt Torque, in-lb	24	24	24	24
Filler	None	RTV 11	RTV 11	RTV 11
Sample Number	1	2	2	2
Joint Length, in.	9	6	6	6
Number of Bolts	3	2	2	2
h_a , Btu/hr ft ² °F	94.1	889	795	669
h_b , Btu/hr ft ² °F	97.6	1892	1466	800

Table 14. Experimental Data—Structural Joint Configuration 3

Run Number	41	42	43	44	45
Date	5/8/65	5/8/65	5/8/65	5/9/65	5/9/65
Pressure, Torr	1×10^{-6}	1×10^{-6}	1×10^{-6}	1×10^{-6}	1×10^{-6}
Absolute T. C.					
1 - °F	70.3	84.5	98.1	69.6	80.0
2 - °F	62.7	62.6	62.2	63.5	63.1
3 - °F	63.0	63.3	63.4	63.9	64.0
Differential T. C.					
1 - °F	1.42	4.55	7.80	1.11	4.06
2 - °F	3.12	9.34	15.78	2.35	7.48
3 - °F	3.83	11.61	19.67	2.84	8.90
4 - °F	3.62	10.91	18.90	3.64	11.20
5 - °F	-0.22	0.36	1.15	0.43	1.55
6 - °F	2.66	8.30	14.35	1.92	6.15
7 - °F	3.11	9.55	16.40	1.98	6.41
8 - °F					
Voltage, volts	21.93	37.94	49.01	21.89	38.04
Current, amps	0.2281	0.3949	0.5106	0.2268	0.3943
Water Flow, ml/min	600	600	600	575	575
Bolt Torque, in-lb	24	24	24	24	24
Filler	None	None	None	None	None
Sample Number	1	1	1	2	2
Joint Length, in.	6	6	6	6	6
Number of Bolts	2	2	2	2	2
h, Btu/hr ft ² °F	147	144.2	142	194	180

Contrails

Table 14. Experimental Data—Structural Joint Configuration 3 (Continued)

Run Number	46	47	48	49	50
Date	5/9/65	5/13/65	5/13/65	5/13/65	5/15/65
Pressure, Torr	1×10^{-6}	6×10^{-7}	6×10^{-7}	6×10^{-7}	5×10^{-7}
Absolute T. C.					
1 - °F	89.7	72.2	86.8	98.3	70.7
2 - °F	62.5	65.0	66.0	64.1	62.4
3 - °F	63.7	65.3	66.9	65.4	62.8
Differential T. C.					
1 - °F	7.11	2.69	7.94	13.30	0.107
2 - °F	12.79	3.82	11.62	19.90	0.583
3 - °F	15.31	4.91	14.60	24.80	0.414
4 - °F	19.00	4.01	11.79	20.30	3.84
5 - °F	1.94	0.07	0.43	0.76	-0.458
6 - °F	10.50	3.71	11.08	18.82	0.307
7 - °F	10.81	3.66	10.52	17.78	0.222
8 - °F					
Voltage, volts	49.01	21.88	37.20	48.00	21.91
Current, amps	0.5084	0.2385	0.4059	0.5244	0.2279
Water Flow, ml/min	575	575	575	575	425
Bolt Torque, in-lb	24	24	24	24	24
Filler	None	None	None	None	RTV 11
Sample Number	2	3	3	3	1
Joint Length, in.	6	6	6	6	6
Number of Bolts	2	2	2	2	2
h, Btu/hr ft ² °F	174.0	112.2	108.5	106.5	1110

Table 14. Experimental Data—Structural Joint Configuration 3 (Continued)

Run Number	51	52	53	54
Date	5/15/65	5/15/65	5/16/65	5/16/65
Pressure, Torr	5×10^{-7}	5×10^{-7}	4×10^{-7}	4×10^{-7}
Absolute T. C.				
1 - °F	87.7	102.5	74.3	91.8
2 - °F	63.7	63.4	66.0	68.0
3 - °F	64.8	65.0	66.3	68.9
Differential T. C.				
1 - °F	0.461	0.827	0.222	0.723
2 - °F	1.560	2.441	0.284	0.991
3 - °F	0.979	1.672	0.418	1.208
4 - °F	11.52	19.50	3.89	11.71
5 - °F	-0.282	-0.218	-0.515	0.491
6 - °F	0.735	1.260	0.391	1.104
7 - °F	0.630	1.088	0.311	0.835
8 - °F				
Voltage, volts	38.00	48.99	21.90	38.00
Current, amps	0.3956	0.5104	0.2278	0.3955
Water Flow, ml/min	375	450	450	575
Bolt Torque, in-lb	24	24	24	24
Filler	RTV 11	RTV 11	G 683	G 683
Sample Number	1	1	1	1
Joint Length, in.	6	6	6	6
Number of Bolts	2	2	2	2
h, Btu/hr ft ² °F	1273	1242	1328	1262

Table 14. Experimental Data—Structural Joint Configuration 3 (Continued)

Run Number	55	56	57	58
Date	5/16/65	5/19/65	5/19/65	5/20/65
Pressure, Torr	4×10^{-7}	7×10^{-7}	7×10^{-7}	4×10^{-7}
Absolute T. C.				
1 - °F	103.2	75.0	87.0	96.8
2 - °F	63.9	68.8	69.2	67.2
3 - °F	65.1	69.2	70.2	68.9
Differential T. C.				
1 - °F	1.273	1.44	4.41	7.60
2 - °F	1.678	3.10	9.46	16.21
3 - °F	2.043	4.10	12.64	21.63
4 - °F	19.85	4.10	12.39	21.08
5 - °F	0.80	0.40	1.50	2.78
6 - °F	1.905	4.64	14.00	23.78
7 - °F	1.440	3.84	11.61	19.60
8 - °F		3.00	9.18	15.47
Voltage, volts	49.01	18.98	32.84	42.45
Current, amps	0.5105	0.3958	0.6852	0.8860
Water Flow, ml/min	625	575	575	575
Bolt Torque, in-lb	24	24	24	24
Filler	G 683	None	None	None
Sample Number	1	1	1	1
Joint Length, in.	6	9	9	9
Number of Bolts	2	3	3	3
h, Btu/hr ft ² °F	1231	142.2	139	135.5

APPENDIX III

SCRIPT F COMPUTER PROGRAM PRINT OUT

\$18FTC MAIN LIST,REF,DECK
C DRIVER FOR SPECULAR-DIRECTIONAL SCRIPT F PROGRAM (AH052A) 10/28/64

DIMENSION ID(ZZ)

DIMENSION RHO(Z0,Z0),F(Z0,Z0),AREA(Z0)

1 ,SF(Z0,Z0),SFA(Z0,Z0)

2 ,B(1000),DI(400)

DIMENSION R(Z0,Z0,Z0),R1(Z0,Z0),R2(Z0,Z0),R3(Z0,Z0),R4(Z0,Z0)

1 ,R5(Z0,Z0),R6(Z0,Z0),R7(Z0,Z0),R8(Z0,Z0),R9(Z0,Z0),R10(Z0,Z0)

2 ,R11(Z0,Z0),R12(Z0,Z0),R13(Z0,Z0),R14(Z0,Z0),R15(Z0,Z0)

3 ,R16(Z0,Z0),R17(Z0,Z0),R18(Z0,Z0),R19(Z0,Z0),R20(Z0,Z0)

C

EQUIVALENCE (R1(1,1),R11(1,1)),(R2(1,1),R12(1,1)),(R3(1,1),R13(1,1)),

1),(R4(1,1),R14(1,1)),(R5(1,1),R15(1,1)),(R6(1,1),R16(1,1)),

2 ,(R7(1,1),R17(1,1)),(R8(1,1),R18(1,1)),(R9(1,1),R19(1,1)),

3 ,(R10(1,1),R20(1,1)),(R11(1,1),R12(1,1)),(R12(1,1),R13(1,1)),

4 ,(R13(1,1),R14(1,1)),(R14(1,1),R15(1,1)),(R15(1,1),R16(1,1)),

5 ,(R16(1,1),R17(1,1)),(R17(1,1),R18(1,1)),(R18(1,1),R19(1,1)),

6 ,(R19(1,1),R20(1,1)),(R20(1,1),R11(1,1)),(R11(1,1),R12(1,1)),

C

CLEAR STORAGE REGIONS

300 DO 310 I=1,20

AREA(I)= 0.

310 CONTINUE

DO 320 I=1,400

RHO(I,1)= 0.

F(I,1)= 0.

320 CONTINUE

DO 330 I=1,8000

R(I,1)= 0.

330 CONTINUE

C

100 WRITE (3,1000)

1000 FORMAT (1H1,5X,13HINPUT FOLLOWS)

C

CALL FIMP(-26,Z,CLR,RHO,F,AREA,R1,R2,R3,R4,R5,R6,R7,R8,R9,R10,R11

1 ,R12,R13,R14,R15,R16,R17,R18,R19,R20, ID

2 , 156HN CLR RHO F AREA R1 R2 R3 R4 R5

3 R6 R7 R8 R9 R10 R11 R12 R13 R14 R15 R16

4 R17 R18 R19 R20 ID)

C

N= Z+.25

```

NN= M+N
2000 DO 2100 I=1,N
IF(RHO(I,1))2020,2070,2070
2020 RMO(I,1)=-RHO(I,1)
DO 2060 J=1,N
RHO(I,J)=RMO(I,1)
DO 2060 K=1,J
2060 R(K,I,J)=RHO(I,1)
2070 DO 2100 J=1,N
IF(J.LT.I)F(J,I)=AREA(I)*F(I,J)/AREA(J)
DO 2100 K=1,J
2100 R(J,I,K)=R(K,I,J)
WRITE (3,1001)
1001 FORMAT ( 1H0,5X,12HEND OF INPUT)
WRITE (3,1010) ID
1010 FORMAT (1H1,26X,56HSPECULAR-DIRECTIONAL SCRIPT F PROGRAM (A#052A),
1 10/28/64 / (1H0,21X,11A6) )
C
WRITE (3,1002)
1002 FORMAT (1H1,5X,15HRHO(I,J) MATRIX)
CALL MPRT (RHO,N)
WRITE (3,1003)
1003 FORMAT (1H1,5X,13HF(I,J) MATRIX)
CALL MPRT (F,N)
WRITE (3,1004) (AREA(I),I=1,N)
1004 FORMAT (1H1,5X,11HAREA VECTOR/(15E20.8))
WRITE (3,1005)
1005 FORMAT (1H1,5X,14HR(I,J,K) ARRAY)
DO 150 K=1,N
WRITE (3,1009) K
1009 FORMAT (1H0/1H0,5X,9HBLOCK NO. 14)
CALL MPRT (R(1,1,K),N)
150 CONTINUE
CALL SCRF (M,NN,RHO,F,AREA,R,D,DI,SF,SFA,IERR)
WRITE (3,1007)
1007 FORMAT (1H1,5X,15HSCRIPT F MATRIX)
CALL MPRT (SF,N)
WRITE (3,1008)
1008 FORMAT (1H1,5X,16HSCRIPT FA MATRIX)
CALL MPRT (SFA,N)
IF (CLR) 300,100,300

```

Confidential

END

\$IBMAP	ERRS	LIST,REF,DECK	ERRS0000
ERRS	ENTRY	ERRS	ERRS0001
	SAVE	4,2,1	ERRS0002
	SXA	EA,4	ERRS0003
	LAC	EA,2	ERRS0004
	SXA	EA,2	ERRS0005
	TXI	*+1,4,-2	ERRS0006
	CLA	1,4	ERRS0007
	STA	IDENTZ	ERRS0008
	CLA*	1,4	ERRS0009
	PAX	,1	ERRS0010
	SXA	CODEO,1	ERRS0011
	CAL	2,4	ERRS0012
	ANA	(PDT)	ERRS0013
	TNZ	ER23	ERRS0014
	CAL*	2,4	ERRS0015
	TRA	ER24	ERRS0016
ER23	CAL	2,4	ERRS0017
ER24	SLW	NAME	ERRS0018
	STZ	ER7	ERRS0019
	CAL	3,4	ERRS0020
	AMA	(PDT)	ERRS0021
	TNZ	ER31	ERRS0022
	CAL	3,4	ERRS0023
	STA	LEAV1	ERRS0024
	AXT	1,2	ERRS0025
	SXA	ER7,2	ERRS0026
	SXD	*+2,4	ERRS0027
	AXC	1,4,2	ERRS0028
	TXI	*+1,2,**	ERRS0029
	SXA	BEG1,2	ERRS0030
	LAC	BEG1,2	ERRS0031
	SXA	BEG1,2	ERRS0032
	SXA	BEG1+3,2	ERRS0033
	AXT	10,4	ERRS0034
	CAL	** ,4	ERRS0035
BEG1	ANA	(PDT)	ERRS0036
	TNZ	ER31	ERRS0037
	CLA	** ,4	ERRS0038
	STA	ARG+10,4	ERRS0039
	TIX	BEG1,4,1	ERRS0040

ERRS0041	EA	•FWRD.,(.UN03.,A)
ERRS0042	TSX	•FCNV.,4
ERRS0043	NAME	
ERRS0044	TSX	•FCNV.,4
ERRS0045	CODEO	
ERRS0046	TSX	•FCNV.,4
ERRS0047	**	
ERRS0048	TSX	•FCNV.,4
ERRS0049	FFIL.,4	
ERRS0050	ER7	
ERRS0051	LEAV1	
ERRS0052	ERRS	
ERRS0053		
ERRS0054		
ERRS0055		
ERRS0056	REM	SIMULATE CALL TO SUBPROGRAM (CNTRL) FROM MAIN PROGRAM
ERRS0057	REM	•••UP TO 10 ARGUMENTS PERMITTED
ERRS0058	LEAV1	**.,4
ERRS0059	RTN	
ERRS0060		
ERRS0061		
ERRS0062		
ERRS0063		
ERRS0064		
ERRS0065		
ERRS0066		
ERRS0067		
ERRS0068		
ERRS0069		
ERRS0070		
ERRS0071		1,
ERRS0072		
ERRS0073		1
ERRS0074		7777777700000
ERRS0075		1
ERRS0076		1, (1H0 3
ERRS0077		1,5H **
ERRS0078		1,*ERRS-
ERRS0079		1,-ERROR
ERRS0080		1, EXIT
ERRS0081		

ERRS0082
ERRS0083
ERRS0084
ERRS0085
ERRS0086
ERRS0087
ERRS0088
ERRS0089
ERRS0090
ERRS0091
ERRS0092
ERRS0093
ERRS0094
ERRS0095

1, FROM L
1, OCATIO
1, N 06,
1, 10H, P
1, PROGRAM
1, A6, B
1, H, I, D
1, = 06
1, 5H(8
1,) = 16
1, 9H(1
1, 0).***
1, *)

BCI
BCI
BCI
BCI
BCI
BCI
BCI
BCI
BCI
BCI
BCI
BCI
BCI
BCI
BCI
BCI
BCI
END

SIBMAP	FIMP	LIST, REF, DECK	FIMP0000
*	FIMP-FORTRAN IV DECEMBER 1964		FIMP0001
TBL	ENTRY	TBLOO	FIMP0002
FIMP	SAVE	(4,1,2)I	FIMP0003
	TXI	*+1,4,-2	FIMP0004
	CLA*	1,4	FIMP0005
	STO	COMMON+28	FIMP0006
	TZE	INPT2	FIMP0007
	SXD	FIMPT,4	FIMP0008
INPT2	LXD	FIMPT,4	FIMP0009
	PXA	0,4	FIMP0010
	SBM*	1,4	FIMP0011
	SUB	1B35	FIMP0012
	COM		FIMP0013
	STA	TBLO2	FIMP0014
	CLA	1,4	FIMP0015
	STA	TBLOO	FIMP0016
	CLA*	1,4	FIMP0017
	STO	COMMON+29	FIMP0018
	ALS	18	FIMP0019
	COM		FIMP0020
	STD	**1	FIMP0021
	TXI	*+1,4,0	FIMP0022
	CLA	0,4	FIMP0023
	STO	GINOO	FIMP0024
	STO	RLOC	FIMP0025
	CLA	1,4	FIMP0026
	ADM	COMMON+29	FIMP0027
	STA	TBLO1	FIMP0028
	STO	ERROR	FIMP0029
*	GINA	READ ONE BCD CARD IMAGE FROM INPUT TAPE	FIMP0030
	CALL	.FRDD.(.UNO2.,=H(14A6))	FIMP0031
	AXT	14,1	FIMP0032
A	TSX	.FCNV.,4	FIMP0033
	STO	COMMON+14,1	FIMP0034
	TIX	A,1,1	FIMP0035
	TSX	.FRTN.,4	FIMP0036
	CLA	COMMON+29	FIMP0037
	TPL	GINA1	FIMP0038
*	WRITE CARD IMAGE ON OUTPUT TAPE.		FIMP0039
	CALL	.FWRD.(.UNO3.,=H(15A6))	FIMP0040

FLAG TO USE PREVIOUS CALL

ALPHA+N

N OR O

FOR HEADER COMPATABILITY
RELATIVE ORIGIN

N

N NO INPUT LIST

FINP0041
FINP0042
FINP0043
FINP0044
FINP0045
FINP0046
FINP0047
FINP0048
FINP0049
FINP0050
FINP0051
FINP0052
FINP0053
FINP0054
FINP0055
FINP0056
FINP0057
FINP0058
FINP0059
FINP0060
FINP0061
FINP0062
FINP0063
FINP0064
FINP0065
FINP0066
FINP0067
FINP0068
FINP0069
FINP0070
FINP0071
FINP0072
FINP0073
FINP0074
FINP0075
FINP0076
FINP0077
FINP0078
FINP0079
FINP0080
FINP0081

CLA	#H	
TSX	.FCNV.04	
AXI	14,1	
CLA	COMMON+14,1	
TSX	.FCNV.04	
TIX	*-2,1,1	
CALL	.FFIL.	
AXC	COMMON,1	
TXI	*+1,1,-12	
SXD	GINC,1	
SXD	GINI1+1,1	
AXC	COMMON,1	
CLA	BLANK	
CAS	0,1	
TXI	GINC+2	
TXI	*+2,1,-1	
TXL	GINC+2	
TXH	GINB,1,**	
TXL	GINA	
AXC	COMMON,1	
LDQ	0,1	
PXD	**	
LGL	6	
STO	PREFIX	
STQ	0,1	
SUB	ME	
T7E	GIN13	
LGL	30	
AMA	MASK1	
STO	ADDIND	
STZ	SUM	
STZ	SIGN	
CLA	0,1	
CAS	MASK2	
TXL	*+2	
TXL	GINO6	
LDQ	0,1	
LGL	6	
AXI	2,4	
PXD	0,0	
LGL	6	

INGORE BLANK CZRD

SAVE PREFIX CODE

E
END

SAVE LAST DIGIT OF ADDRESS

TEST FOR BLANK ADDRESS

BLANK
DETERMINE COMMA POSITION

SUB	MASK4	COMMA	FINP0082
TZE	**3		FINP0083
TXH	GIN17-2,4,3	NOT MATRIX	FINP0084
TXI	*-5,4,1		FINP0085
PXA	4	POSITION OF COMMA	FINP0086
TSX	MTX00,4	MATRIX	FINP0087
TRA	GINER	OUTSIDE MATRIX	FINP0088
TRA	GIN20		FINP0089
MASK4	73		FINP0090
AXT	5,4		FINP0091
LDQ	0,1		FINP0092
PXD			FINP0093
LGL	6		FINP0094
PAX	0,2		FINP0095
TXL	GIN18,2,9		FINP0096
TXH	GIN19,2,48		FINP0097
TXL	GIN19,2,47		FINP0098
TXI	GIN17,4,1		FINP0099
TXL	GIN16		FINP0100
CLA	0,1	SYMBOLIC	FINP0101
ORA	MASK3		FINP0102
TSX	TBLOO,4		FINP0103
LLS	35		FINP0104
STA	GIN00		FINP0105
STA	SGINO3		FINP0106
CLA	MASK3		FINP0107
STO	ADDIND		FINP0108
TXL	GIN07		FINP0109
CLA	ADDIND	TEST FOR OCTAL	FINP0110
SUB	MASK3		FINP0111
TZE	GIN04		FINP0112
LXA	5835,2	SET-UP OCTAL ADDRESS	FINP0113
TSX	OCTAL,4		FINP0114
TXH	5,*,**		FINP0115
TXL	GIN07,*,**		FINP0116
LXA	100B35,2	SET UP DECIMAL ADDRESS	FINP0117
CLA	4B35		FINP0118
TSX	DECIM,4		FINP0119
TRA	GINER	ERROR	FINP0120
TXH	6,*,**		FINP0121
TXL	GINER,2,100		FINP0122

GINO6	TXL	GINO7							FINP0123
GINO7	LDQ	MASK2							FINP0124
	STQ	CRDADD							FINP0125
	LXA	PREFIX,4							FINP0126
	TXH	GINER,4,48							FINP0127
	TXL	GINO8,4,47							FINP0128
	LXD	100B35,4							FINP0129
	TXL	GINO9							FINP0130
GINO8	TXH	GINER,4,41							FINP0131
	TXL	**2,4,32							FINP0132
	TXI	GINO9,4,-23							FINP0133
	TXH	GINER,4,25							FINP0134
	TXX	GINER,4,16							FINP0135
GINO9	TXI	GINO9+1,1,-1							FINP0136
	TRA	GIN10,4							FINP0137
	TXL	RGINOO							FINP0138
	TXL	GINER							FINP0139
	TXL	GINER							FINP0140
	TXL	GINER							FINP0141
	TXL	NGINOO							FINP0142
	TXL	MCDOO							FINP0143
	TXL	MCDOO							FINP0144
	TXL	KGINOO							FINP0145
	HTR*	CRDADD							FINP0146
	TXL	IGINOO							FINP0147
	TXL	HGINOO							FINP0148
	TXL	GGINOO							FINP0149
	TXL	FGINOO							FINP0150
	TXL	GINER							FINP0151
	TXL	DGINOO							FINP0152
	TXL	CGINOO							FINP0153
	TXL	BGINOO							FINP0154
	TXL	ACDO							FINP0155
GIN10	TXL	LGINOO,12							FINP0156
GIN11	TXI	GIN11+1,1,-1							FINP0157
	TXH	GINO1-1,1,**							FINP0158
GIN12	TXL	GINA							FINP0159
GIN13	NZI	ERROR							FINP0160
	TRA	GIN15							FINP0161
GIN15	RETURN	FIMP							FINP0162
	CALL	-FXEM.(CODE40)							FINP0163

SET-UP TRA TO
SUB-PROGRAM

R RELATIVE ORIGIN
Q
P
O
N RELATIVE INDEX VALUE
M MATRIX IJ,ZERO
L MATRIX IJ-NO ZERO
K SKIP CELLS
J
I INTEGER
H HEADER
G TABLE ORIGIN
F FIXED FOINT
E
D BCD
C SAVE NEXT LOCATION
B OCTAL
A SYMBOLIC
BLANK FLOATING
TEST END CARD
TO NEXT CARD

GINER	CALL	EXIT		FINP0164
	STZ	ERROR		FINP0165
	CLA	COMMON+29		FINP0166
	TPR	GIN12		FINP0167
	CALL	•FWRD•(•UN03•,•H(14A6))		FINP0168
	AXT	10,1		FINP0169
	CLA	•H		FINP0170
	TSX	•FCNV•,4		FINP0171
	TIX	*-2,1,1		FINP0172
	AXT	4,1		FINP0173
	CLA	GINRC+4,1		FINP0174
	TSX	•FCNV•,4		FINP0175
	TIX	*-2,1,1		FINP0176
	CALL	•FFIL•		FINP0177
	TXL	GIN12		FINP0178
GINRC	BCI	4, ABOVE CARD IN ERROR		FINP0179
ME	BCI	1,00000E		FINP0180
BLANK	BCI	1,		FINP0181
GGIN00	CLA	CRDADD		FINP0182
	CAS	MASK2		FINP0183
	TXL	*+2		FINP0184
	TXL	GIN12	BLANK	FINP0185
	LDQ	CRDADD		FINP0186
	MPY	11835		FINP0187
	LLS	35		FINP0188
	TZE	*+2	SYMBOLIC	FINP0189
	SUB	10835		FINP0190
	STO	CRDADD		FINP0191
	AXT	11,1		FINP0192
	LDQ	COMMON+12,1		FINP0193
	TSX	SGIN00,4		FINP0194
	CLA	MASK2	SET TO BLANK	FINP0195
	STO	CRDADD		FINP0196
	TIX	*-4,1,1		FINP0197
	TXL	GIN12		FINP0198
GGIN00	CLA	ADDIND		FINP0199
	SUB	MASK3		FINP0200
	TZE	GGIN01		FINP0201
	PXD			FINP0202
	TXL	GGIN02		FINP0203
GGIN01	CAL	GIN00		FINP0204

GGINO2	SUB	1835			FINP0205
	ADD	CRDADD			FINP0206
	STA	SGINO3			FINP0207
	TXL	GIN12			FINP0208
BGINO0	STZ	SUM			FINP0209
	STZ	SIGN		6	FINP0210
	LXA	M6B35,2			FINP0211
	TSX	OCTAL,4			FINP0212
	TXI	BGINO4,1,-1			FINP0213
	TXI	BGINO1,1,-1			FINP0214
BGINO1	LXA	M6B35,2		6	FINP0215
	TSX	OCTAL,4			FINP0216
	TXH	4			FINP0217
BGINO2	TSX	SGINO0,4			FINP0218
BGINO3	TXL	GIN11,***			FINP0219
BGINO4	TXH	BGINO3,2,5			FINP0220
	TXL	BGINO2			FINP0221
IGINO0	TSX	DECNO,4			FINP0222
	TXH	GINER,2,1			FINP0223
	TXL	BGINO2,2,0			FINP0224
	CLM				FINP0225
DVP		10835			FINP0226
TMZ		GINER			FINP0227
TRA		BGINO2			FINP0228
DGINO0	LDQ	0,1			FINP0229
	TSX	SGINO0,4			FINP0230
	CLA	MASK2			FINP0231
	STO	CRDADD			FINP0232
	LDQ	1,1			FINP0233
	TXI	BGINO2,1,-1			FINP0234
DECNO	SXD	BGINO3,4			FINP0235
	CLA	0,1			FINP0236
	STO	COMMON+33			FINP0237
	CLA	1,1			FINP0238
	STO	COMMON+34			FINP0239
	ALS	24			FINP0240
	SLW	COMMON+20			FINP0241
	STZ	SUM			FINP0242
	STZ	SIGN			FINP0243
	LXA	100B35,2			FINP0244
	CLS	M6B35		6	FINP0245

EXIT FOR NEW PREFIX
BLANK
INTERGER FORMAT
DECIMAL PLACES
STORE INTEGER

NOT .0
STORE INTEGER

TSX DECIM,4						FINP0246
TRA DECER						FINP0247
TXI DECN2+1,1,-1				ERROR		FINP0248
TXI DECN1,1,-1				END ON BLANK		FINP0249
DECN1 CLA 4835			4			FINP0250
TSX DECIM,4						FINP0251
TXI DECER,1,1				ERROR		FINP0252
DECN2 TXH 2,***						FINP0253
TXL DECN4,2,99						FINP0254
TXL GIN11,2,100						FINP0255
DECN3 LXD 1835,2						FINP0256
DECN4 LXD BGINO3,4						FINP0257
LXD BGINO3,4						FINP0258
TRA 1,4						FINP0259
DECEN SXD GINO3,4						FINP0260
TSX DECNO,4						FINP0261
STQ COMMON+13						FINP0262
SXD DECN2,2						FINP0263
CLA DECN2						FINP0264
STZ SUM						FINP0265
STZ SIGN						FINP0266
LDO COMMON+20						FINP0267
STQ 0,1						FINP0268
TSX DECIM,4						FINP0269
TXI DECER,1,1				ERROR		FINP0270
TXH						FINP0271
LXD GINO3,4						FINP0272
TRA 1,4						FINP0273
DECER CLA COMMON+33						FINP0274
STO 0,1						FINP0275
CLA COMMON+34						FINP0276
STO 1,1						FINP0277
TRA ACDO						FINP0278
FGINOO TSX DECN,4				FIXED PT. CONVERSION		FINP0279
STQ COMMON						FINP0280
CAL DECN2						FINP0281
COM						FINP0282
ADD 1B17						FINP0283
PDX 0,2						FINP0284
CLA COMMON						FINP0285
SUB BREF,2						FINP0286

FINP0287	TMI GINER		
FINP0288	STA FGINO1		
FINP0289	LDG COMMON+13		
FINP0290	MPY FREF *2		
FINP0291	FGINO1 LRS **		
FINP0292	TNZ GINER		
FINP0293	TXL BGINO2,**		
FINP0294	TSX DECEN *4	FLTG. PT. CONVERSION	
FINP0295	STO COMMON		
FINP0296	LXD DEC2 *2		
FINP0297	PXD *2		
FINP0298	ARS 18		
FINP0299	SSM		
FINP0300	ADD COMMON		
FINP0301	LRS 35		
FINP0302	DVP 10B35		
FINP0303	SUB M9B35		
FINP0304	PAX *2		
FINP0305	CLM		
FINP0306	LLS 35		
FINP0307	ADD 5B35	HIGH DIGIT	
FINP0308	TMI GINER		
FINP0309	PAX *4		
FINP0310	SXD FGINO1+2,1	SAVE ADD REFERENCE	
FINP0311	CLA XREF1 *2		
FINP0312	ADD XREF2 *4		
FINP0313	ADD 126B35		
FINP0314	TPL LGINOA		
FINP0315	STZ COMMON+13		
FINP0316	LGINOA PAX 0,1		
FINP0317	LDG FREF1 *2		
FINP0318	MPR FREF2 *4		
FINP0319	LRS 35		
FINP0320	MPY COMMON+13		
FINP0321	LLS 2		
FINP0322	TZE LGINO3		
FINP0323	TZE LGINO2		
FINP0324	LRS 1		
FINP0325	TXI LGINO1,1,1		
FINP0326	LGINO2 LLS		27
FINP0327	RND		

LRS	27				FIMP0328
TZE	**3				FIMP0329
LRS	1				FIMP0330
TXI	**1,1,1				FIMP0331
PXA	0				FIMP0332
LLS	8				FIMP0333
LRS	8				FIMP0334
LGINO3	LXD	FGINO1+2,1			FIMP0335
TNZ	GINER				FIMP0336
TXL	BGINO2		EXIT TO STORE		FIMP0337
SGINOO	CLA	CRDADD	STORE ROUTINE		FIMP0338
SUB	MASK2				FIMP0339
TZE	SGINO1				FIMP0340
CLA	ADDIND				FIMP0341
SUB	MASK3				FIMP0342
TZE	SAAL				FIMP0343
CLA	CRDADD				FIMP0344
TXL	SGINO2				FIMP0345
SAAL	CLA	CRDADD	ONLY IF CRDADD HAS		FIMP0346
TZE	SGINOA				FIMP0347
CAL	CRDADD				FIMP0348
SUB	1B35		RELATIVE LOCATION IN		FIMP0349
STA	CRDADD				FIMP0350
SGINOA	CAL	GINOO			FIMP0351
ACL	CRDADD				FIMP0352
TXL	SGINO2				FIMP0353
SGINO1	CAL	SGINO3	ADD 1 TO OLD ADDRESS		FIMP0354
ACL	1B35				FIMP0355
SGINO2	STA	SGINO3			FIMP0356
SGINO3	STQ	**			FIMP0357
TRA	1,4				FIMP0358
*					FIMP0359
KGINOO	TSX	DECNO,4	SKIP CELLS		FIMP0360
TXH	GINER,2,0		NON INTEGER		FIMP0361
XCA					FIMP0362
TMI	GINER				FIMP0363
ADM	SGINO3				FIMP0364
STA	SGINO3				FIMP0365
TRA	GIN11				FIMP0366
*					FIMP0367
CGINOO	CLA	0,1			FIMP0368

CGIN01	TSX	TBLO0,4	FINP0369
	CAL	SGIN03	FINP0370
	ADD	1835	FINP0371
	AXI	**2	FINP0372
	STA*	TBLO2	FINP0373
	TXI	GIN11,1,-1	FINP0374
*	SAVE	RELATIVE LOCATION AND ABSOLUTE LOCATION	FINP0375
NGIN00	CLA	0,1	FINP0376
	TSX	TBLO0,4	FINP0377
	LXA	CGIN01,2	FINP0378
	TXI	**1,2,1	FINP0379
	CLA*	TBLO1	FINP0380
	SUB	BLANK	FINP0381
	TNZ	GINER	FINP0382
	TXI	**1,2,-2	FINP0383
	XEC	TBLO2	FINP0384
	XCA		FINP0385
	STA	NGIN01	FINP0386
	TXI	**1,2,1	FINP0387
	CAL	SGIN03	FINP0388
	ADD	1835	FINP0389
	STA*	TBLO2	FINP0390
	ADD	1835	FINP0391
	SUB	RLOC	FINP0392
	STZ*	**1	FINP0393
NGIN01	STA	**	FINP0394
	TXI	GIN11,1,-1	FINP0395
RGIN00	CLA	0,1	FINP0396
	TSX	TBLO0,4	FINP0397
	STZ	RLOC	FINP0398
	XCA		FINP0399
	STA	RLOC	FINP0400
	TXI	GIN11,1,-1	FINP0401
*	OCTAL	LDQ 0,1	FINP0402
	OCTAL1	PXD	FINP0403
	LGL	3	FINP0404
	TNZ	OCTAL2	FINP0405
	CAL	SUM	FINP0406
	LGL	3	FINP0407
	SLW	SUM	FINP0408
			FINP0409

TIX OCTAL1,2,1	FIMP0410
TXI OCTAL3,4,-1	FIMP0411
OCTAL2 LGL 3	FIMP0412
SUB MASK3	FIMP0413
TNZ GINER	FIMP0414
OCTAL3 LDQ SUM	FIMP0415
TRA 1,4	FIMP0416
DECIM SXD DECIM2,4	FIMP0417
PAX ,4	FIMP0418
DECIM1 CLM	FIMP0419
LDQ 0,1	FIMP0420
LGL 6	FIMP0421
STQ 0,1	FIMP0422
SUB 10B35	FIMP0423
TMI DECIM6	FIMP0424
SBM M6B35	FIMP0425
TZE DECIM7	FIMP0426
SUB 11B35	FIMP0427
TNZ DECIM3	FIMP0428
LXD 10B35,2	FIMP0429
DECIM2 TXL DECIM7, **	FIMP0430
DECIM3 SUB 5B35	FIMP0431
TMI DECIM9	FIMP0432
SUB 10B35	FIMP0433
TNZ DECIM4	FIMP0434
SUB 10B35	FIMP0435
DECIM4 TPL DECIM5	FIMP0436
STO SIGN	FIMP0437
TXL DECIM6	FIMP0438
DECIM5 ADD M6B35	FIMP0439
TZE DECIM8	FIMP0440
SUB 11B35	FIMP0441
TNZ DECIM9	FIMP0442
TRA DECIM7	FIMP0443
DECIM8 LXD DECIM2,4	FIMP0444
LDQ SUM	FIMP0445
CLA SIGN	FIMP0446
LRS 0	FIMP0447
TRA 2,4	FIMP0448
DECIM6 ADD 10B35	FIMP0449
STO COMMON+14	FIMP0450

GENERATE DECIMAL INTEGER

**+

BLANK

IGNORE COMMA
END ON BLANK

```

LDQ SUM          FIMP0451
MPY 10B35        FIMP0452
LLS 35           FIMP0453
ADD COMMON+14    FIMP0454
STO SUM          FIMP0455
TXI DECIM7,2,1  FIMP0456
TIX DECIM1,4,1  FIMP0457
LXD DECIM2,4     FIMP0458
TXI DECIM8,1,4,-1 FIMP0459
DECIM9 LXD       FIMP0460
TRA             FIMP0461
DEC 133         FIMP0462
100B35 DEC 100  FIMP0463
DEC 67          FIMP0464
DEC 34          FIMP0465
1B35           FIMP0466
DEC 1           FIMP0467
DEC -33        FIMP0468
DEC -66        FIMP0469
DEC -99        FIMP0470
DEC -132       FIMP0471
XREF2 DEC .918354961680
DEC .788860905380
DEC .677626357980
DEC .582076609280
DEC .580
DEC .858993459280
DEC .737869763080
DEC .633825300280
DEC .544451787180
FREF2 DEC 30
DEC 27
DEC 24
DEC 20
17B35 DEC 17
DEC 14
10B35 DEC 10
DEC 7
4B35 DEC 4
BREF DEC 1
M6B35 DEC -3
DEC -6
END ON DIGIT COUNT
ERROR EXIT

```

M9835	DEC -9	FIMP0492
	DEC -13	FIMP0493
	DEC -16	FIMP0494
	DEC -19	FIMP0495
	DEC -23	FIMP0496
	DEC -26	FIMP0497
	DEC -29	FIMP0498
XREF1	DEC .931322574780	FIMP0499
	DEC .745058059780	FIMP0500
	DEC .596046447880	FIMP0501
	DEC .953674316580	FIMP0502
	DEC .762939453180	FIMP0503
	DEC .610351562580	FIMP0504
	DEC .976562580	FIMP0505
	DEC .7812580	FIMP0506
	DEC .62580	FIMP0507
FREF	DEC .580	FIMP0508
	DEC .880	FIMP0509
	DEC .6480	FIMP0510
	DEC .51280	FIMP0511
	DEC .819280	FIMP0512
	DEC .6553680	FIMP0513
	DEC .52428880	FIMP0514
	DEC .898860880	FIMP0515
	DEC .6710886480	FIMP0516
FREF1	DEC .53687091280	FIMP0517
5835	DEC 5	FIMP0518
12835	PZE 126	FIMP0519
MASK1	OCT 0000000000077	FIMP0520
MASK2	OCT 6060606060000	FIMP0521
MASK3	OCT 0000000000060	FIMP0522
1817	OCT 1000000	FIMP0523
2835	DEC 2835	FIMP0524
3835	PZE 3	FIMP0525
8835	DEC 8835	FIMP0526
11835	PZE 11	FIMP0527
12835	PZE 12	FIMP0528
*		FIMP0529
MTX00	SXA MTX10.4	FIMP0530
	COMMON+35	FIMP0531
STO		FIMP0532
SSM		

CLA LOC COMMA
 TSX MTX00.4
 NO CHAR I

ADD	5B35	NO CHAR J	FIMP0533
STO	COMMON+36	IJ RETURN	FIMP0534
AXT	2,4	NORMAL RETURN	FIMP0535
MTX01	MTX02,4		FIMP0536
SXA	SIGN		FIMP0537
STZ	SUM		FIMP0538
STZ	100B35,2		FIMP0539
LXA	COMMON+37,4		FIMP0540
CLA	DECIM,4		FIMP0541
TSX	GINER		FIMP0542
TRA	MTX11	LES THAN N CHADS	FIMP0543
TRA	GINER,2,100		FIMP0544
TXL	** ,4		FIMP0545
AXT	I+2,4	I,J	FIMP0546
STQ	MTX01,4,1		FIMP0547
TIX	** ,4		FIMP0548
MTX10	J		FIMP0549
AXT	IB35		FIMP0550
CLA	IMAX		FIMP0551
SUB			FIMP0552
XCA			FIMP0553
MPY			FIMP0554
XCA			FIMP0555
ADD	I		FIMP0556
LDO	IJ		FIMP0557
TLQ	1,4	LOC GTR MAX	FIMP0558
XCA			FIMP0559
TRA	2,4		FIMP0560
LXA	MTX02,4		FIMP0561
TXH	GINER,4,1	I ERROR	FIMP0562
TRA	MTX02-1	J	FIMP0563
SET UP	IJ WORD		FIMP0564
SXA	MCD02,4		FIMP0565
CAL	GINOO		FIMP0566
SUB	1B35		FIMP0567
STA	SGIN03		FIMP0568
LDO	0,1	DETERMINE COMMA POSITION	FIMP0569
LGL	6		FIMP0570
AXT	2,4		FIMP0571
PXD	0,0		FIMP0572
LGL	6		FIMP0573
SUB	MASK4	COMMA	
TZE	**3		

TXH	GINER,4,3	NOT MATRIX	FIMP0574
TXI	*-5,4,1		FIMP0575
PXA	,4	POSITION OF COMMA	FIMP0576
TSX	MTX00,4		FIMP0577
NOP	**		FIMP0578
LDQ	I		FIMP0579
STQ	IMAX		FIMP0580
MPY	J		FIMP0581
STQ	IJ		FIMP0582
LXA	MCD02,4		FIMP0583
TXL	MCD04,4,12		FIMP0584
LXA	IJ,4		FIMP0585
CAL	GIN00		FIMP0586
ADM	IJ		FIMP0587
STA	*+1	ZERO MATRIX	FIMP0588
STZ	**+4		FIMP0589
TIX	*-1,4,1		FIMP0590
TXI	GIN11,1,-1		FIMP0591
MCD04			FIMP0592
*			FIMP0593
ACD0	CTR		FIMP0594
	PASS		FIMP0595
	PF		FIMP0596
ACD1	5,2	BLANK	FIMP0597
	SYM00,4		FIMP0598
	0,4		FIMP0599
	ACD6,2,1		FIMP0600
	ACD12,4,0	NULL AND BLANK	FIMP0601
	ACD6+1	NULL	FIMP0602
ACD6	PF	BLANK	FIMP0603
	ACD10,4,0		FIMP0604
	1,2		FIMP0605
	SYM00,4		FIMP0606
	0,4	BLANK	FIMP0607
	ACD10,2,1	NULL	FIMP0608
			FIMP0609
	15		FIMP0610
	PF		FIMP0611
	PF		FIMP0612
ACD10	PASS		FIMP0613
	PASS		FIMP0614
	ACD15		

Contrails

STQ	WORD	NOT BLANK	FINP0615
TXH	ACD1,4,0		FINP0616
LXA	CTR,4		FINP0617
TXH	ACD14,4,6		FINP0618
TXI	**1,1,-1		FINP0619
TXL	**3,4,1	BLANK	FINP0620
LDQ	WORD		FINP0621
TSX	SGIN00,4		FINP0622
TXL	GIN11		FINP0623
ACD15	18		FINP0624
SLO	WORD		FINP0625
TXL	ACD12		FINP0626
* SYM00	SYM02,2	LXA L(NO CHARACTERS),2	FINP0627
SXA	SYM14,4	TSX SYM00,4	FINP0628
STZ	PSYM	BALNK	FINP0629
AXT	1,2	NORMAL IR2=1 IF NULL	FINP0630
CLA	CTR		FINP0631
ADD	1835		FINP0632
STO	CTR		FINP0633
SUB	10B35+1		FINP0634
TMZ	**2		FINP0635
TXI	**1,1,-1		FINP0636
LDQ	0,1		FINP0637
CAL	PSYM		FINP0638
LGL	6		FINP0639
SLW	PSYM		FINP0640
STQ	0,1		FINP0641
AMA	MASK1		FINP0642
SUB	MASK3		FINP0643
TZE	SYM20	BLANK	FINP0644
SUB	11B35		FINP0645
TZE	SYM21	COMMA	FINP0646
TXI	**1,2,1		FINP0647
TXL	SYM01,2,**		FINP0648
CAL	PSYM		FINP0649
TXI	**1,2,-1		FINP0650
SXA	SYM06,2	NO CHARACTERS	FINP0651
LDQ	MASK2		FINP0652
LGL	6		FINP0653
TXI	**1,2,1	LEFT JUSTIFY	FINP0654
			FINP0655

Contrails

	SYM04,2,5		FIMP0656
TXL	SYMBL		FIMP0657
SLW	PSYM		FIMP0658
CAL	BLANK		FIMP0659
ANA	SYM10	SYMBOLIC	FIMP0660
TNZ	**2	NO CHARACTERS	FIMP0661
AXT	SYMBL		FIMP0662
LDQ	SUM		FIMP0663
STZ	SIGN		FIMP0664
STZ			FIMP0665
TXL	SYM08,2,4	DECIMAL	FIMP0666
TSX	OCTAL1,4	OCTAL	FIMP0667
TXL	GINER		FIMP0668
TSX	SYM14,2		FIMP0669
CLA	0,1		FIMP0670
STQ	0,1		FIMP0671
STO	SYMBL		FIMP0672
PXA	*2		FIMP0673
TSX	DECIM,4		FIMP0674
TRA	GINER	ERROR	FIMP0675
TXL	GINER		FIMP0676
CLA	SYMBL		FIMP0677
STO	0,1		FIMP0678
TSX	SYM14,2		FIMP0679
CLA	SYMBL		FIMP0680
TSX	TBLOO,4		FIMP0681
AXT	**2,4		FIMP0682
TRA	2,4	EXIT	FIMP0683
TXI	**1,4,1	BLANK	FIMP0684
SXA	SYM14,4		FIMP0685
TXL	SYM14+1,2,1	NULL FIELD	FIMP0686
CAL	PSYM		FIMP0687
ARS	6		FIMP0688
SLW	PSYM		FIMP0689
TXL	SYM03		FIMP0690
LXA	**2	N	FIMP0691
CAS	**2	BCD+N-N	FIMP0692
TXL	**2		FIMP0693
TXI	TBLO2,2,-2		FIMP0694
TIX	TBLO1,2,1		FIMP0695
TXL	GINER,0,-1		FIMP0696
LDQ	**2	ALPHA+N-(N-2)	

SIBFTC	MAT9	LIST,REF,DECK	MAT90000
	SUBROUTINE	MAT9(A,X,KR,KC,LC,LA)	MAT90001
	DIMENSION	A(KR,KC),X(KR,LC)	MAT90002
	M=KR		MAT90003
	M=LC		MAT90004
	MM=KC		MAT90005
	DO 15 I=2,N		MAT90006
	II=I-1		MAT90007
	DO 15 J=1,II		MAT90008
	IF(A(I,J))9,15,9		MAT90009
9	IF (ABS(A(J,J))-ABS(A(I,J)))	11,10,10	MAT90010
10	R=A(I,J)/A(J,J)		MAT90011
	GO TO 13		MAT90012
11	R=A(J,J)/A(I,J)		MAT90013
	DO 12 K=1,MM		MAT90014
	B=A(J,K)		MAT90015
	A(J,K)=A(I,K)		MAT90016
12	A(I,K)=B		MAT90017
13	JJ=J+1		MAT90018
	DO 14 K=JJ,MM		MAT90019
14	A(I,K)=A(I,K)-R*A(J,K)		MAT90020
15	CONTINUE		MAT90021
	IF (ABS(A(M,N))-1.0E-10)	16,16,17	MAT90022
16	CALL ERRS(1,4HMAT9)		MAT90023
	LA=-1		MAT90024
	RETURN		MAT90025
17	DO 20 J=1,M		MAT90026
	KK=N+J		MAT90027
	X(N,J)=A(N,KK)/A(N,N)		MAT90028
	DO 28 I=2,N		MAT90029
	JJ=N-I+1		MAT90030
	B=0.		MAT90031
	II=N-I+2		MAT90032
	DO 25 K=II,N		MAT90033
25	B=B+A(JJ,K)*X(K,J)		MAT90034
	IF (ABS(A(JJ,JJ))-1.0E-10)	26,26,28	MAT90035
26	CALL ERRS(2,4HMAT9)		MAT90036
	LA=-1		MAT90037
	RETURN		MAT90038
28	X(JJ,J)=(A(JJ,KK)-B)/A(JJ,JJ)		MAT90039
	LA=+1		MAT90040

Contrails

MAT90041
MAT9004+

RETURN
END

```
SIBFTC MPRT LIST,REF,DECK  
C MPRT PRINTS THE FIRST N ROWS AND COLUMNS OF A 20X20 ARRAY  
SUBROUTINE MPRT (A,N)  
DIMENSION A(20,20)  
DO 100 I=1,N  
WRITE (3,1001) I,(A(I,J),J=1,N)  
1001 FORMAT (4HROW,14,5E20.8/(8X,5E20.8))  
100 CONTINUE  
RETURN  
END
```



```

$IBFTC SCRF LIST,REF,DECK
C SCRF COMPUTES AN NXN SCRIPT F MATRIX (( SCRIPT F(I,J) ))
C
C SUBROUTINE SCRF (N,MN,RHO,F,AREA,R,D,DI,SF,SFA,IERR)
C
C DIMENSION RHO(20,20),F(20,20),AREA(20),R(20,20,20)
1 ALPHA(20,20),A(20,20),B(20,20),C(20,20),DD(20,20)
2 D(M,MN),DI(N,N)
3 SF(20,20),SFA(20,20)
4 WK(10)
C
100 M2= N*MN
MN2= 2*MN2
IERR= 0
C CLEAR STORAGE REGIONS
DO 120 I=1,400
DD(I,1)= 0.
SF(I,1)= 0.
SFA(I,1)= 0.
CONTINUE
120 DO 150 I=1,MN2
D(I,1)= 0.
CONTINUE
150
C COMPUTE ABSORBITIVITIES AND EMISSITIVITIES.
C
200 DO 210 I=1,N
DO 210 J=1,N
ALPHA(I,J)= 1.-RHO(I,J)
CONTINUE
210
C COMPUTE MATRICES A,B,C,AND D.
C
300 DO 390 I=1,N
DO 390 J=1,N
WK(3)= ALPHA(J,I)*F(I,J)
WK(1)= ALPHA(I,J)*WK(3)
WK(2)= 0.
WK(4)= 0.
C
DO 320 K=1,N
WK(5)= R(J,K,I)*F(I,K)*F(K,J)
WK(6)= WK(5)*RHO(J,K)

```

```

C
WK(7) = WK(5)*ALPHA(J,K)

WK(1) = WK(1) + ALPHA(I,K)*WK(7)
WK(2) = WK(2) + ALPHA(I,K)*WK(6)
WK(3) = WK(3) + WK(7)
WK(4) = WK(4) + WK(6)
320 CONTINUE
C
A(I,J) = -WK(1)
B(I,J) = -WK(2)
C(I,J) = WK(3)
D(I,J) = -WK(4)
IF (I-J) 390,330,390
I=J, DIAGONAL ELEMENTS
330 D(I,J) = 1.-WK(4)
IM=IAN
D(I,IM) = 1.
390 CONTINUE
C
C COMPUTE SMALL P PRINIPAL
400 LA=1
CALL MATH (D,DI,M,MM,M,LA)
IF (LA) 410,410,500
410 WRITE (3,1000)
1000 FORMAT (68H) ERROR. MATRIX D CAN NOT BE INVERTED. CHECK DIAGONAL E
LEMENTS OF D./1H0.5X. @MATRIX D)
IERR=1
CALL VMPRT (D,N)
GO TO 900
C
C COMPUTE CAPITAL D MATRIX
500 DO 590 I=1,N
DO 590 J=1,N
WK=0.
DO 520 K=1,N
WK = WK + D(I,J,K)*C(K,I)
520 CONTINUE
DD(I,J) = WK
590 CONTINUE

```

```
C
C  COMPUTE SCRIPT F MATRIX
600  DO 690 I=1,N
      DO 690 J=1,N
        WK= A(I,J)
        DO 620 K=1,N
          WK= WK + B(I,K)*DD(J,K)
        CONTINUE
        SF(I,J)= -WK
        SFA(I,J)= -WK*AREA(I)
620  CONTINUE
690  RETURN
900  END
```

```
SIBFTC VMPRT LIST,REF,DECK  
C VMPRT PRINTS AN MXN ARRAY  
SUBROUTINE VMPRT (A,N)  
DIMENSION A(N,N)  
DO 100 I=1,N  
WRITE (3,1001) I,(A(I,J),J=1,N)  
1001 FORMAT (4HROW,I4,5E20.8/(8X,5E20.8))  
100 CONTINUE  
RETURN  
END
```

INPUT FELLOWS

H1 DIRECTIONAL SPECULAR, ALUM. PAINT

H2 BLACK, BLACK

N 4

01,030.7075

02,030.07

03,020.07

MF 20,20

04,010.2

3 0.25

MR1 20,20

MR2 20,20

MR3 20,20

01,020.16583

04,010.752091

01,040.7283

02,040.1275

03,040.1275

02,010.2

04,020.2

AREA

4 0.75

01,020.07

01,030.07

01,020.07

01,030.16583

03,010.692613

04,020.13368

MRHO 20,20

03,010.2

04,030.2

1

0.25

01,030.07

02,030.07

02,011.519

02,010.692613

03,020.07

04,030.13368

01,020.7075

02,010.1275

03,010.1275

03,020.2

04,040.4

2

0.25

03,020.07

MR4 20,20

02,030.07

END

END OF INPUT

SPECULAR-DIRECTIONAL SCRIPT F PROGRAM (AH052A), 10/28/64

DIRECTIONAL SPECULAR, ALUM. PAINT

BLACK, BLACK

RHO(I, J) MATRIX

ROW 1	0.	0.7075000E 00	0.7075000E 00	0.7283000E 00
ROW 2	0.1275000E-00	0.	0.7000000E-01	0.1275000E-00
ROW 3	0.1275000E-00	0.7000000E-01	0.	0.1275000E-00
ROW 4	0.	0.	0.	0.

F(I,J) MATRIX

ROW 1	0.	0.20000000E-00	0.20000000E-00	0.59999999E 00
ROW 2	0.20000000E-00	0.	0.20000000E-00	0.59999999E 00
ROW 3	0.20000000E-00	0.20000000E-00	0.	0.59999999E 00
ROW 4	0.20000000E-00	0.20000000E-00	0.20000000E-00	0.40000000E-00

Contracts

AREA VECTOR
0.2500000E-00 0.2500000E-00 0.2500000E-00 0.7500000E 00

R(I, J, K) ARRAY

BLOCK NO. 1
ROW 1 0. 0.70000000E-01 0.70000000E-01 0.
ROW 2 0. 0. C.70000000E-01 0.
ROW 3 0. 0.70000000E-01 0. 0.
ROW 4 0. 0.1658299E-00 0.1658299E-00 0.

BLOCK NO. 2
ROW 1 0. 0. 0.70000000E-01 0.
ROW 2 0. 0. C.70000000E-01 0.
ROW 3 0.1518999E 01 0. 0.
ROW 4 0.69261300E 00 0. 0.70000000E-01 0.

BLOCK NO. 3
ROW 1 0. 0.70000000E-01 0. 0.
ROW 2 0.1518999E 01 0. 0. 0.
ROW 3 0. 0.70000000E-01 0. 0.
ROW 4 0.69261300E 00 0.70000000E-01 0. 0.

BLOCK NO. 4
ROW 1 0. 0.1658299E-00 0.1658299E-00 0.

Contracts

RDM	2	0.69261300E 00	0.	C.70000000E-01	0.
RDM	3	0.69261300E 00	C.70000000E-01	0.	0.
RDM	4	0.75209100E 00	0.13388000E-00	0.13388000E-00	0.

SCRIPT F MATRIX

RDM	1	0.48790440E-03	0.52023036E-01	0.52023036E-01	0.17548605E-00
RDM	2	0.52221070E-01	0.43687483E-02	0.21963776E-00	0.60985991E 00
RDM	3	0.52221070E-01	0.21963776E-00	0.43687482E-02	0.60985991E 00
RDM	4	0.58681963E-01	0.20385623E-00	0.20385623E-00	0.53362094E 00

SCRIPT FA MATRIX

ROM 1	0.12197610E-03	0.13005759E-01	0.13005759E-01	0.43871512E-01
ROM 2	0.13055267E-01	0.10921870E-02	0.54909441E-01	0.15246497E-00
ROM 3	0.13055267E-01	0.54909441E-01	0.10921870E-02	0.15246497E-00
ROM 4	0.44011472E-01	0.15289217E-00	0.15289217E-00	0.40021570E-00

APPENDIX IV
EXPERIMENTAL DATA —
RADIATION EXCHANGE EXPERIMENT

Contrails

The experimental data used in the verification of the analytical techniques described in Section 6 are shown in Table 15. The predicted receiver temperature was calculated from a heat balance between the surfaces of the experimental enclosure. The heat balance equation for the receiver is

$$A_S \bar{\eta}_{S-R} (\sigma T_S^4 - \sigma T_R^4) + A_M \bar{\eta}_{M-R} (\sigma T_M^4 - \sigma T_R^4) = A_R \bar{\eta}_{R-O} (\sigma T_R^4 - \sigma T_O^4) + Q_{LOSS}$$

$$\sigma T_R^4 = \frac{A_S \bar{\eta}_{S-R} \sigma T_S^4 + A_M \bar{\eta}_{M-R} \sigma T_M^4 + A_R \bar{\eta}_{R-O} \sigma T_O^4 - Q_{LOSS}}{A_S \bar{\eta}_{S-R} + A_M \bar{\eta}_{M-R} + A_R \bar{\eta}_{R-O}}$$

For Configuration 3, run number 7, using the directional analysis to obtain the $\bar{\eta}$'s

$$\sigma T_R^4 = \frac{0.0593(201.84) + 0.0013(62.85) + 0.159(1.0) - 0.57}{0.2196}$$

$$\sigma T_R^4 = 53.0$$

$$T_R = 419.4^\circ R$$

This temperature can be compared to the experimentally measured value of $428.2^\circ R$.

The net heat lost by the source, Q_S , is computed by summing the heat leaving the source and received by each surrounding surface

$$Q_S = Q_{S-M} + Q_{S-R} + Q_{S-O} + Q_{LOSS}$$

$$Q_{S-M} = A_S \bar{\eta}_{S-M} (\sigma T_S^4 - \sigma T_M^4)$$

$$Q_{S-R} = A_S \bar{\eta}_{R-S} (\sigma T_S^4 - \sigma T_R^4)$$

$$Q_{S-O} = A_S \bar{\eta}_{R-O} (\sigma T_S^4 - \sigma T_O^4)$$

Contrails

Using the data from Run 7, directional analysis

$$Q_S = 0.0013(201.84 - 62.85) + 0.0593(201.84 - 57.62) + 0.159(201.84 - 1.0)$$

$$Q_S = 40.68 \text{ Btu/hr}$$

This value compares to the experimental quantity of 41.29 Btu/hr.

As described in Section 6, a guard heater method was used to minimize the extraneous heat losses from each test surface. Figure 38 shows the measured heat losses from a vacuum deposited aluminum coated surface and a 3M black paint coated surface. These results were used to correct the experimentally measured source radiation and in the prediction of the temperature of the receiver temperature.

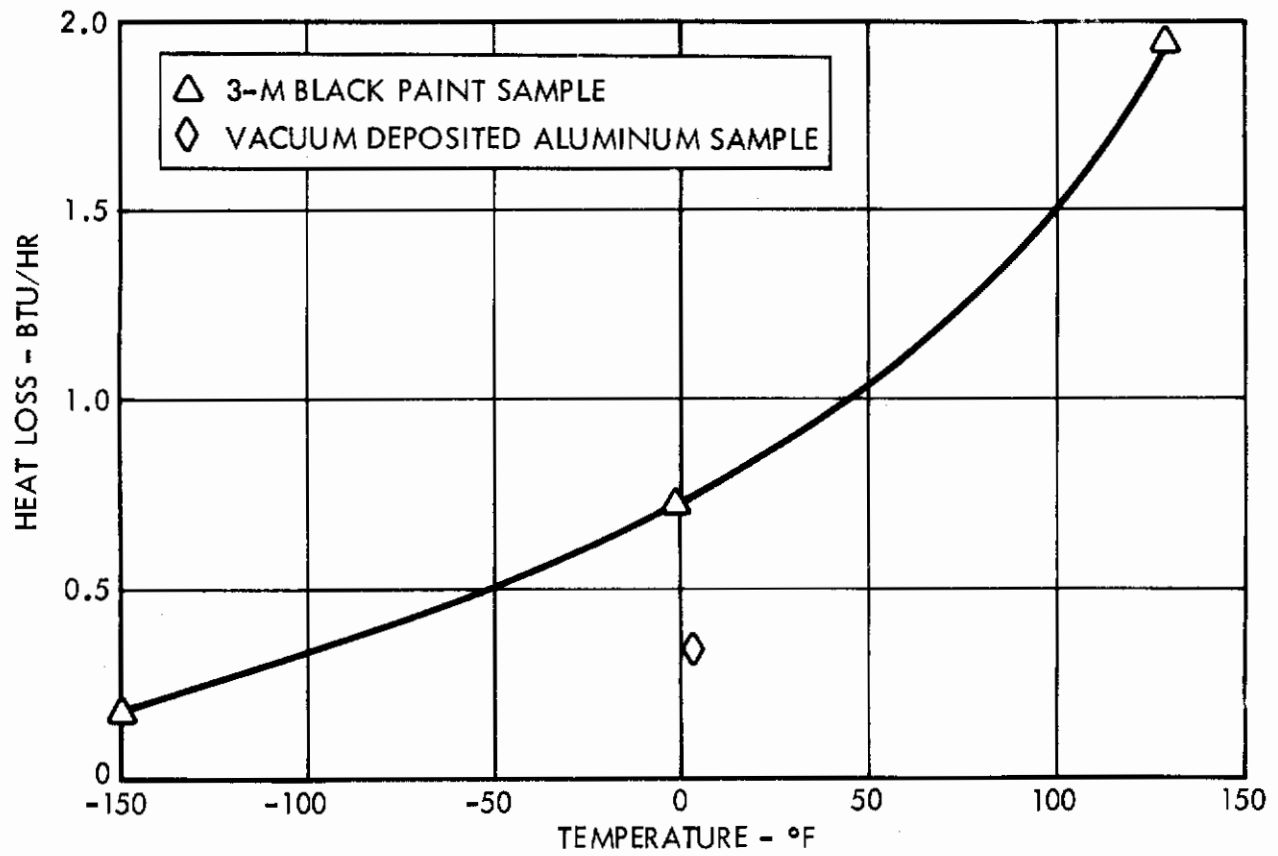


Figure 38. Measured Heat Loss from Test Surfaces of Radiation Experiment

Contrails

Table 15. Summary of the Data Obtained in the Experimental Testing of the Analytical Prediction

Run Number	1	2	3	4	5
Date	3/18/65	3/19/65	3/19/65	3/23/65	3/4/65
Pressure	4×10^{-6}	4×10^{-6}	3×10^{-6}	4×10^{-6}	5×10^{-6}
Configuration	*	*	*	**	1
Source					
Center T. C. - °F	129.9	-1.0	-150.9	+4.4	73.8
Corner T. C. - °F	129.1	-2.5	-151.7	+4.1	72.2
Guard T. C. - °F	129.9	-0.3	-147.4	+1.0	73.1
Mirror					
Center T. C. - °F					
Corner T. C. - °F					
Guard T. C. - °F					
Receiver					
Center T. C. - °F					-114.5
Corner T. C. - °F					-115.0
Guard T. C. - °F					-114.8
Source Voltage, volts	50.5	30.4	13.5	6.86	41.11
Source Current, amps	0.276	0.167	0.0776	0.0373	0.2266

* Single black plate

** Single vacuum deposited aluminum plate

Contrails

Table 15. Summary of the Data Obtained in the Experimental Testing of the Analytical Prediction (Continued)

Run Number	6	7	8	9	10
Date	3/28/65	4/1/65	4/5/65	4/6/65	4/8/65
Pressure	2×10^{-6}	3×10^{-6}	4×10^{-6}	5×10^{-6}	7×10^{-6}
Configuration	2	3	4	5	6
Source					
Center T. C. - °F	124.6	125.8	124.7	125.0	124.5
Corner T. C. - °F	124.5	125.8	124.3	124.6	124.1
Guard T. C. - °F	125.1	125.3	123.7	126.7	125.5
Mirror					
Center T. C. - °F		-22.4	-51.8	-74.7	-63.5
Corner T. C. - °F		-22.4	-51.7	-74.7	-62.6
Guard T. C. - °F		-23.7	-51.7	-73.5	-60.3
Receiver					
Center T. C. - °F	-66.1	-31.0	-36.5	-50.3	-61.3
Corner T. C. - °F	-66.4	-31.7	-37.0	-50.3	-61.3
Guard T. C. - °F	-65.4	-24.4	-35.2	-52.4	-61.7
Source Voltage, volts	48.7	48.0	47.7	47.3	47.4
Source Current, amps	0.267	0.2635	0.2615	0.259	0.2592

**APPENDIX V
BIBLIOGRAPHY FOR
JOINT THERMAL CONDUCTANCE**

APPENDIX V

BIBLIOGRAPHY FOR JOINT THERMAL CONDUCTANCE

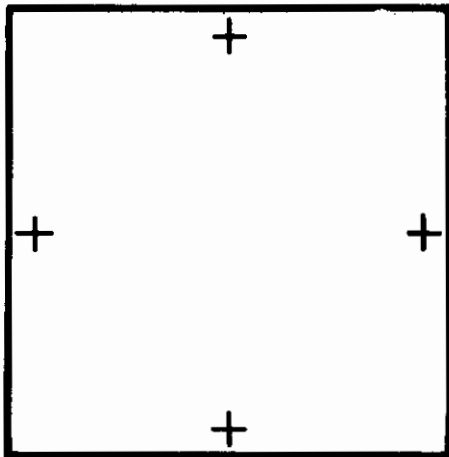
1. Ambrosio, A. and Lindh, K. "Thermal Contact Resistance of Riveted Joints," UCLA Engineering Report No. C55-4, February 1955.
2. Ambrosio, A. and Lindh, K. "Thermal Contact Resistance of Spot Welded Titanium Joints," UCLA Engineering Report No. C55-12, March 1955.
3. Blum, H. A. and Moore, C. J. "Heat Transfer Across Surfaces in Contact Transient Effects of Ambient Temperatures and Pressures," NASA-CR-57137, 1964.
4. Bernard, J. "The Thermal Resistance of Joints: Translation 951," AD 202, 822, 1961.
5. Clausing, A. H. and Chao, B. T. "Thermal Contact Resistance in a Vacuum Environment," ASME Journal of Heat Transfer, 87:243-251, May 1965.
6. Gurr, G. W. and Cote, H. S. "A Study of the Thermal Conductance of Metallic Joints," Engineering Report No. LB-25705, Douglas Aircraft Company, 23 January 1958.
7. Lindh, K. "Measurement of Thermal Contact Resistance," UCLA Engineering Report No. C14-53, July 1953.
8. Lindh, K. "Thermal Contact Resistance Study," UCLA Engineering Report No. C15-53, August 1953.
9. Lindh, K. "Progress Report Contract," North American P. O. No. L522-138792, Thermal Resistance, UCLA Engineering Report No. 56-28, 1 June 1956.
10. Lindh, K., Lieb, B. A., Knuth, E. L., Ishimoto, T., and Kaysen, H. M. "Studies in Heat Transfer in Aircraft Structure Joints," UCLA Engineering Report No. 57-50, May 1957.
11. Little, R., Smith, S., et al. "Electrical Breakdown in Vacuum NRL 5671," AD 266603, 2 October 1961.
12. Lobbet, J. and Robb, E. "Thermo-Mechanical Analysis of Structural Joint Study," WADD TR 61-151, January 1962.
13. Miller, Y. S. "Thermal Resistances in Contact Areas of Heating Elements," (Prokontakt TUI TERMICHNI OPORY U TEPLOVDILYA YUCHYKH ELEMENTAKH) March 1964, Translation into English from Akad. Nauk Ukr RSR, Inst. Teploenerg, 2b Prats (Kiev) no 24, 1962, NASA-TT-F-8839.

**APPENDIX VI
COMPONENT JOINT TEST DATA
USED FOR CORRELATION TASK**

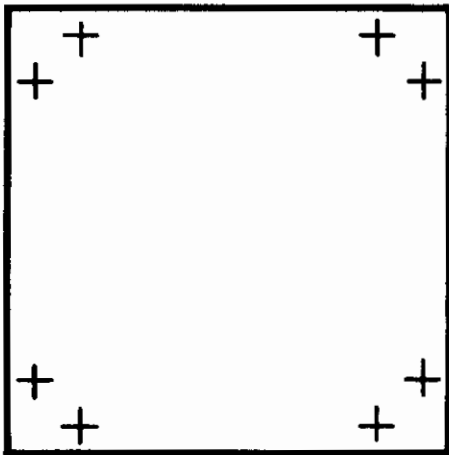
Contrails

Three experimental tests were conducted to verify the results of the correlation task. The experimental measurements are given in Table 16. The thermocouple locations and data reduction technique are described in Appendix I. The bolt locations for these three tests are shown in Figure 39.

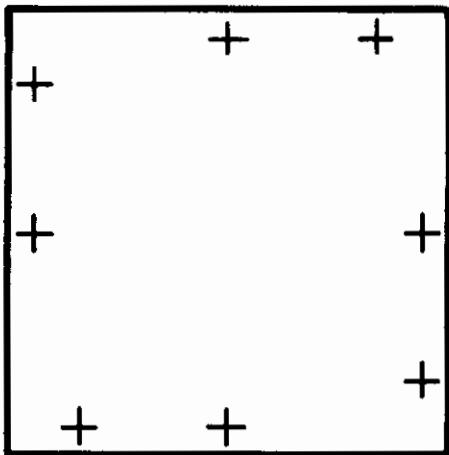
BOLT LOCATION-CORRELATION TASK



4 BOLTS
RUN NO. 41



8 BOLTS
RUN NO. 43



8 BOLTS
RUN NO. 42

Figure 39. Bolt Locations for Correlation Task Experiments

Table 16. Additional Component Joint Correlation Data

Run Number	41	42	43
Date	11/24/64	11/25/64	11/25/64
Pressure	5×10^{-7}	5×10^{-6}	5×10^{-6}
Absolute T. C.			
1 - °F	92.6	88.4	92.7
2 - °F	81.8	74.9	75.0
3 - °F	66.6	65.9	66.4
4 - °F	67.0	66.4	66.9
Differential T. C.			
1 - °F	17.64	14.32	18.42
2 - °F	17.70	13.93	18.45
3 - °F	11.94	7.36	10.19
4 - °F	7.46	4.97	10.59
5 - °F	1.80	1.11	9.44
6 - °F	7.80	4.26	7.95
7 - °F	10.18	3.26	3.64
8 - °F	10.40	2.53	1.61
Voltage, volts	52.96	52.95	52.95
Current, amps	0.1880	0.1880	0.1880
Water Flow, ml/min	700	575	550
Bolt Torque, in-lb	24	24	24
Filler	None	None	None
Sample Number	3	3	3
Number of Bolts	4	8	8
h, Btu/hr ft ² °F	13.4	22.0	13.7

Unclassified

Security Classification

DOCUMENT CONTROL DATA - R&D		
<i>(Security classification of title, body of abstract and indexing annotation must be entered when the overall report is classified)</i>		
1. ORIGINATING ACTIVITY (Corporate author) AFFDL (FDPE) WPAFB, Ohio		2a. REPORT SECURITY CLASSIFICATION Unclassified
		2b. GROUP
3. REPORT TITLE Prediction of Space Vehicle Thermal Characteristics		
4. DESCRIPTIVE NOTES (Type of report and inclusive dates) TR		
5. AUTHOR(S) (Last name, first name, initial) J. T. Bevans, T. Ishimoto, B. R. Loya, E. E. Luedke		
6. REPORT DATE October 1965	7a. TOTAL NO. OF PAGES	7b. NO. OF REFS
8a. CONTRACT OR GRANT NO.	8b. ORIGINATOR'S REPORT NUMBER(S)	
b. PROJECT NO. 6146		
c. Task No. 614617	8c. OTHER REPORT NO(S) (Any other numbers that may be assigned this report) AFFDL-TR-65-139	
10. AVAILABILITY/LIMITATION NOTICES Not to be released to the U.S. Department of Commerce, CFSTI, for a period of two years from date of publication.		
11. SUPPLEMENTARY NOTES	12. SPONSORING MILITARY ACTIVITY AF Flight Dynamics Laboratory	
13. ABSTRACT The work reported herein is the first phase of a program to improve the prediction of spacecraft thermal performance. The study has consisted of measuring actual joint thermal conductances, correlation of the measured joint conductances, programing an improved method of thermal radiation analysis, and performing an experimental comparison of predicted radiation exchange for a simple geometrical system. Three types of structural and three sizes of component mounting joints were tested and the conductances measured. A successful method of correlation was developed for the unfilled component mounting joints. A method of radiation analysis has been programed which uses directional thermal radiation properties and accounts for the specularity and/or diffuseness of these properties. The results of this program can be readily incorporated into most existing thermal analysis programs. The user has the choice of the specular, the diffuse, or the specular-diffuse assumption. The prediction of radiation exchange using these assumptions for simple geometrical arrangements has been compared to experiment. Although the results were within the overall experimental tolerances, further improvement in the predicted values is believed possible.		

DD FORM 1473
1 JAN 64

Unclassified

Security Classification

Unclassified
Security Classification

14.	KEY WORDS	LINK A		LINK B		LINK C	
		ROLE	WT	ROLE	WT	ROLE	WT
	1. Space vehicles.						
	2. Passive temperature control systems.						
	3. Radiant heat transfer.						
	4. Thermal conductance of joints.						

INSTRUCTIONS

1. **ORIGINATING ACTIVITY:** Enter the name and address of the contractor, subcontractor, grantee, Department of Defense activity or other organization (*corporate author*) issuing the report.
- 2a. **REPORT SECURITY CLASSIFICATION:** Enter the overall security classification of the report. Indicate whether "Restricted Data" is included. Marking is to be in accordance with appropriate security regulations.
- 2b. **GROUP:** Automatic downgrading is specified in DoD Directive 5200.10 and Armed Forces Industrial Manual. Enter the group number. Also, when applicable, show that optional markings have been used for Group 3 and Group 4 as authorized.
3. **REPORT TITLE:** Enter the complete report title in all capital letters. Titles in all cases should be unclassified. If a meaningful title cannot be selected without classification, show title classification in all capitals in parenthesis immediately following the title.
4. **DESCRIPTIVE NOTES:** If appropriate, enter the type of report, e.g., interim, progress, summary, annual, or final. Give the inclusive dates when a specific reporting period is covered.
5. **AUTHOR(S):** Enter the name(s) of author(s) as shown on or in the report. Enter last name, first name, middle initial. If military, show rank and branch of service. The name of the principal author is an absolute minimum requirement.
6. **REPORT DATE:** Enter the date of the report as day, month, year, or month, year. If more than one date appears on the report, use date of publication.
- 7a. **TOTAL NUMBER OF PAGES:** The total page count should follow normal pagination procedures, i.e., enter the number of pages containing information.
- 7b. **NUMBER OF REFERENCES:** Enter the total number of references cited in the report.
- 8a. **CONTRACT OR GRANT NUMBER:** If appropriate, enter the applicable number of the contract or grant under which the report was written.
- 8b, 8c, & 8d. **PROJECT NUMBER:** Enter the appropriate military department identification, such as project number, subproject number, system numbers, task number, etc.
- 9a. **ORIGINATOR'S REPORT NUMBER(S):** Enter the official report number by which the document will be identified and controlled by the originating activity. This number must be unique to this report.
- 9b. **OTHER REPORT NUMBER(S):** If the report has been assigned any other report numbers (*either by the originator or by the sponsor*), also enter this number(s).
10. **AVAILABILITY/LIMITATION NOTICES:** Enter any limitations on further dissemination of the report, other than those

imposed by security classification, using standard statements such as:

- (1) "Qualified requesters may obtain copies of this report from DDC."
- (2) "Foreign announcement and dissemination of this report by DDC is not authorized."
- (3) "U. S. Government agencies may obtain copies of this report directly from DDC. Other qualified DDC users shall request through _____."
- (4) "U. S. military agencies may obtain copies of this report directly from DDC. Other qualified users shall request through _____."
- (5) "All distribution of this report is controlled. Qualified DDC users shall request through _____."

If the report has been furnished to the Office of Technical Services, Department of Commerce, for sale to the public, indicate this fact and enter the price, if known.

11. **SUPPLEMENTARY NOTES:** Use for additional explanatory notes.
12. **SPONSORING MILITARY ACTIVITY:** Enter the name of the departmental project office or laboratory sponsoring (*paying for*) the research and development. Include address.
13. **ABSTRACT:** Enter an abstract giving a brief and factual summary of the document indicative of the report, even though it may also appear elsewhere in the body of the technical report. If additional space is required, a continuation sheet shall be attached.

It is highly desirable that the abstract of classified reports be unclassified. Each paragraph of the abstract shall end with an indication of the military security classification of the information in the paragraph, represented as (TS), (S), (C), or (U).

There is no limitation on the length of the abstract. However, the suggested length is from 150 to 225 words.
14. **KEY WORDS:** Key words are technically meaningful terms or short phrases that characterize a report and may be used as index entries for cataloging the report. Key words must be selected so that no security classification is required. Identifiers, such as equipment model designation, trade name, military project code name, geographic location, may be used as key words but will be followed by an indication of technical context. The assignment of links, rules, and weights is optional.

Unclassified
Security Classification